ALTERED PROTEIN EXPRESSION PATTERNS IN OESOPHAGEAL CANCER

Widaad Zemanay

This thesis is submitted in fulfillment of the academic requirements

for the degree of

Doctor of Philosophy in Medical Biochemistry

in the Faculty of Health Sciences

University of Cape Town

February 2009

Declaration

I hereby declare that: (1) the above thesis is my own unaided work, both in conception and execution, and that apart from the normal guidance of my supervisor, I have received no assistance apart from that stated below; (2) except as stated below, neither the substance or any part of the thesis has been submitted in the past, or is being, or is to be submitted for a degree in the University or any other University. I am now presenting the thesis for examination for the Degree of Doctor of Philosophy in Medical Biochemistry.

Signature: _____

Name: Widaad Zemanay Date: _____15 February 2009_____

Abstract

Oesophageal squamous cell carcinoma presents a significant health burden in South Africa. It is one of the most common causes of cancer-related mortality of South African black males, as a result of its asymptomatic progression leading to late diagnosis and poor prognosis.

The aim of this study was to identify membrane or membrane-associated proteins that are expressed at different levels in oesophageal tumour tissue when compared to normal tissue. The identification of such proteins would be an important step towards the development of better diagnostic and therapeutic strategies for this disease.

Two proteomic approaches, were employed to identify differentially expressed proteins. 2D-DIGE linked to MALDI-MS was used to identify altered protein levels in tumour tissue in comparison with normal tissue from OSCC patients. Collectively, 60 differentially expressed proteins were identified using this technique and a subset of proteins was selected for validation. The altered expression levels of gelsolin, HSP90B1 and annexin 2 were confirmed using immunohistochemical analysis, and the increased levels of annexin 2 were assessed as a potential marker for prognosis. The increased expression of several glycolytic enzymes was noted, including pyruvate kinase and GAPDH (confirmed by IHC). This presented a potential therapeutic target, and we proceeded to explore the glycolytic pathway as a target for therapeutic intervention in OSCC, using DCA. Unfortunately, the results achieved, reported that DCA is not an effective chemotherapeutic agent in OSCC. However, annexin 2, pending further investigation, could potentially be used as an early diagnostic marker.

REQUA linked to ESI-QUAD-TOF MS was used in a cell culture system to compare a cultured oesophageal cancer cell line to a cultured normal oesophageal cell line. Higher levels of CD98 hc were observed in the tumour cell line and IHC validation of this observation revealed that

increased CD98 hc levels occur as early as dysplasia, re-affirming CD98 as a molecular target for therapeutic intervention of OSCC.

This study identified several regulated proteins that may be of use as markers or therapeutic targets to improve the diagnosis and prognosis of squamous cell carcinoma of the oesophagus.

Acknowledgements

In no particular order, I would like to thank everybody who has contributed to me being able to complete this work.

Dr Denver Hendricks played more than a supervisory role, and even though he writes it off as just being part of his job, he has supported me in more ways than one and I would never have completed this without him.

Prof Parker is the reason I was fortunate enough to be part of this group and in addition to being my supervisor; he has been like a father figure. I will always be thankful for that!

To Dr John Timms and all in the members in the lab in the UK, for allowing me to complete a big chunk of the work for this thesis at the Ludwig Institute for Cancer Research, UCL.

To the lab members, present and past: Jacs, Nelusha, Pauline, Luke, Michelle, Kate, Bo, Wei, Dong Ping, Beverly, Kevin, Laja, Maurice and all the honours students. Thanks for always being there, whether it be just to chat or figure out a protocol.

A special thanks to Dr Catherine Whibley and Adrianne Arendse, for support and encouragement in every way!

To the lab members in other laboratories: Ray and Roshan, for allowing me to invade your space! To Ingrid Baumgarten and everyone in the NHLS Chemical Pathology lab at Red Cross.

To the guys in Anatomical Pathology, Nafiesa, Heather, Dr Komala Pillay and Prof Dhiren Govender for teaching and guiding me in the world of IHC.

To Prof Lutz Thilo, for being my unofficial other supervisor. Also, thanks to Dr Virna Leaner, for all the encouraging words of support.

To my Lab family: Haji, Robbie, Lamize, Lee-ann, Graham and Aunty Sia.

And to my family: My parents (Nadeema and Yousuf), for teaching me the importance of my studies and always encouraging me. For supporting me, even if it meant driving me to the lab at 2 am in the morning to complete experiments! To my brother and sister (Yousrie and Rashidah), for always being

the responsible ones and taking care of me! To Amirah and Shamsudeen, for providing me with the unconditional love only kids can give!

To my Limbada parents and siblings: Fatima (thanks for proof-reading!), Ahmed, Aneesa, Faeez and Nailah, for support rendered during the final stages!

To my friends, Ayesha, Nailah, Amaal, Yumna, Tasneem, Fayrous, Fuad, Yazeed and Faizel! Thanks for all your support and lending an ear!

Last but obviously, never least…thanks to my husband…Rashid Limbada, without you, I would never have had the strength…thanks for being my rock, my strength…my life…you can have me back now…and now I can come to your cricket matches again!

Finally, to my Creator, for everything we do in life, our faith is the one thing that never fails!

Table of Contents

Glossary

2D-DIGE - Two dimensional in Difference Gel Electrophoresis
2DE - Two dimensional gel electrophoresis
ADC - Adenocarcinoma of the oesophagus
AML - Acute Myeloid Leukemia
AQUA - Absolute Quantification of Abundance
ATP - Adenosine triphosphate
Beta Gal - beta galactosidase
CA125 - Cancer Antigen 125
CANSA- Cancer Association of South Africa
CBER - Center for Biologics Evaluation and Research
CCB - colloidal coomassie blue
CCR - Center for Cancer Research
CD98 hc - CD98 heavy chain
CHAPS - 3-[(3-Cholamidopropyl)-dimethylammonio]-1-propanesulfonate
CI – Confiidence interval
COFRADIC - Combined FRActional DIagonal Chromatography
dATP - Deoxyadenosine triphosphate
DCA - sodium dichloroacetic acid
dCTP - deoxycytidine triphosphate
dGTP - deoxyguanosine triphosphate
DMEM - Dulbeccos modified Eagles medium
DMF - N,N-dimethylformamide
DNA - deoxyribonucleic acid
dpm - disintegrations per minute
DTT - Dithiothreitol
dTTP - deoxythymidine triphosphate
ECM - extracellular matrix
EC50 – effective concentration at 50%
EDTA - ethylenediaminetetraacetic acid
EGFR-2 - Epidermal growth factor receptor 2
ELISA - Enzyme-Linked ImmunoSorbent Assay
ESI-QUAD-TOF-MS - electron spray ionisation linked to quadropole time of flight mass spectrometry
FBS - fetal bovine serum
FDA - Food and Drug administration
FTICR - Fourier transform ion cyclotron resonance
GAPDH - Glyceraldehyde-3-phosphate dehydrogenase
Gleevec/imatinib mesylate
GT - galactosyl transferase
H_2O - distilled water
HAT complex - Heteromeric Amino acid Transporter complex

Herceptin/trastuzumab
HPLC - High Performance Liquid Chromatography
HPV - Human Papilloma virus
ICAT - Isotope-coded affinity tag
IEF – iso electric focusing
IHC - immunohistochemistry
IPG – immobilized pH gradient
ISO - International Organization for Standardization
IT - Ion trap
iTRAQ - isobaric tag for relative and absolute quantitation
KCl - potassium chloride
kVh – kilo volt hours
KSFM - keratinocyte serum free media
LAT-1 - L-amino acid transporter
LC - liquid chromotography
LCM - Laser capture microdissection
m/z - mass to charge ratio
MALDI-MS - Matrix-assisted laser desorption/ionization mass spectrometry
$MgCl_2$ - magnesium chloride
MS - mass spectrometry
MS/MS/ Tandem MS/ MS^2
MTT - 3-[4,5-dimethylthiazol-2-yl]-2,5-diphenyltetrazolium bromide
MuDPIT - multidimensional protein identification technology
MW - molecular weight
MWM - molecular weight marker
Mylotarg/Gemtuzumab Ozogamicin
NaF - sodium fluoride
Na_3VO_4 - sodium vanadate
NCI - National Cancer Institute
NHS - N-hydroxy succinimidyl
OSCC - Oesophageal Squamous Cell Carcinoma
O/N - overnight
PARP - poly ADP ribose polymerase
PBS - phosphate buffered saline
PDH - pyruvate dehydrogenase
PDK - pyruvate dehydrogenase kinase
PET - Positron emission tomography
PI - propidium iodide
PK2 - Pyruvate kinase M2 isozyme
PMSF - phenylmethanesulphonylfluoride or phenylmethylsulphonyl fluoride
PMT - photomultiplier tube
PNS - post nuclear supernatant
PSA - Prostate Specific Antigen
QUAD - quadrupole

REQUA - Relative Quantification of glycosylated proteins
RNA - ribonucleic acid
ROS - reactive oxygen species
RT - room temperature
SA - South Africa
SDS - sodium dodecyl sulphate
SDS - PAGE - sodium dodecyl sulphate polyacrylamide gel electrophoresis
SELDI-MS - Surface-enhanced laser desorption ionization mass spectrometry
SILAC - Stable Isotope Labeling with Amino acids in Cell culture
TBS - tris buffered saline
TBST - tris buffered saline plus Tween
TOF - time of flight
U - units
UDP - Uridine diphosphate (diphospho)
WB - western blot

1 Overview

1.1 Introduction

Squamous cell carcinoma of the oesophagus is a disease that disproportionately affects certain communities in developing countries (including South Africa) and is associated with a high mortality in these communities. Although various studies have provided a wealth of information describing possible mechanisms involved in the development and progression of cancer so that more effective treatment and diagnostic strategies can be developed, many questions remain. This, in part, reflects the complexity of the processes underlying tumourigenesis, which include genetic predisposition, the tissue involved, specific agents involved, certain chemicals and various other environmental factors. This particular study seeks to identify and characterize some of the proteins that may be involved in oesophageal cancer, since this knowledge may contribute to the development of better diagnostic or therapeutic strategies for this disease.

1.2 Pathology

Oesophageal cancer is classified into two main pathological types based on location and morphology of the tumour. Adenocarcinoma (ADC) occurs in the lower third of the oesophagus including the gastro-oesophageal junction (Fig. 1.1). The second type, oesophageal squamous cell carcinoma (OSCC) occurs in the upper two thirds of the oesophagus (Fig. 1.1). ADC develops in the distal part of the oesophageal epithelium primarily comprising columnar or cuboidal cells (in a glandular epithelium), whereas OSCC arises from stratified squamous epithelia, located more proximally in the oesophagus (Fig. 1.1). There are other important differences between these two cancers. ADC usually occurs in developed countries and is associated with obesity and gastro-oesophageal reflux. The observation that gastro-oesophageal reflux predisposes subjects to the development of ADC facilitates the identification of subjects that are at risk for developing ADC and can thus be used as

part of an early diagnosis program. OSCC usually occurs in developing countries and is a result of a different set of aetiological factors in comparison to ADC. Adequate/effective markers for early identification of OSCC have yet to be developed. Consequently, the early diagnosis of OSCC is not feasible and is generally associated with a high mortality rate, primarily a result of the late clinical presentation of the disease.

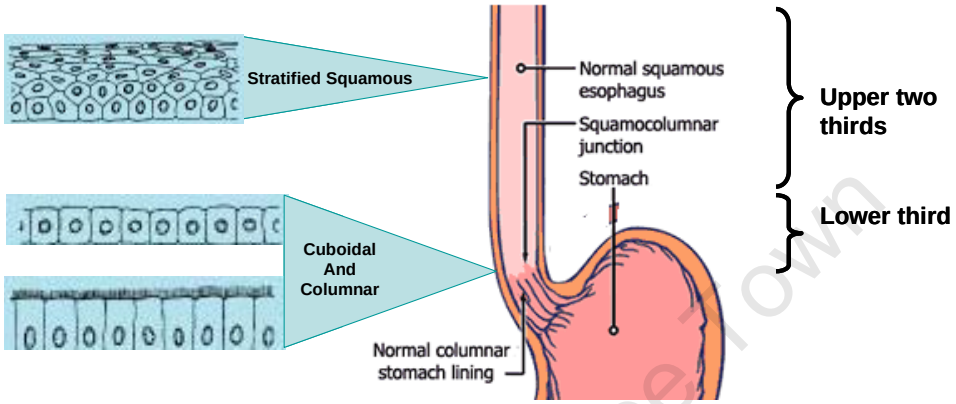

Figure 1.1: Schematic diagram of oesophagus: Upper two thirds of the oesophagus comprises of squamous epithelia and the lower third is made up of cuboidal and columnar epithelia. (Images adapted from (1,2)

The development of OSCC can be distinguished by five stages. Stage 0 is characterized by the presence of intra-epilthelial neoplasia (dysplasia and carcinoma *in situ*) (Fig. 1.2). Stage 1 is typified by the invasion of the tumour into the submucosal layer. Stage 2 can be divided into two categories, where Stage 2A refers to a tumour that has infiltrated the muscle layer of the oesophagus and Stage 2B describes a tumour that has invaded all layers of the oesophagus as well as the lymph nodes.

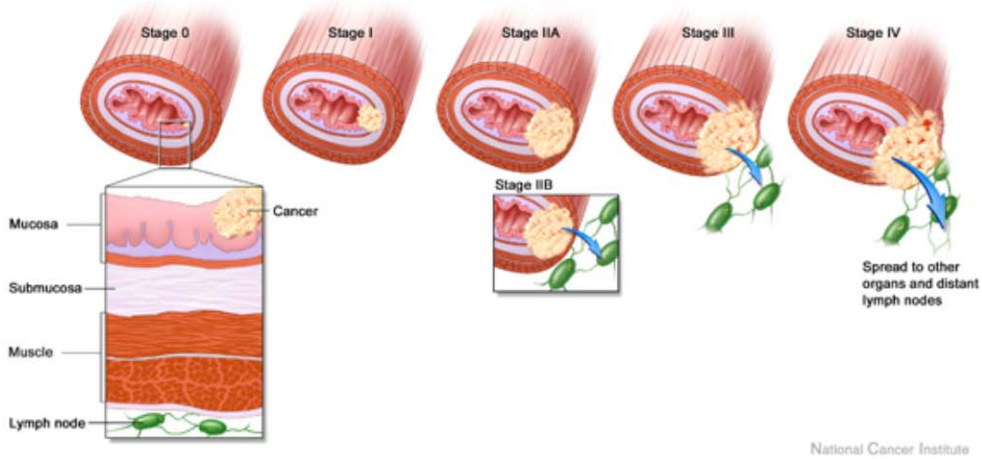

Figure 1.2: Schematic diagram depicting the progression of oesophageal cancer. Stage 0 – intra-epithelial neoplasia; Stage 1 – tumour invasion of the sub-mucosa; Stage 2 – tumour invasion of the muscle layers and lymph nodes; Stages 3 and 4 – tumour metastasis (image reproduced from (3).

Stages 3 and 4 are usually associated with metastasis. Stage 3 tumours have metastasized to proximal tissues and lymph nodes and stage 4 tumours have metastasized to distal organs and lymph nodes (4). Most OSCC patients present with symptoms at stages 2 to 4, which are associated with poor prognosis. This late presentation of the disease contributes to the poor survival rate of patients diagnosed with OSCC.

1.3 Epidemiology

OSCC ranks as the eighth most common cancer in the world, affecting more males than females (Fig. 1.3) (5). It predominantly occurs in developing countries with areas of particularly high incidence localized to the Linxian District in China, parts of Iraq and Iran as well as parts of South America and certain regions in Africa (Fig. 1.4) (6-9).

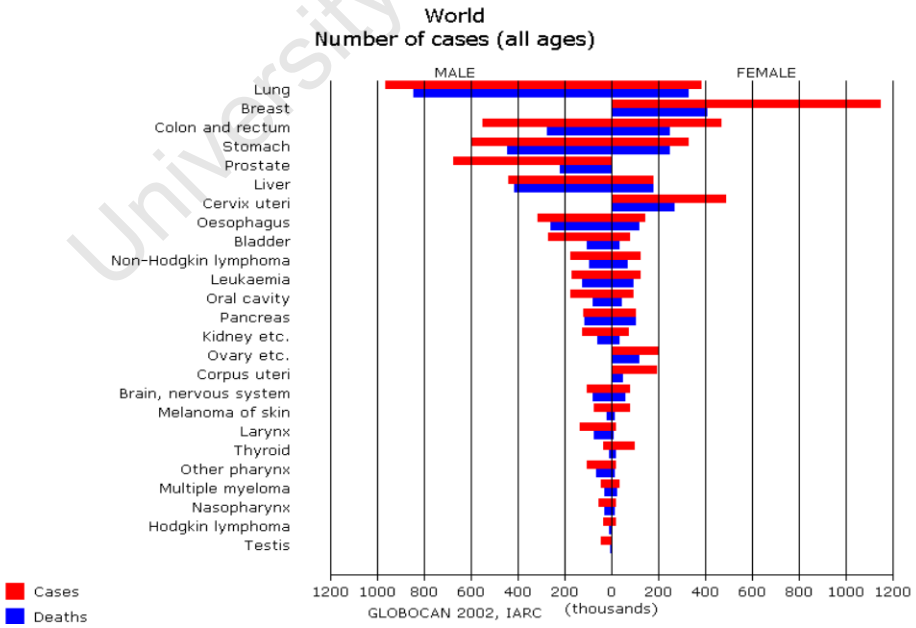

Figure 1.3: Estimated ranking of most common cancers by number of cases (for all ages) in the world for the year 2002, where males are shown on the left and females are on the right (reproduced from Globocan, IARC, 2002) (9)

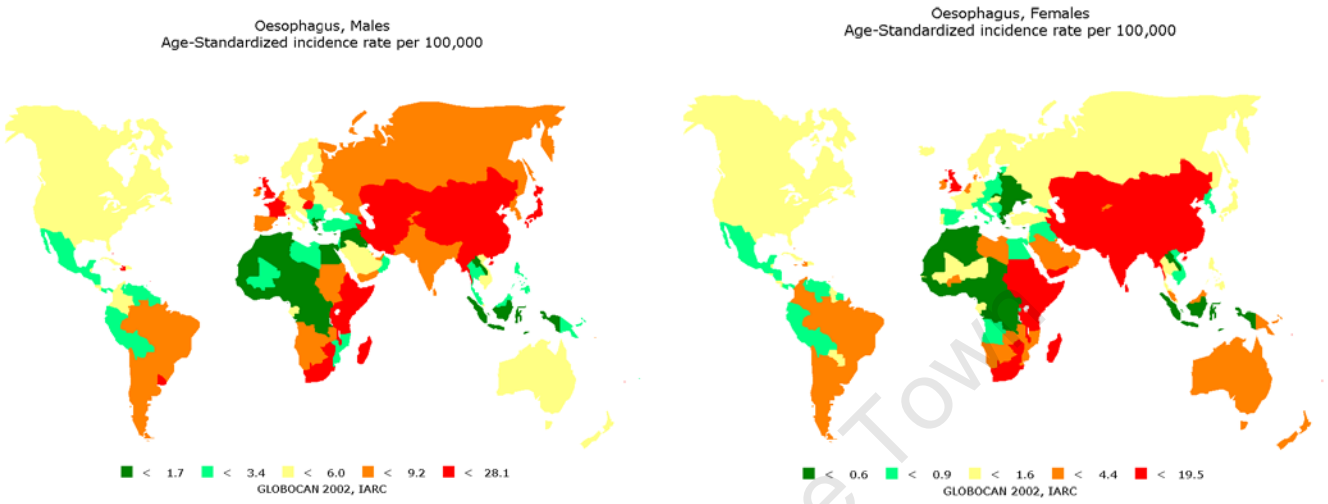

Figure 1.4: World map depicting estimated age standardized incidence rates per 100 000 for oesophageal cancer in (a) males and (b) females for the year 2002 (reproduced from Globocan, IARC, 2002) (9)

In South Africa (SA), OSCC presents a significant health burden, with an age-standardized incidence of 11.3 per 100,000 for males and 5.5 per 100,000 for females (5). The incidence of OSCC ranks third in the South African male population, preceded only by prostate and lung cancer (5). In South African females, the incidence of OSCC ranks as the fourth most common cancer with breast cancer, cervical cancer and colorectal cancer as the three leading cancers (5). Although it has been reported that the risk for developing OSCC has decreased in SA between 1998 and 1999 (5), these reports are yet to be reproduced. The South African National Burden of Disease studies estimates that 1.1% of total deaths in SA in the year 2000 was due to OSCC (Table 1.1) (5,10). The data in Table 1.1 suggests that OSCC is one of the most common causes of cancer-related deaths in SA, emphasizing the high incidence, poor survival rates and public health burden of this disease.

Table 1.1: Ranking causes of death in SA in the year 2000, according to the National Burden of Disease reports (reproduced from (10))

Deaths (Persons)			
Rank	**Cause**	**Total**	**%**
1	HIV/AIDS	132 990	25.5
2	Ischaemic heart disease	34 402	6.6
3	Stroke	33 866	6.5
4	Tubercolosis	28 907	5.5
5	Interpersonal violence	27 563	5.3
6	Lower respiratory infections	22 910	4.4
7	Hypertensive disease	16 648	3.2
8	Diarrhoreal diseases	16 006	3.1
9	Road traffic accidents	15 993	3.1
10	Diabetes Mellitus	13 546	2.6
11	Chronic obstructive pulmonary disease	12 768	2.5
12	Low birth weight	11 597	2.2
13	Asthma	7 006	1.3
14	Trachea/bronchi/lung cancer	6 885	1.3
15	Nephritus/nephrosis	6 760	1.3
16	Septicaemia	6 234	1.2
17	Oesophageal cancer	5 579	1.1
18	Protein/energy malnutrition	5 499	1.1
19	Suicide	5 461	1.0
20	Cirrhosis of liver	5 442	1.0
	Top twenty %		79.8
	All causes	521 082	

1.4 Aetiology

A variety of environmental factors have been associated with the development of OSCC in various parts of the world (11). In the South African population, excessive smoking and alcohol consumption are the leading factors associated with the development of OSCC (5,6,12), although, other factors have also been associated with the development of this disease. These include, HPV infection status, the use of emetics, consumption of fumonisin contaminated maize, home-brewed beers made from fusarium-infected maize and nutritional deficiencies (specifically lack of Vitamin A and C, riboflavin, folic acid and magnesium) (5,11-16). Interestingly, the diets of those in the high incidence areas in SA primarily consists of maize, which contains low levels of niacin, riboflavin, vitamin C, zinc, calcium, folic acid and magnesium (5,17).

Although a number of environmental factors have been implicated in the development of OSCC, worldwide, a few common themes have emerged. These include chronic exposure to smoke, alcohol and other factors, such as drinking hot beverages (5,11,18) (observed in South America and Iran) and the use of emetics in traditional health practices in SA (19), that lead to chronic irritation of the oesophagus. The link between chronic inflammatory processes and cancer has previously been summarized in a review by Coussens *et al* (20).

Even though various environmental factors have been linked to the development of OSCC, the molecular events leading to the development of the disease are, as yet, poorly understood. Investigating the molecular mechanisms involved in the development of OSCC could lead to the identification of molecular events associated with the development of the disease, or identify genes/proteins that maintain tumour progression. Tumourigenesis is underpinned by the dysreglated expression and function of a wide range of genes and proteins that lead to uncontrolled cell growth. Cancer biologists have in recent years gained considerable insight into some of the molecular mechanisms that are responsible for the development of some cancers,

facilitating the design of better diagnostic tools allowing the identification of at risk individuals and also developing cancer therapeutic agents that specifically target irregular cellular processes (21). Although the review by Hanahan and Weinberg (22) is slightly dated, it still provides a particularly clear perspective of the bewildering variety of molecular alterations associated with the development of cancer. It also catergorizes these alterations into distinct classes (or hallmarks), which include self-sufficiency in growth signals, evasion of apoptosis as well as tissue invasion and metastasis, among others. A recent review by Ullah and Aatif (23) further outlines how the development of cancer can be targeted for cancer therapeutic intervention. To illustrate this point, two different cancers (breast cancer or colon cancer) may display alterations in different genes, (Her2/Neu or Ras) with each alteration resulting in self-sufficiency in growth signals in that specific cancer (22). This sort of information has effectively been used to develop a therapeutic agent (Herceptin) for the treatment of those breast cancer patients with elevated levels of Her2/Neu (24-26).

By using a variety of new techniques, cancer biologists are constantly identifying new targets for therapeutic purposes and simultaneously contributing to the molecular understanding of the neoplastic process. Approaches used to explore these molecular alterations include the use of either genomic and/or proteomic techniques.

1.5 Challenges associated with oesophageal cancer

Considering that most patients with OSCC are diagnosed at a late stage, with a 5-year survival rate of 14% (6,11), current treatments are primarily aimed at extending the life expectancy and quality of life of patients (27). In patients with advanced stage OSCC, palliative treatment as opposed to therapeutic intervention is provided (4). Since the present treatment options (which include radiotherapy, surgery and chemotherapy) are not effective in treating late stage OSCC, efforts to

improve the low survival rate associated with OSCC should include either earlier diagnosis or developing better treatment options.

1.6 Approaches to challenges

Developing procedures for the early diagnosis of OSCC (when the disease is more manageable) and/or designing better or more specific drugs, could significantly improve the prognosis for OSCC patients. The identification of biomolecular markers (biomarkers) in the early stages of OSCC would facilitate early diagnosis, thereby improving the prognosis for OSCC patients.

The identification and development of biomarkers (for the early detection of cancer) hold considerable promise for OSCC patients, especially considering that some biomarkers are already used clinically for other cancers. Current biomarkers used for early detection in a clinical setting include, CA125 for ovarian cancer (28-30) and PSA (prostate specific antigen) for prostate cancer (31-33). Despite the high rate of false positives, CA125 serves as a good prognostic indicator for ovarian cancer. CA125 has been clinically useful in determining disease re-occurrence as well as serving as an indicator for post-operative/follow-up surgery (34). PSA is effective in the diagnosis of prostate cancer, but has no prognostic significance (31). PSA has improved the diagnosis of prostate cancer dramatically since its discovery and has paradoxically led to an apparent increase in the incidence of prostate cancer observed, due to its widespread use as a screening tool for prostate cancer (35,36).

Current thinking suggests that the sensitivity and specificity of a diagnostic tool, based on biomarkers, would improve if multiple biomarkers were incorporated in the assay (37). There is clearly a need to identify and characterize potential biomarkers for the early detection of OSCC.

Although early diagnosis is often associated with a better prognosis (38), current treatment options are either very invasive (surgery) or associated with a number of side-effects (chemo-and radiotherapy). The side-effects of chemo- and radiotherapy reflect the method of action of these treatments, i.e. that they often target all rapidly dividing cells. Unfortunately, chemotherapeutic approaches also affect normal rapidly dividing cells, such as those found in hair follicles, bone marrow, and the lining of the gastrointestinal tract. Side-effects experienced during cancer chemotherapy therefore usually include, alopecia (hair loss), myelo-suppression (reduction in activity of the bone marrow), and nausea (39-42). Therefore, in addition to the requirement for the development of a robust panel of specific and sensitive biomarkers for the early detection of OSCC, there is also a need to develop therapeutic agents that selectively target OSCC cells more effectively than current treatment regimes.

In recent years, scientists have been able to identify some of the molecular changes leading to cancer development, enabling them to develop treatments that specifically target abnormal cells. These treatments target only tumour cells and not normal cells and are known as targeted therapies. Various research groups, in collaboration with pharmaceutical companies have (and still are) investing an immense amount of time and money in identifying molecular targets for the purpose of targeted therapy (Genentech Inc, AstraZeneca Int. and Wyeth Pharmaceuticals). Some of the major categories of this new generation of cancer chemotherapeutic agents are monoclonal antibody therapy, small molecule inhibitors and apoptosis inducing drugs (43).

In breast cancer, increased levels of human epidermal growth factor receptor 2 (EGFR-2 or Her-2/Neu) in breast cancer cells compared to normal cells have been exploited through the use of a monoclonal antibody that blocks homodimerization of the receptor by binding to its extracellular domain and subsequently flags the cell for destruction via the immune system (25). This monoclonal antibody therapy, Herceptin ® (made by Genentech Inc.) is already being used in a clinical setting.

Although, this therapy is only available to those patients displaying increased levels of EGFR-2 in their tumours (about 25% of breast cancer patients) (25), results from clinical trials indicate the risk of breast cancer recurrence is decreased by 52% when Herceptin ® is used in conjunction with standard chemotherapeutic agents, compared to the use of standard chemotherapeutic agents on their own (26).

An alternative approach to monoclonal antibody therapy is demonstrated by Gemtuzumab Ozogamicin (Mylotarg® made by Wyeth Pharmaceuticals), which is a calicheamicin-conjugate linked to an antibody to CD33 that selectively targets leukemia cells (44). This selectivity is based on the observation that acute myeloid leukemia (AML) cells have increased levels of CD33 compared to normal hematopoietic stem cells in more than 80% of patients with AML (44-46). Data reflecting its effectivity in decreasing risk of mortality as well as its prognostic significance is yet to be released.

The second type of targeted therapy includes the use of small molecule inhibitors. These have been designed to target surface proteins involved in cell signaling for example. Iressa ® (ZD1839 or gefitinib - AstaZeneca Int.) targets epidermal growth factor receptor (EGFR), which is elevated in many cancers (47-49). Although both Iressa ® and Herceptin ® target EGFR, Iressa ® acts by competing for binding of ATP to the tyrosine kinase domain of EGFR, thereby inhibiting receptor autophosphorylation and resulting in inhibition of signal transduction (50,51). Clinical trial results showed that treatment with Iressa ® alone failed to improve prognosis of patients (51,52).

The third type of targeted therapy involves the use of apoptosis-inducing drugs. One of these therapies includes, Genasense ® (oblimersen - Genta Inc.), which inhibits the production of BCL–2, an anti-apoptotic signal promoting the survival of tumour cells. Some tumours express elevated levels of BCL-2, protecting these abnormal cells from apoptotic signals (53,54). By reducing BCL–2 levels in cells, Genasense ® increases the sensitivity of cancer cells to other conventional anticancer drugs.

Genasense ® is currently in clinical trials for the treatment of leukemia, non-Hodgkin's lymphoma, and solid tumours (55-57).

An underlying theme in recent drug development programmes that involve targeted therapy is the exploitation of proteins that are either overexpressed in cancer cells or that play critical roles in the maintenance of the cancer phenotype. The potential development of these novel therapies require the identification of protein targets like EGFR-2, CD33 or BCL-2 in those cancers that are characterized by poor prognosis, like OSCC.

In OSCC, the identification of a surface protein displaying markedly elevated levels in tumour cells compared to normal in OSCC patients, would be a first step in the development of a targeted therapy approach. This study aims to address this issue by identifying and characterising altered surface protein levels in tumour cells compared to normal cells in OSCC using two proteomic approaches.

1.7 Rationale for proteomic approach

Current approaches to cancer therapeutics have in recent years been informed by novel findings in biomedical science, and our increased understanding of the molecular events occurring during the process of tumourigenesis. Methods have been developed that allow parallel examination of expression of genes or proteins (genomics and proteomics), enabling the determination of differential gene/protein expression. The differences in gene/protein expression between normal and cancer cells could facilitate the identification of molecules important in cancer development, which could conceivably serve as targets for the development of novel agents.

Genomic methods for identifying potential therapeutic targets include differential gene profiling by subtractive hybridization, serial analysis of gene expression (SAGE), differential display reverse transcription polymerase chain reaction *(*DDRT-PCR*)* and micro-array technologies (58-60). These

technologies have contributed to the identification of a number of diagnostic markers that are involved in cell signaling and are also potential targets for developing cancer therapeutics (60,61).

Using SAGE, researchers identified mesothelin (a protein normally expressed on the surface of certain cell types) as an overexpressed protein in pancreatic tumour tissue compared to normal cells (62). Other cancers characterized by very high surface mesothelin expression include mesothelioma and ovarian carcinoma (63). This protein has been identified as a target for cancer therapy and an immunotoxin to mesothelin, SS1(dsFv)-PE38 (SS1P), is in phase 1 clinical trials (Clinical trial identifier: NCT00024687).

In recent years micro-array analysis have been used more often as the technology became more accessible and amenable to high throughput processing (60). Micro-array technology has led to the development of a 21-gene array to select appropriate treatments for a subset of breast cancer patients (64-67). This multi-gene array is currently used as a test to predict distant recurrence in ER-positive (estrogen receptor positive) breast cancer patients. The cost of these tests are relatively high, but it has been suggested that the potential saving in selecting the correct treatment would outweigh this initial expense (68).

The sequencing of the human genome has enabled a revolution in identifying genes that display altered expression in tumour compared to normal tissue. However, considering that less than 35 000 genes code for more than 500 000 proteins, the human proteome also provides a substantial amount of information that can be mined to identify differences in expression (69).

1.8 Proteomic tools used for separation of proteins

Methods used in quantitative proteomics rely on the fact that the same protein, obtained from different complex samples (e.g. tumour and cancer), would separate in a similar manner, thereby allowing comparative expression analysis. Sample complexity is an important factor to consider when

choosing a method of protein separation. The reduction of sample complexity can be achieved in a variety of ways. In plasma samples, highly abundant proteins (such as albumin and immunoglobulins) should be removed to focus on separating and identifying lower abundance proteins. In protein samples obtained from cultured cells, sample complexity can be reduced by fractionation methods that allow one to analyze proteins from various compartments within the cell (membrane, nucleus or cytoplasm). Sample complexity can also be reduced by isolating proteins on the basis of their post-translational modifications, such as glycosylation (as will be discussed later) or amino acid composition (targeting cysteine containing peptides).

Laser Capture Micro-dissection (LCM) can also be used to isolate cells of interest and excludes contaminating proteins from surrounding tissue (70). Unfortunately, LCM is often not easily accessible and generally expensive and time-consuming. Essentially, reducing sample complexity would facilitate better protein separation.

The primary aim of the separation step is to separate proteins by virtue of their size, charge or hydrophobicity or a combination of these. Protein separation can be achieved either by gel-free or gel-based methods (Fig. 1.5).

Gel-free methods include methods such as MudPIT - Multidimensional Protein Identification Technology- (71), ICAT - Isotope-Coded Affinity Tags - (72), iTRAQ - Isobaric tags for relative and absolute quantitation - (73) and SILAC - Stable Isotope Labelling by Amino acids in Cell culture - (74,75). The latter mentioned methods all involve differentially labelling samples either at cell/tissue, protein or peptide level, digesting the sample (where required), separation on the basis of its ionic status and subjected to MS. Other gel-free methods include SELDI-MS (Surface Enhanced Laser Desorption Ionization Mass Spectrometry) and protein arrays.

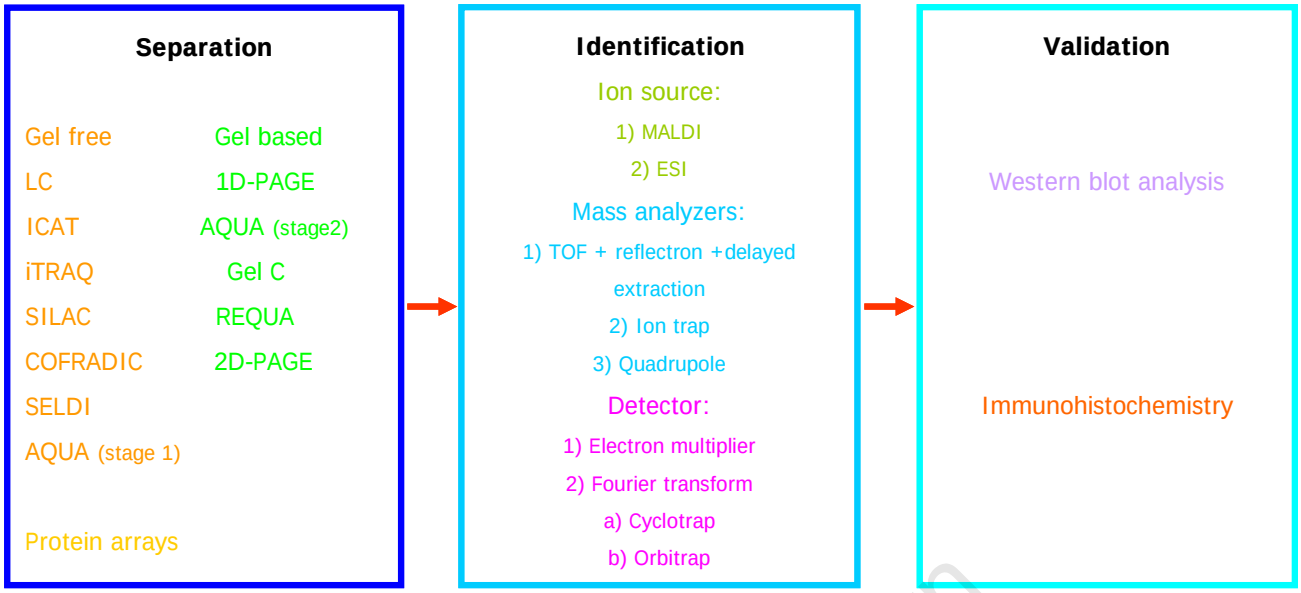

Figure 1.5: Schematic diagram illustrating the basic workflow of a quantitative proteomic approach, which includes three main phases; separation, identification and validation. Separation techniques include either gel-free or gel based methods. Identification can be achieved using a combination of different ion sources, mass analyzers and detectors. Validation is considered a critical step in the workflow.

Principally, all gel-free based separation methods allow the separation of peptides either by virtue of its size, charge or hydrophobicity. In the case of MudPIT, peptides are first separated by nature of their charge, using a strong cation exchange and followed by separation by nature of their hydrophobicity, using reverse phase chromatography. The latter is linked directly to an ion source and peptides are subjected to MS analysis. Both ICAT and iTRAQ involve labelling peptides with isotope-labelled reagents. In ICAT peptides are labelled at their cysteine residues, whereas iTRAQ involves labelling the N-terminus of peptides. Both ICAT and iTRAQ labelling methods occur after protein digestion, as opposed to SILAC, in which isotope labelling occurs in vivo. SILAC relies on the incorporation of amino acids with substituted stable isotopic nuclei (74).

These methods have contributed to the rapid evolution of proteomic technologies. However, there are a few disadvantages associated with the use of these high-throughput methods that should be highlighted.

Although, MudPIT is a high throughput method that can be utilized for complex protein mixtures, it is not able to detect any modifications to proteins in complex mixtures. MudPIT also yields a substantial amount of MS data, however, special programmes and algorithms have been developed to cope with the immense amount of spectra produced from this method (76,77).

Even ICAT is limited by the fact that it does not account for those proteins that have little or no cysteine residues. Furthermore, like MudPIT, ICAT does not facilitate the observation of changes in post-translational modifications.

iTRAQ, on the other hand, is considered to be more sensitive than ICAT labelling, as more peptides per protein are identified resulting in better statistics (78). Unfortunately, iTRAQ is very expensive in comparison to other methods.

ICAT and iTRAQ use chemical labelling methods that require the two proteomes being analyzed to be purified and fractionated, separately. The drawback is that the purification and fractionation steps, from the two separate proteomes, needs to be exactly the same in order to facilitate relative quantification. SILAC, however, is a metabolic labelling method that allows purification and fractionation of mixed populations allowing a more accurate quantification, as minimal errors could be introduced. SILAC displays a high degree of labelling, quantitation is simple and it is a relatively inexpensive method. The disadvantages of SILAC, however, include that one can only label cells in culture and that in some instances cells do no respond well to the media used during labelling (75).

Various software packages have been developed to cope with the enormous amounts of information generated from these gel-free techniques. Despite the disadvantages associated with the above high-throughput proteomic tools, they offer the opportunity to reveal a number of potential targets for cancer therapeutic intervention (69,79). More recently, the drive towards proteomic based profiling of diseases has sparked an interest in clinical proteomics. A gel-free separation approach that recently

attracted attention is SELDI-MS (Surface-enhanced laser desorption/ionization linked to mass spectrometry) (80). This approach involves separating proteins using various chromatographic surfaces with different chemical characteristics (hydrophobic, cationic, anionic, metal presenting or hydrophilic). This high-throughput technology was earmarked as the technique to identify potential biomarkers of disease from serum, urine or other clinical samples, (80-82).

Protein arrays are another example of a gel-free based method that would be ideal in a clinical setting as it can be likened to an ELISA assay. The overall concept is more like a micro-array. Protein arrays are both quantitative and qualitative and allow complex analyses in one operation. Protein arrays are very expensive and high risk. Furthermore, this technique also only allows for the identification of known proteins and is suitable for analyzing treatment effects over populations of samples, but is not well suited to assess individual patients (83,84). Proteomic techniques are rapidly advancing and other gel-free methods that are either novel or developed from current proteomic methods have entered the market (85-92). Generally, gel-free methods of separation mainly out-compete gel-based methods when a high-throughput technique is required.

Gel-based methods of separation should not be discounted though, considering that various laboratories have generated valuable information using these methods (70,93,94).

Gel-based methods of separation can be divided into 1-dimensional gel electrophoresis or 2-dimensional gel electrophoresis. 1-dimensional gel electrophoresis allows the separation of proteins by virtue of its size. Although this approach is not popular, it is used in the first stage of AQUA (92), GelC (95) and REQUA (Relative quantification of glycosylated proteins) (96-98), which will be described in detail later.

The most commonly utilized gel-based method is 2DE and conceptually involves the separation of protein mixtures by virtue of their charge and size (99). However, there are a number of problems

associated with this approach that include the poor detection of some proteins (mainly low abundance proteins, highly charged proteins and hydrophobic proteins), imperfect separation, reproducibility and lack of automation (78).

Recently an advance in 2DE technology, where protein samples are separately labelled with different fluorescent dyes, combined and separated on the same 2 dimensional gel was developed and termed 2D-DIGE (two-dimensional difference gel electrophoresis) (100). Although this method does not address the separation of low-abundant, highly charged or hydrophobic proteins, it does allow increased reproducibility and sensitivity to allow better quantification. Furthermore, the software and scanning methods allow automated detection of proteins of interest that are highlighted for identification. This approach was selected as one of the separation techniques used in this project.

1.9 Proteomic tools used for identification of proteins

The rapid advance in proteomic technologies has led to the development of various software packages and databases to facilitate the identification of proteins of interest. The proteomic tools used for the identification of proteins can be divided into the ion source, the mass analyzer and the detector (Fig. 1.5). The ion source can either be electron spray ionization (ESI) or the protein/peptide target can be immobilized on a matrix via matrix assisted laser desorption ionization (MALDI). Typically LC-based separation methods are directly linked to ESI in order to achieve a higher sensitivity. The disadvantage of ESI though is that once the sample has been sprayed/nebulized, a large volume is lost as a result of evaporation. Conversely, MALDI allows immobilization of the target protein/peptide, facilitating multiple ionizations of the same target.

The resolution and added sensitivity of identification is nonetheless dependant on the mass analyzer. Mass analyzers are either based on the time of flight (TOF) that the ionized peptide takes to travel a set distance within a vacuum, or by trapping ions in an oscillating electrical field (Ion trap-IT) or by

filtering ions using 4 rods, which utilize a combined alternate and direct current, based on the ionization status (quadrupole). The resolution of the TOF mass analyzer can further be improved with the addition of a reflectron and delayed extraction of the ions. In addition, by having two mass analyzers in tandem, where the first would serve as a collision cell and the second would be the mass analyzer, one would increase the sensitivity level of identification. Tandem MS (aka MS/MS and MS^2) facilitates the identification of a protein at an amino acid level.

These mass analyzers are in turn connected to a detector that amplifies and digitizes the signal. The most common type is the electron multiplier tubes, nevertheless, the more expensive, yet more sophisticated, is the Fourier transform ion cyclotron resonance detector (FTICR). The latter detector is based on, as the name suggests, Fourier transform technology. Briefly, it is a type of particle accelerator in which electrons are captured in orbits by an exceptionally strong magnetic field, whilst acceleration is facilitated by an applied voltage. This technology is currently utilized in only a handful of laboratories around the world.

In spite of this, a recent technological advance yielded the Orbitrap. The Orbitrap is a much cheaper system that yields nearly the same efficacy as that of the FTICR. It generates an electrostatic field using one electrode within another that allows the ions to oscillate along the axis of the tubes. Similarly to FTICR, Orbitrap also utilizes Fourier transform technology to clarify individual frequencies that are related to the *m/z* (mass/ charge) ratio.

Various combinations of each part of the mass spectrometer result in machines of varying speeds, sensitivities and resolutions in identifying proteins of interest. The combination of choice relies on availability of instruments. Regardless of the combination of choice used to identify the proteins, it is imperative to validate the expression level of the protein of interest using an alternative method.

1.10 Protein validation

It is important to validate the information produced from the previous techniques before further work is carried out. The methods of validation most frequently used are western blot analysis and immunohistochemical analyses (of frozen tissue or archived paraffin blocks of tissue).

Western blot (WB) involves confirming the expression levels of a protein of interest observed from the same protein sample used in the first stage of the proteomic approach. Multiple samples can be analyzed using this approach, to determine reproducibility. This method has the advantage in that multiple proteins can quantitatively be analyzed in a simple and effective manner. However, western blot does also not allow one to visualize the sub-cellular localization of proteins.

Immunohistochemistry (IHC) allows both quantitation and visualization of sub-cellular localization of the proteins of interest. This approach requires careful selection of antibodies to minimize non-specific reactions and the assistance of pathologists to interpret the stained sections accurately. Identifying and validating altered levels of proteins in tumour compared to normal is the first step towards identifying potential diagnostic markers or targets for cancer therapeutic intervention.

1.11 Objectives of this study

Our laboratory has previously embarked on identifying genes that are differentially expressed in tumour tissue compared to normal tissue in oesophageal cancer, using differential display and micro-array technology. A subset of genes identified are currently being further investigated as potential early biomarkers for oesophageal cancer (101).

Genomics and proteomics complement one another and in this context, we developed this project to determine the proteomic profile of tumour tissue compared to normal tissue, from OSCC patients, with the primary focus on identifying potential therapeutic targets (given that most drug targets are proteins) (102). Furthermore, current therapeutic approaches do not effectively target tumour cells as opposed to normal cells in OSCC. This has created the demand to identify proteins on the surface of

the cell that displays increased levels in tumour cells compared to normal cells that could potentially serve as targets for cancer therapeutic intervention.

In this study, we used a combination of proteomic approaches to address our objectives, which include:

Objective 1

To identify plasma membrane proteins that display altered levels in tumour cells compared to normal in OSCC using two different approaches. In the first approach, we intend on using proteins extracted from tumour and corresponding normal tissue. In the second approach, we intend on using proteins extracted from oesophageal cancer cell lines and an immortalized normal oesophageal cell line.

Objective 2

To validate the altered levels displayed by proteins' of interest in OSCC by using a method that allows visualisation of the sub-cellular localisation of the proteins of interest.

Objective 3

To determine the value of altered protein levels as markers for OSCC or as targets for therapeutic intervention.

2 2D-DIGE analysis of tumour tissue compared to normal tissue

2.1 Introduction

The most commonly utilised application in proteomics is two-dimensional gel electrophoresis (2DE), for separation of proteins, coupled with mass spectrometry (MS) for the identification of proteins. More recently, two-dimensional difference gel electrophoresis (2D-DIGE) has been applied for the

separation and accurate quantitation of protein for differential expression profiling of multiple biological samples. 2D-DIGE avoids the variation associated with conventional 2DE by pre-electrophoretic covalent labelling of proteins with different fluorescent tags, allowing three different samples to be compared on a single gel (103). This innovation substantially simplifies the comparison and analysis of paired samples (normal and tumour tissue for example), since the comparison takes place within the same gel. Furthermore, by using one of the tags to label an internal standard, spot matching across gels and accuracy of quantitation can be improved. 2D-DIGE has previously been used to identify proteins that are differentially expressed in tumour compared to normal cells in cancer of the breast (104), oesophagus (70,105), pancreas (106), colon (107) and liver (108), using whole cell protein lysates.

The aim of this study was to identify differentially expressed proteins in the cell membrane and cytoplasmic fractions of tumour tissue compared to normal tissue from oesophageal cancer patients.

2.2 Materials and methods

2.2.1 Tissue procurement

This study was approved by the Ethics Committee at the University of Cape Town (Reference: 146/2004). Oesophageal tumour and adjacent normal tissue was obtained by informed consent from

44 oesophageal cancer patients who had undergone oesophageal biopsies at Groote Schuur and Tygerberg Hospitals in Cape Town, South Africa. Health personnel administered the consent forms and patient confidentiality was strictly maintained throughout. Tumour samples were only used for the study if greater than 90% of the tissue was identified as neoplastic by the attending pathologist. Normal oesophageal epithelium distant from the tumour biopsies were used after it had been determined that these samples were free of tumour tissue. The tissue samples were frozen in liquid nitrogen and stored at -70°C until further use.

2.2.2 Preparation of samples

Tissue from oesophageal tumour biopsies were pooled, and, normal tissue from the corresponding patients were pooled. Pooling took place prior to protein preparation, to give separate tumour tissue and normal tissue pools. Membrane and cytoplasmic fractions were isolated from the pooled tissue biopsies, using published methods (109). Briefly, the tissue was homogenized in ice-cold HEPES buffer (10mM HEPES, 1 mM EDTA, pH 7.4) using an Ultra Turrax homogenizer (Janke and Kunkel, Switzerland). The homogenate was subjected to differential centrifugation in order to collect a crude membrane fraction and a cytoplasmic fraction. The homogenate was centrifuged for 10 minutes at 500Xg in a Sigma 302K (Sigma-Aldrich, St Louis, USA) at 4°C, in order to remove large debris. Subsequently, the supernatant was centrifuged for 75 min at 180, 000Xg at 4°C in a Beckman SW 40 Ti (Beckman Coulter Inc, Calif). The pelleted membrane fractions were re-suspended and stored in 50 µL HEPES buffer containing a cocktail of protease inhibitors (*cOmplete*, Roche) (see appendix A), whereas cytoplasmic fractions were lyophilised. All fractions were stored at -70ºC, until further use. Unfortunately, no method was used to determine the effectiveness of the membrane and cytosolic fractionation. Pooled crude membrane fractions were re-suspended in HEPES buffer and centrifuged at 100,000 X g for 20 minutes at 4°C using a TLA-110 rotor in a Beckman Optima Ultracentrifuge (Beckman Coulter Inc, Calif) to pellet the membrane proteins. Membrane proteins

were solubilized in 400 µL of 2D lysis buffer (8M urea, 2M thiourea, 4% (w/v) CHAPS, 0.5% (w/v) NP-40, 10mM Tris-HCl pH 8.3). Lyophilised cytoplasmic protein fractions were re-suspended in 500 µL of 2D lysis buffer. All samples were subsequently centrifuged at 13,000 X g in a benchtop centrifuge for 15 minutes, to pellet debris. Protein concentrations were determined using the Coomassie Plus Protein Assay Reagent (Pierce, USA) using BSA (bovine serum albumin) as a standard.

2.2.3 Protein labeling, separation and gel imaging

Protein lysates were fluorescently labelled with *N*-hydroxy succinimidyl (NHS) ester-derivatives of the cyanine dyes Cy2, Cy3 and Cy5 as previously described (110) . Briefly, 75µg of protein from the membrane fraction or 150 µg of protein from the cytoplasmic fraction were minimally labelled with 4 pmol of dye per µg protein with either NHS-Cy3 or NHS-Cy5 (Table 2.1) for 30 min on ice in the dark, in as small a volume as possible. Reactions were quenched with a 20-fold molar excess of free lysine to dye for 10 min on ice. DTT was added to 65mM and the samples mixed appropriately (Cy3 + Cy5). The volume was made up for IPG strip rehydration (450 uL for 24 cm strips) to a final concentration of 65mM DTT (Dithiothreitol), 2% ampholytes/pharamalytes and bromophenol blue (Appendix A).

In parallel, equal amounts of protein from both normal and tumour were pooled and minimally labelled with Cy2, to serve as an internal standard (Table 2.1). Samples are thereby in-gel linked to a common standard, giving accurate quantitation and separating gel-to-gel variation from inherent biological variation (Fig. 2.1).

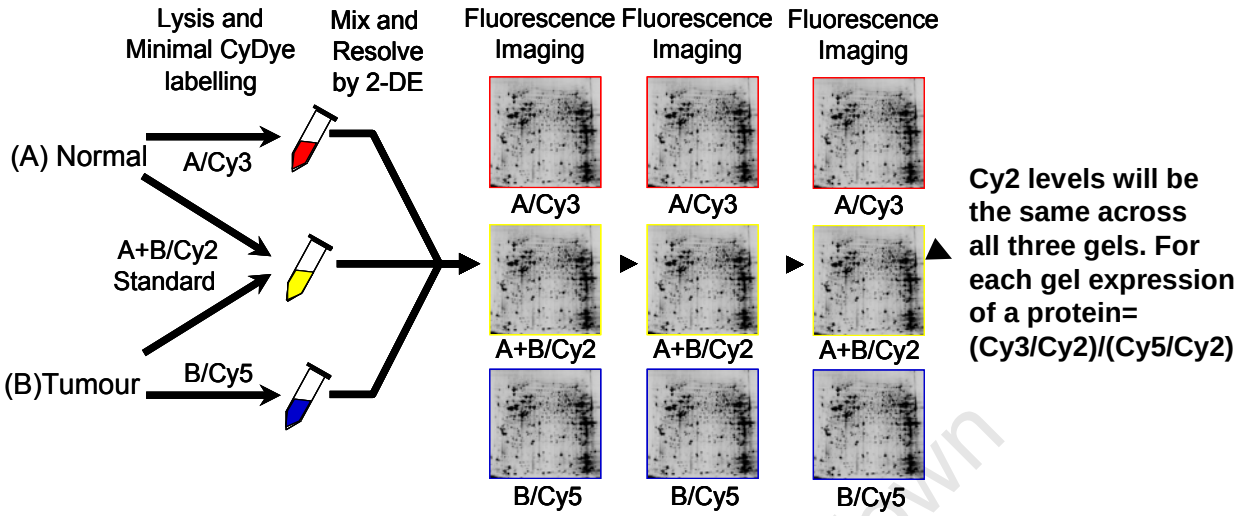

Figure 2.1: Protein labelling protocol. Proteins from normal and tumour lysates were fluorescently labelled with either Cy3 or Cy5. Equal amounts of protein lysates from normal and tumour origin were pooled and labelled with Cy2. This served as an internal control to minimize gel to gel variation. Relative protein abundance in tumour compared to normal was calculated as indicated (images courtesy of John Timms, Ludwig Institute for Cancer Research, University College of London).

Table 2.1: Amount of labelled proteins separated on analytical gels. In gels 1-3, membrane protein preparations (denoted by ^{m}) were separated on triplicate gels, where N indicates protein from normal tissue and T indicates protein from tumour tissue. Proteins from normal and tumour tissue were reciprocally labelled in gel 2. In gels 4 - 7, cytoplasmic protein preparations (denoted by ^{s}) were separated on quadruplicate gels, where N indicates protein from normal tissue and T indicates protein from tumour tissue. Proteins from normal and tumour tissue were reciprocally labelled in gels 5 and 7. In parallel, equal amounts of protein from both normal and tumour were pooled and minimally labelled with Cy2, to serve as an internal standard.

Gel number	Cy3	Cy5	Cy2 (internal standard)
1	75 µg N^m	75 µg T^m	37.5 µg N^m and 37.5 µg T^m
2	75 µg T^m	75 µg N^m	37.5 µg N^m and 37.5 µg T^m
3	75 µg N^m	75 µg T^m	37.5 µg N^m and 37.5 µg T^m
4	150 µg N^s	150 µg T^s	75 µg N^s and 75 µg T^s
5	150 µg T^s	150 µg N^s	75 µg N^s and 75 µg T^s
6	150 µg N^s	150 µg T^s	75 µg N^s and 75 µg T^s
7	150 µg T^s	150 µg N^s	75 µg N^s and 75 µg T^s

Protein separation was carried out using methods previously described (110), with minor modifications. Protein separation was carried out in a clean room ISO (International Organization for Standardization) class 6, reserved for protein handling, to minimize any contaminating proteins or fibres. IPG strips (pH range: 3 – 10, 24 cm) (GE Healthcare, United Kingdom) were run on a Multiphor II electrophoresis unit (GE Healthcare, United Kingdom) for a total of 77 kVh at 17°C, to separate proteins on the basis of their iso-electric points. Equilibrated IPG strips were transferred onto 12.5% polyacrylamide gels poured between low-fluorescence glass plates. Gels were bonded to the inner plate using bind-saline solution (PlusOne, GE Healthcare, United Kingdom). IPG strips in the polyacrylamide gels were overlaid with 0.5% (w/v) low melting point agarose in 1X SDS electrophoresis buffer (Severn Biotech, United Kingdom) containing bromophenol blue. Gels were run in an Ettan DALT *twelve* electrophoresis unit (GE Healthcare, United Kingdom) at 2.8 Watts per gel until the dye front had run off the bottom. 2D gels were scanned between the plates directly after electrophoresis using a Typhoon 9400 multi-wavelength fluorescence imager and ImageQuant software (GE Healthcare, United Kingdom). Images were acquired using the optimal excitation/emission wavelengths for each fluorescent dye i.e. 488/520 nm for Cy2, 532/580 nm for Cy3 and 633/680 nm for Cy5. Low resolution scans (1000 µm) were first taken to optimise

photomultiplier tube (PMT) voltages to give maximum pixel values to within 10% for each Cy channel and below the saturation threshold of the imager. Final scans were performed at 100 µm resolution.

2.2.4 Image analysis, post-staining, spot picking and digestion

Images were analysed using DeCyder software v5.0 (GE Healthcare, United Kingdom) as previously described (110). Features matching on all images displaying ≥2.0 -fold average increase or≤ -2.0-fold average decrease in abundance in cancer versus normal and with *P*-values ≤0.05 (Student T-test) were selected for excision and MS analysis. To visualise separated proteins, the same gels were post-stained with colloidal Coomassie Brilliant Blue (CCB) G-250 using a modified version of the protocol by Neuhoff *et al.* (111,112). Briefly, gels were fixed in fixing solution from 3 hours to overnight followed by three 30 min washes with distilled water. Staining solution was added and gels were left placed on shaker for 1 hour at room temperature. An amount of 0.5 g/L crushed solid Coomassie Blue G-250 was added to the gel in staining solution and placed on a shaker for up to 3 days at room temperature. Gels were then rinsed in distilled water and scanned on the Typhoon 9400 imager using the red laser (633 nm) and no emission filter. CCB images were then matched with the corresponding Cy dye images using DeCyder software and a pick list of coordinates generated for excision using an Ettan automated spot picker (GE Healthcare, United Kingdom). For illustration purposes, images were also pseudo-coloured and superimposed using Adobe PhotoShop (Adobe Systems Inc., California). Excised protein spots from the post-stained gel were in-gel digested with modified trypsin (Promega, USA) and peptides extracted for MS analysis as previously described (103).

2.2.5 MALDI-TOF MS peptide mass fingerprinting

Peptide extracts (0.5 µL) were spotted onto a MALDI target with 1 µL of matrix solution (saturated aqueous 2,5-dihydroxybenzoic acid). Matrix-assisted laser-desorption/ionisation time-of-flight (MALDI-

TOF) MS was performed using an externally calibrated Ultraflex TOF/TOF mass spectrometer (Bruker Daltonics) in the reflector mode. External calibration was achieved by using commercially available Cal Mix standards (Applied Biosystems, United Kingdom) (details outlined in appendix A). The standards were spotted adjacent to sample on each plate used. After internal calibration using trypsin autolysis peaks, prominent peaks in the mass range m/z 500-5000 were used to generate a peptide mass fingerprint. Common contaminating peaks in all samples were excluded using the in-house software 'CommonContam' (Developed by Dr Richard Jacobs, Ludwig Institute, UCL, London). Mass fingerprints were then searched against the updated IPI database using Mascot version 2.0.02 (Matrix Sciences). Identifications were accepted when a minimum of 6 peptide masses matched a particular protein (mass error of ±50 ppm allowing 1 missed cleavage), sequence coverage was >25%, MOWSE scores were higher than the threshold value (P=0.05), the predicted protein mass and pI agreed with the gel-based mass and pI and the proteins identified were human.

2.2.6 Immunohistochemistry (IHC)

Archived paraffin-embedded sections of tumour and normal tissue from up to 18 oesophageal cancer patients were used in order to confirm expression of a subset of proteins. Slides were heat-fixed for 10 min on a heating block at 70 °C, de-paraffinised and rehydrated, followed by antigen retrieval by incubating slides in 10 mM sodium citrate buffer (pH 6) in a pressure cooker for 5 min. Sections were blocked for endogenous peroxidase activity by submerging the slides in 3% hydrogen peroxide for 20 min. The slides were then incubated at room temperature with a 1/20 dilution of goat serum (Dako, California) for 30 minutes. Antibodies to annexin 2 (rabbit polyclonal) and GP96/HSP90B1 (goat polyclonal) (Santa Cruz Biotechnologies, Inc., California) were used at a dilution of 1/250 and 1/500, respectively. The monoclonal mouse antibody to gelsolin (clone GS-2C4, Sigma-Aldrich, St Louis, USA) was used at a dilution of 1/1000. The LSAB-2 detection system (DAKO, California) was used

according to the manufacturer's instructions to detect the rabbit and mouse antibodies to annexin 2 and Gelsolin. In the case of the goat antibody, a 1/600 dilution of biotinylated rabbit anti-goat immunoglobulins (DAKO, California) was used.

Monoclonal mouse antibodies to glyceraldehyde-3-phosphate dehydrogenase (GAPDH) and pyruvate kinase were used at a dilution of 1/400 and 1/100, respectively. Furthermore, the antigen retrieval method for the antibodies to GAPDH and pyruvate kinase involved incubating slides in 10 mM sodium citrate (pH 6) at sub-boiling point for 10 min. Also, the Envision Pollyalomer-HRP detection system (Dako, California) was used, according to manufacturer's instructions, for the latter two mentioned antibodies as opposed to the LSAB-2 system.

Omission of the primary antibody served as a negative control in each case. Sections were counterstained with haemotoxylin and subsequently dehydrated. The slides were independently evaluated by a qualified pathologist.

2.2.7 Statistical evaluations and survival test

In order to determine if there is an association between annexin 2 expression and patient survival, 59 archived paraffin-embedded sections (Table A4 in Appendix A) of tumour tissue were stained for annexin 2, as described above. The statistical power of the study was calculated using published methods (113).

The slides were independently evaluated by a qualified pathologist and annexin 2 staining in tumour tissue was scored as indicated in Table 2.2.

Table 2.2: Criteria used by independent pathologist for scoring IHC slides. Slides were assigned a score of 0 to 4+ based on the percentage membrane staining observed in tissue section.

Intensity	Percentage membrane staining in field of view
0	less than 5% stained
1+	between 5 and 25% stained
2+	between 26 and 50% stained
3+	between 51 and 75% stained
4+	more than 75% stained

The Kaplan Meier Survival test was applied to the data, using STATA™ (version 8) (Stata Corporation, USA). The power of the sample size used in this study was calculated using the PS program (version 2.1.31).

2.3 Results

2.3.1 Protein quantitation and labeling

As described in Materials and Methods, tissue from oesophageal tumour biopsies were pooled and similarly normal tissue, from the corresponding patients, were pooled prior to protein preparation, to yield a separate tumour tissue pool and a normal tissue pool. Tissue samples were pooled since biopsy sample were very small (most were approximately 0.07g in size) (Table 2.3). Subsequently membrane and cytoplasmic protein preparations were prepared and quantitated (Table 2.3).

Table 2.3: Quantitation of protein fractions. Biopsies from normal and tumour tissue pools were weighed, prior to processing into membrane and cytoplasmic fractions. The corresponding protein preparations were subsequently quantitated and fractions from tumour biopsies were diluted to their equivalent counterparts as outlined in Table 2.1.

Pool	Normal (pool of 44 patients)		Tumour (pool of 44 patients)	
Mass (g)	3.14		3.07	
Fraction	membrane	soluble	membrane	soluble
Concentration (µg/µl)	0.885	0.855	2.163	1.183

Although, the amount of tumour and normal biopsies were similar, the yield from the tumour biopsies was higher. Nevertheless, protein fractions from tumour biopsies were diluted to the same concentration as their normal counterparts, labelled and separated, as previously outlined (Table 2.1).

2.3.2 2D-DIGE and MS protein expression profiling

2D-DIGE analysis was used to examine changes in protein expression in pooled biopsy samples of primary oesophageal tumours and adjacent normal oesophageal tissue with the aim of identifying potential biomarkers or therapeutic targets for oesophageal cancer. In order to improve proteomic coverage, samples were fractionated into crude membrane and cytoplasmic fractions by ultracentrifugation. Separation of proteins on large format 2D-gels allowed the resolution of ~2500 Cy dye-labelled protein features in the crude membrane preparations (Fig. 2.2). Fluorescent images of differentially labelled (Cy3 and Cy5) proteins from normal and tumour membrane fraction were compared with a Cy2-labelled internal standard using the DeCyder image analysis software allowing accurate quantitation and separating gel-to-gel variation from tumour versus normal variation. 150 significantly differentially expressed protein features were selected ($P \leq 0.05$) using a filtering threshold

of 2.0-fold up- or down-regulation (Fig. 2.3a). Post-staining of gels with CCB (Fig. 2.3b), however, allowed matching of only 71 of these features with the fluorescently-labelled features, suggesting that the expression levels of the other 79 features were too low for CCB detection and most likely, for successful MS-based identification. Similarly, ~3000 Cy dye-labelled features were identified from gels on which the proteins from the cytoplasmic fraction were resolved (Fig. 2.4). Fluorescent images of differentially labelled cytoplasmic proteins from normal and tumour samples were compared and 55 protein features were shown to be significantly differentially expressed ($P \leq 0.05$) when filtering using a 2.0-fold threshold (Fig. 2.5a). CCB post-staining (Fig. 2.5b) allowed detection of only 32 of these features, again reflecting low protein levels in some gel spots. The matched protein spots were subsequently picked, digested with trypsin and subjected to MALDI-TOF MS peptide mass fingerprinting for identification.

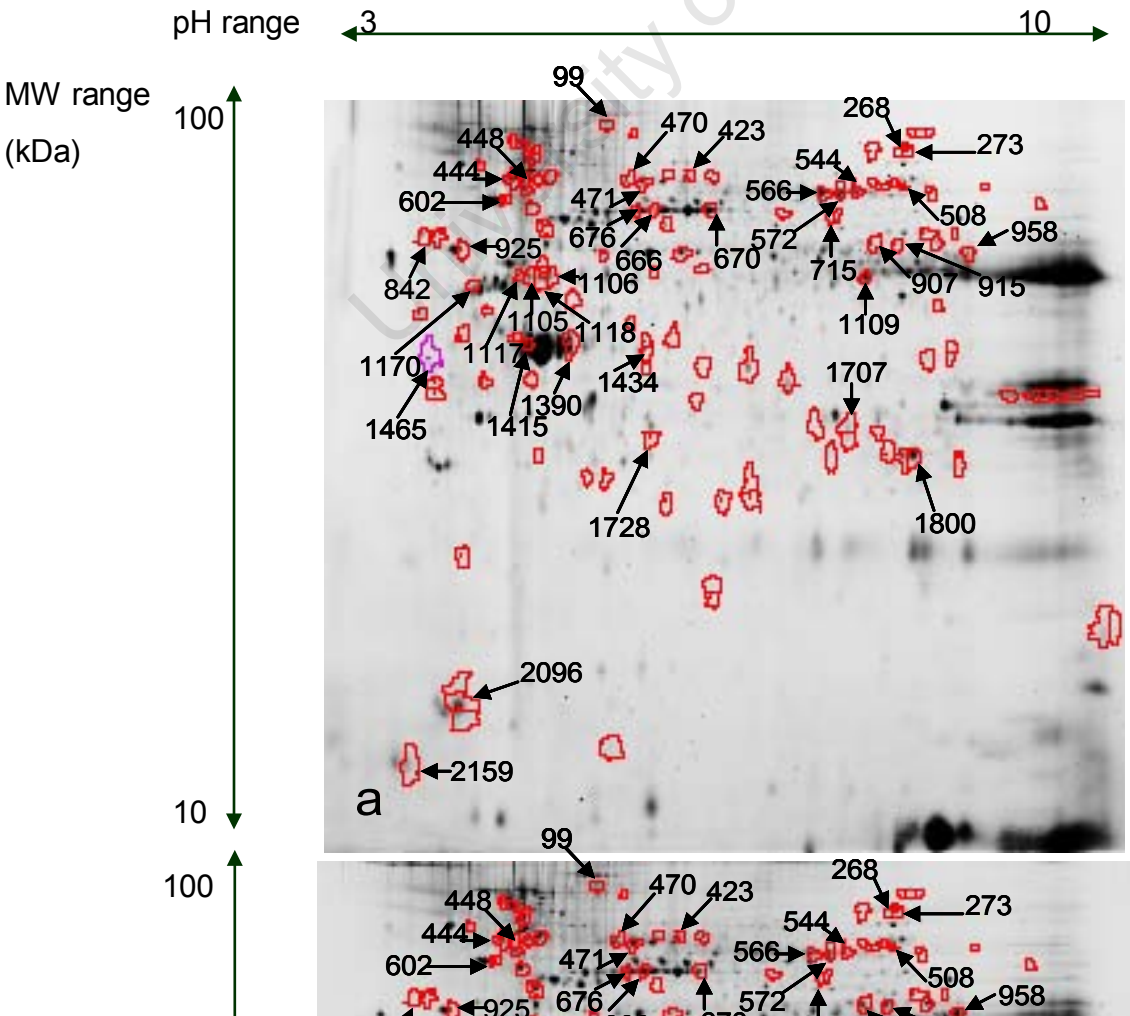

Figure 2.2: Comparison of the grayscale images depicting the protein profile of (a) a crude membrane protein fraction from oesophageal tumour tissue, labelled with Cy 3 and (b) a crude membrane protein fraction from normal oesophageal tissue, labeled with Cy 5. Proteins differentially expressed by 2-fold ($P<0.05$) are outlined in red. Spot numbers are indicated for proteins identified by MALDI-MS and peptide mass fingerprinting. Molecular weight (MW) range is indicated on the left and pH range on the top of the image.

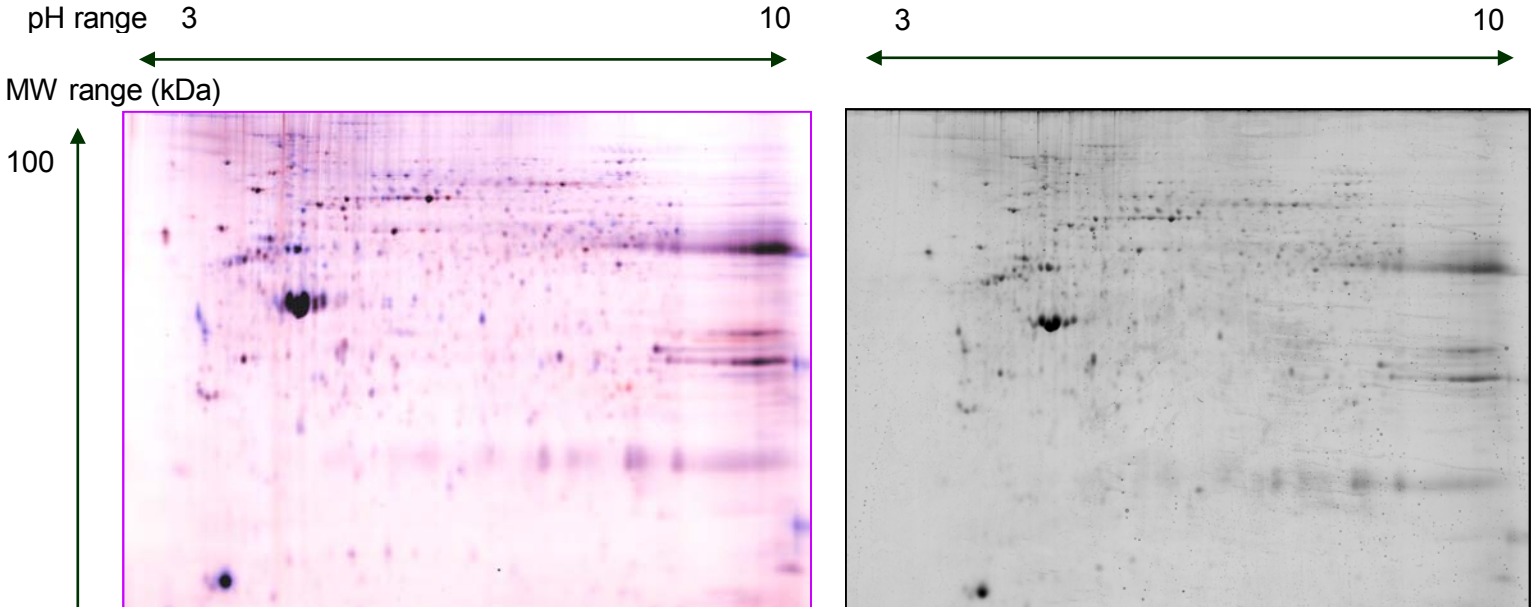

Figure 2.3: (a) Merged Cy dye image of a crude membrane protein fraction from oesophageal tumour tissue, labeled with Cy 3 (red) and a crude membrane protein fraction from normal oesophageal tissue, labeled with Cy 5 (blue). (b) The same gel was post-stained with colloidal coomassie blue. Molecular weight (MW) range is indicated on the left and pH range on the top of the image.

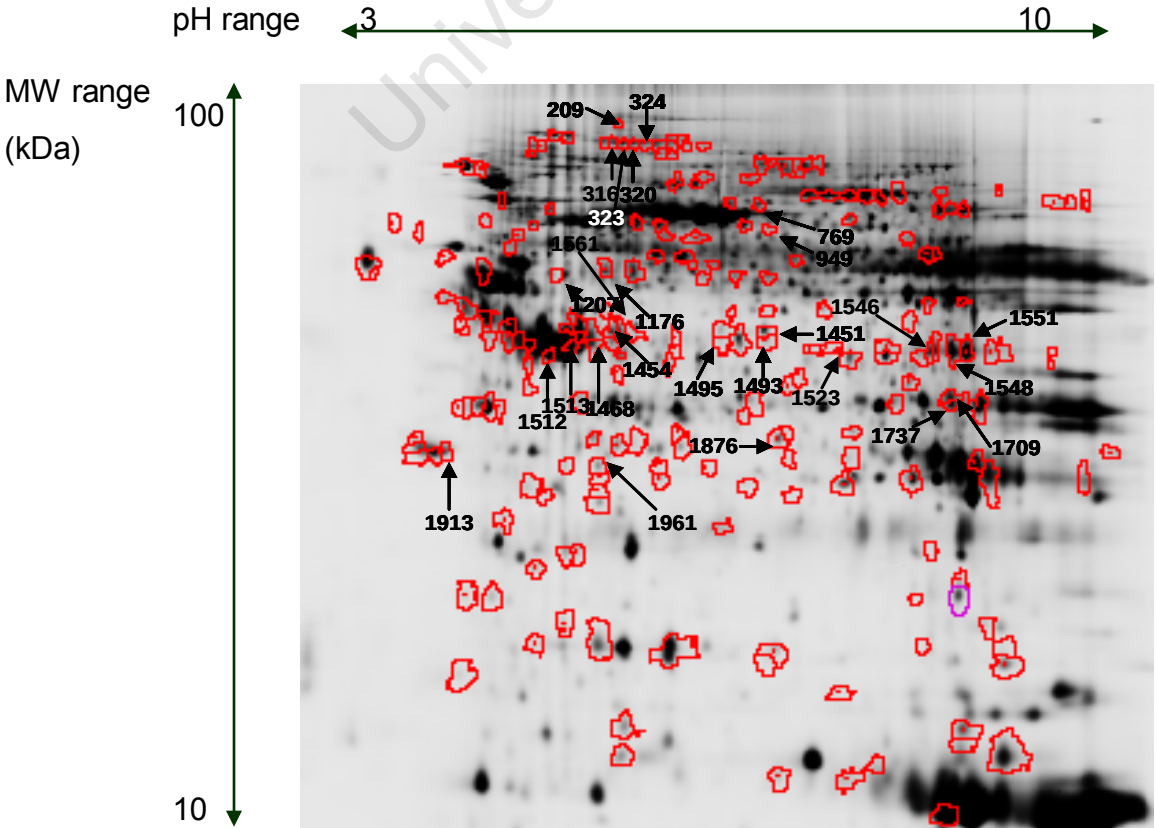

Figure 2.4: Comparison of the grayscale images depicting the protein profile of (a) cytoplasmic protein fraction from oesophageal tumour tissue, labeled with Cy 5 and (b) cytoplasmic protein fraction from normal oesophageal tissue, labeled with Cy 3. Proteins differentially expressed by 2-fold ($P<0.05$) are outlined in red. Spot numbers are indicated for proteins identified by MALDI-MS and peptide mass fingerprinting. Molecular weight (MW) range is indicated on the left and pH range on the top of the image.

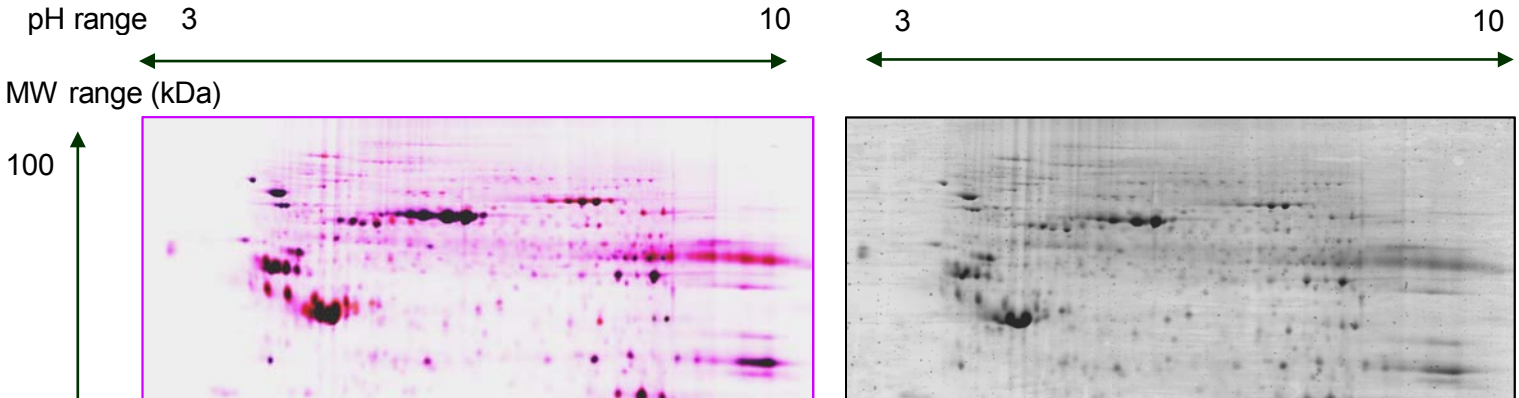

Figure 2.5: (a) Merged Cy dye image of cytoplasmic protein fraction from oesophageal tumour tissue, labeled with Cy 5 (blue) and cytoplasmic protein fraction from normal oesophageal tissue, labeled with Cy 3 (red). (b) The same gel was post-stained with colloidal coomassie blue. Molecular weight (MW) range is indicated on the left and pH range on the top of the image.

A total of 37 differentially expressed protein features corresponding to 24 gene products were identified from the crude membrane fraction (Table 2.4) and 26 features corresponding to 18 gene products were identified from the cytoplasmic fraction (Table 2.5). Several proteins were identified in more than one gel spot (Figure 2.2 and Table 2.4), possibly reflecting variable post-translational modification of these proteins. There was some overlap in the proteins identified from both the crude membrane and cytoplasmic fractions and these are highlighted in Tables 2.4 and 2.5.

Table 2.4: Summary of differentially expressed proteins in tumour compared to normal (from the membrane fraction) identified by MALDI-MS. (a) Average ratio: (-) indicates protein is down-regulated in tumour compared to normal and (+) indicates protein is up-regulated in tumour compared to normal (b) Spot number: Refers to spot numbers in Figure 2.2 (c) IPI number: International protein index reference number (d) predicted pI according to protein database (e) Molecular weight in Daltons according to protein database (f) pI according to position on gel (g) Molecular weight in Daltons according to position for gel (h) Number of peptides matching the top hit from Mascot Daemon programme versus the total number of masses submitted (i) Amino acid sequence coverage for the identified protein. *, ** and *** highlight proteins that overlap with proteins identified from the cytoplasmic fraction (see Table 2.5).

Tumour/Normal										
Av. Ratio [a]	Spot No. [b]	Name	IPI No. [c]	Chromosome	pI (pred) [d]	Mw (pred) [e]	pI (gel) [f]	Mw (gel) [g]	Score [h]	%Cov [i]
-8.77	1118	Desmin **	IPI00465084	2q35	5.21	53588	5.17	57170	230	60
-7.05	1105	Desmin **	IPI00465084	2q35	5.21	53588	5.08	53588	286	69
-6.7	2096	Myosin regulatory light chain 2, smooth muscle isoform	IPI00220278	20q11.23	4.94	19894	4.54	19894	88	77
-5.29	1465	Tropomyosin 2 (beta) isoform 2	IPI00220709	9p13.2-p13.1	4.63	33027	4.31	33027	91	41
-4.26	508	Glutaminyl t-RNA synthetase	IPI00026665	3p21.3-p21.1	6.71	88655	7.97	75659	66	16
-3.74	915	Coronin (Actin Binding protein 1C)	IPI00008453	12q24.1	6.65	53899	7.91	53809	72	23
-3.51	715	Keratin 10	IPI00295684	17q21	5.09	59020	7.4	68882	148	33
-3.45	1117	Desmin **	IPI00465084	2q35	5.21	53588	5	53588	64	18
-2.99	423	Keratin 10	IPI00295684	17q21	5.09	59020	6.32	78098	82	25
-2.79	1415	Actin Aortic Smooth Muscle	IPI00008603	10q23.3	5.23	42381	5.08	42294	161	65
-2.79	1434	Actin Gamma Enteric Smooth Muscle	IPI00025416	2p13.1	5.31	42249	5.97	42249	136	56
-2.71	471	Gelsolin Isoform B	IPI00377087	9q33	5.58	80876	5.96	80876	135	33
-2.63	958	T-complex protein, ETA subunit	IPI00018465	2p13.2	7.55	59842	8.46	61318	78	23
-2.6	666	Human serum Albumin precursor	IPI00022434	4q11-q13	5.92	71317	5.8	71317	87	27
-2.6	907	Keratin Type 2 cytoskeletal 5	IPI 00009867	12q12-q13	8.14	62651	7.73	63211	222	39
-2.59	1106	Desmin **	IPI00465084	2q35	5.21	53588	5.24	53588	247	60
-2.44	676	Human serum Albumin precursor	IPI00022434	4q11-q13	5.92	71317	5.91	70076	92	25
-2.4	268	Plasminogen precursor	IPI00019580	6q26	7.04	93247	7.9	93247	76	16
-2.3	99	Collagen alpha 2(VI)	IPI00073454	21q22.3	5.7	88373	5.68	91401	69	12
-2.3	470	Gelsolin Isoform B	IPI00377087	9q33	5.58	80876	5.83	80876	64	17
-2.25	273	Plasminogen precursor	IPI00019580	6q26	7.04	93247	8	93247	68	16
-2.09	1390	Actin, Cytoplasmic 1 *	IPI00021439	7p15-p12	5.29	42052	5.28	42052	101	58
-2.02	2159	Myosin light polypeptide 6, smooth muscle and non-muscle	IPI00029208	12q13.2	4.46	16990	4.14	12770	112	50
-2.01	1170	Tubulin Beta-2 chain	IPI00007752	6p25	4.79	50255	4.65	50255	92	36
2.06	566	Serotransferrin Precursor	IPI00022463	3q22.1	6.81	79280	7.5	79280	122	27
2.14	1728	Pyruvate kinase 3 isoform 2	IPI00220644	15q22	7.6	58538	6.01	34964	84	23
2.15	925	Keratin 6B	IPI00293665	12q12-q13	8.09	60247	4.56	62134	134	24
2.19	572	Serotransferrin Precursor	IPI00022463	3q22.1	6.81	79280	7.47	79280	101	25
2.42	1109	Pyruvate kinase 3 isoform 1	IPI00383237	15q22	7.95	58701	7.67	57170	142	47
2.55	544	Serotransferrin Precursor	IPI00022463	3q22.1	6.81	79280	7.61	79280	129	26
2.62	602	Keratin 10	IPI00295684	17q21	5.09	59020	5.1	59020	101	27
2.69	444	HSP90B1; GRP94; Endoplasmin precursor;Tumour rejection antigen (gp96)	IPI00027230	12q24.2-q24.3	4.76	92696	4.92	77481	138	28
2.94	842	Keratin 10	IPI00383111	17q21	5.01	57384	4.26	64990	91	26
3.06	670	Human serum Albumin precursor	IPI00022434	4q11-q13	5.92	71317	6.47	71317	189	40
3.11	1707	Annexin A2 isoform 2 **	IPI00455315	15q21-q22	7.57	38808	7.54	36282	76	37
3.23	448	HSP90B1; GRP94; Endoplasmin precursor;Tumour rejection antigen (gp96)	IPI00027230	12q24.2-q24.3	4.76	92696	5.04	77379	138	28
7.74	1800	Glyceraldehyde 3 phosphate dehydrogenase	IPI00219018	12p13	8.57	36201	8.04	36201	62	19

Table 2.5: Summary of differentially expressed proteins in tumour compared to normal (from the cytoplasmic fraction) identified by MALDI-MS. (a) Average ratio: (-) indicates protein is down-regulated in tumour compared to normal and (+) indicates protein is up-regulated in tumour compared to normal (b) Spot number: Refers to spot numbers in Figure 2.4 (c) IPI number: International protein index reference number (d) predicted pI according to protein database (e) Molecular weight in Daltons according to protein database (f) pI according to position on gel (g) Molecular weight in Daltons according to position for gel (h) Number of peptides matching the top hit from Mascot Daemon programme versus the total number of masses submitted (i) Amino acid sequence coverage for the identified protein. *, ** and *** highlight proteins that overlap with proteins identified from the membrane fraction (see Table 2.4).

Tumour/Normal										
Av. Ratio [a]	Spot No. [b]	Name	IPI No. [c]	Chromosome	pI (pred) [d]	Mw (pred) [e]	pI (gel) [f]	Mw (gel) [g]	Score [h]	%Cov [i]
-4.47	1454	Creatine Kinase B chain	IPI00022977	14q32	5.34	42902	5.34	42902	72	34
-3.96	949	Tumour related protein	IPI00297056	1q21	5.73	53740	6.31	95919	115	29
-3.84	1468	Creatine Kinase B chain	IPI00022977	14q32	5.34	42902	5.18	51668	158	49
-3.3	769	Protein-glutamine glutamyltranferase	IPI00300376	20q11.2	5.62	76926	6.26	110724	149	28
-2.96	1451	VAT-1 (vesicle amine transport)	IPI00156689	17q21	5.88	42122	6.3	52441	69	34
-2.88	1513	Actin, Cytoplasmic 1 *	IPI00021439	7p15-p12	5.29	42052	5.19	48569	79	39
-2.86	1493	Leukocyte elastase inhibitor; SERPINB1	IPI00027444	6p25	5.9	42829	6.31	49417	66	34
-2.34	209	Smooth Muscle and Non-muscle Myosin alkali light chain	IPI00335168	12q13.13	4.56	17090	5.36	178953	81	39
-2.25	1523	Acetyl-CoA Acetyltransferase, cytosolic	IPI00291419	6q25.3-q26	6.47	41838	7.09	47616	89	28
-2.18	1561	Hurpin; serpinB13	IPI00006560	18q21.3-q22	5.48	44305	5.37	45542	81	34
-2.18	1207	Desmin **	IPI00465084	2q35	5.21	53588	4.95	72700	118	31
-2.16	323	Alpha 2 Macroglobulin	IPI00465313	12p13.31	6.06	167505	5.38	158910	64	11
-2.16	1512	Actin, Cytoplasmic 1 *	IPI00021439	7p15-p12	5.29	42052	4.8	48689	60	32
-2.1	1176	Fibrinogen	IPI00219713	4q28	5.7	50092	5.28	75263	94	31
-2.09	1495	Leukocyte elastase inhibitor; SERPINB1	IPI00027444	6p25	5.9	42829	6.02	49173	100	38
-2.08	320	Alpha 2 Macroglobulin	IPI00465313	12p13.31	6.06	167505	5.45	159304	185	21
-2.05	316	Alpha 2 Macroglobulin	IPI00465313	12p13.31	6.06	167505	5.33	160094	166	19
-2.04	324	Alpha 2 Macroglobulin	IPI00465313	12p13.31	6.06	167505	5.5	167505	112	15
2.04	1876	Glutathione S-transferase	IPI00019755	10q25.1	8.14	33430	6.39	27626	87	31
2.11	1709	Annexin A2 ***	IPI00455315	15q21-q22	7.57	38808	7.5	38808	76	33
2.11	1961	Nicotinamide N-methyltransferase	IPI00027681	11q23.1	5.56	30011	5.23	23579	73	26
2.23	1913	14-3-3 Protein Zeta or Delta	IPI00021263	8q23.1	4.73	27899	4.24	25713	110	57
2.46	1737	Aldo-keto Reductase Family member B10	IPI00105407	7q33	7.12	362266	7.51	36226	70	28
4.78	1548	Creatine Kinase M chain	IPI00027487	19q13.2-q13.3	6.77	43302	7.51	46338	160	45
5.85	1546	Creatine Kinase M chain	IPI00027487	19q13.2-q13.3	6.77	43302	7.4	46915	87	21
9.34	1551	Creatine Kinase M chain	IPI00027487	19q13.2-q13.3	6.77	43302	7.6	46109	209	49

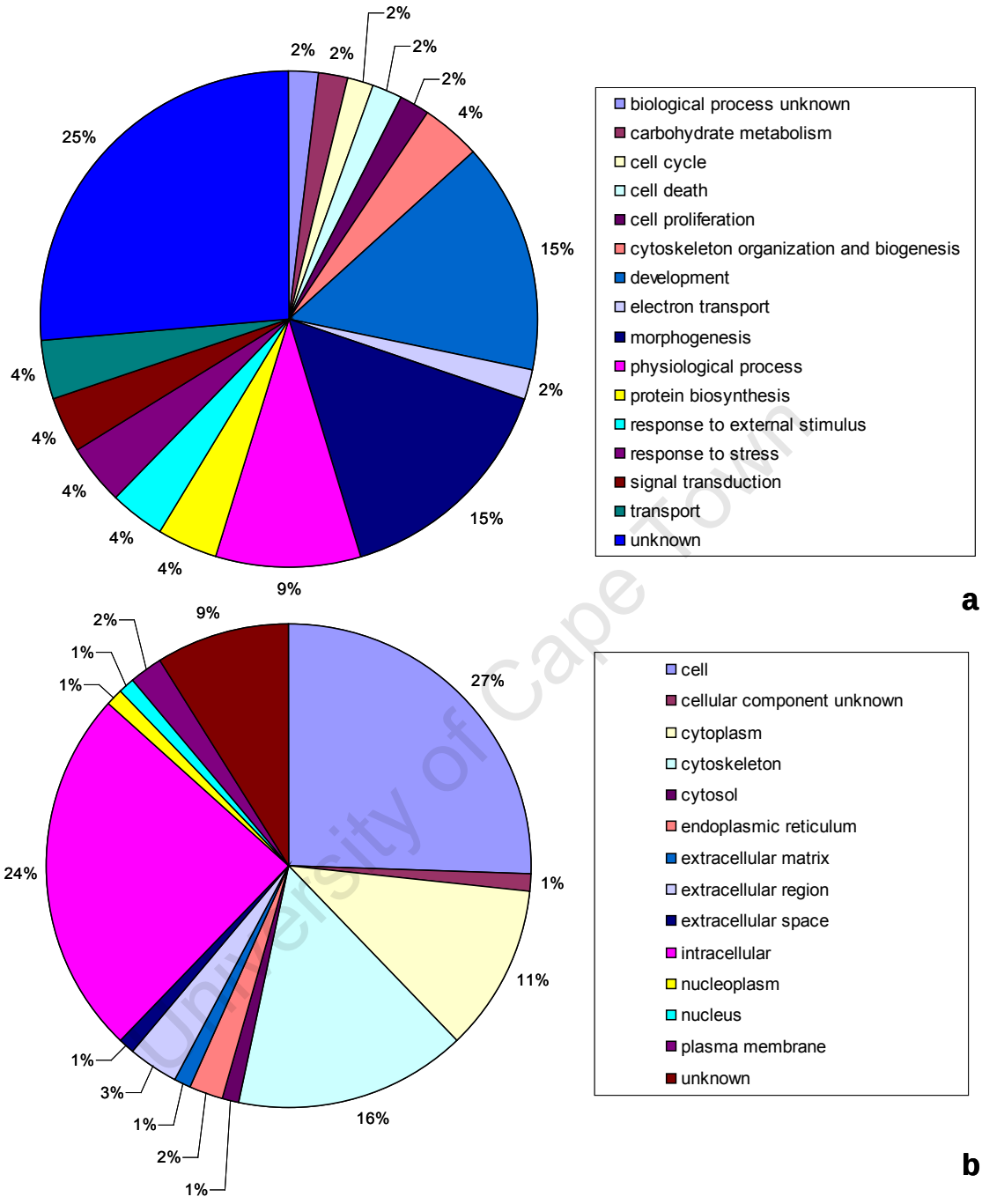

Figure 2.6: Gene ontology for all identified proteins that displayed altered expression in OSCC compared to normal tissue based on data from tables 2.4 and 2.5. (a) Pie graph illustrating the biological processes that the identified proteins are implicated in (b) Pie graph illustrating the biological compartment of origin of the identified proteins (images were kindly generated by software

designed by Dr Richard Jacob, Ludwig Institute for Cancer Research, University College of London, United Kingdom)

The data set of proteins identified to be differentially expressed were categorized according to both biological processes (Fig 2.6a) that the proteins contribute to; as well as according to the compartment the proteins are localized in (Fig 2.6b).

The differentially expressed proteins from the membrane fraction identified by MALDI-MS analysis comprised a small range of functional categories, including cytoskeletal/attachment/ extracellular matrix (ECM) elements, metabolic enzymes, and stress-related proteins. It is probably not surprising that the cytoskeletal/attachment/ ECM proteins comprised the largest category since these proteins are probably present at relatively high concentrations in cells, facilitating their detection in the system used. These include myosin, tropomyosin, actin, collagen, coronin, desmin and tubulin, most of which are decreased in tumour tissue (Table 2.4).

Human serum albumin precursor (Spots numbered 666 and 676 in Table 2.4 and Fig. 2.2) displayed decreased expression in tumour tissue compared to normal tissue. However, in an apparent anomaly further down in Table 2.4, this same protein (human serum albumin precursor) was over-expressed 3-fold in tumour, relative to normal tissue (spot number 670 in Table 2.4 and Fig. 2.2). This apparent contradiction presumably reflects differential post-translational processing of this protein in tumour tissue compared to normal tissue since the same protein occurs at the same molecular weight, but different pI positions. A similar result is observed for keratin 10 (spots numbered 423 and 715 versus spots numbered 602 and 842 in Table 2.4 and Fig. 2.2).

It was also observed that the levels of two glycolytic enzymes (glyceraldehyde 3 phosphate dehydrogenase - Table 2.4 and Fig 2.2: Spot 1800 and pyruvate kinase - Table 2.4 and Fig 2.2: Spots 1109 and 1728) were markedly elevated in tumour tissue compared to normal tissue. The two spots, identified for pyruvate kinase, represent two different isoforms.

A decrease in glutaminyl t-RNA synthase levels, in tumour tissue compared to normal in the membrane fraction, was also observed and although involved in transcription there is also evidence to suggest that this protein inhibits pro-apoptotic mediators (114).

The proteins displaying altered expression levels in normal and tumour tissue from the cytoplasmic fraction identified by MALDI-MS displayed a range of functional categories similar to that observed for the membrane fraction i.e. cytoskeletal/attachment/ extracellular matrix (ECM) elements, metabolism, stress-related proteins and signal transduction. The cytoskeletal/attachment/ extracellular matrix (ECM) proteins represented the bulk of the proteins identified. The metabolic enzymes identified in the cytoplasmic fraction are primarily involved in metabolism of xenobiotic compounds, in contrast to the glycolytic enzymes identified in the membrane fraction. Aldo-keto reductase, glutathione-S-transferase and nicotinimide N-methyltransferase are involved in detoxification of foreign compunds and although no function exists for VAT-1, it is believed to be part of the alcohol dehydrogenase family. Furthermore, acetyl Coenzyme A acetyltransferase is involved in ketone body metabolism, for the production of energy.

The stress related protein, cornulin (identified as tumour related protein in Table 2.5), which is a squamous epithelial heat shock protein and is part of a novel heat shock response in squamous epithelium was down-regulated in tumour similar to the observation in oral squamous cell carcinoma (115,116).

14-3-3 ζ (or Δ) was identified to be up-regulated in the cytoplasmic fraction of tumour tissue compared to normal and plays a role in signal transduction, mitogenesis, cell survival, cell cycle control and apoptosis (117).

Other proteins that displayed altered levels of expression included, human serum albumin precursor, plasminogen precursor, fibrinogen and serotransferrin. Their presence in these samples could reflect

varying levels of serum contamination in the biopsy samples. Also, alpha 2 macroglobulin, hurpin (Serpin B13) and leukocyte elastase inhibitor fall under the umbrella of protease inhibitors that are usuall present in the serum or cytoplasm and are thought to play roles in proliferation, differentiation and regulation (118-120).

Of the differentially expressed proteins listed in Table 2.4 and 2.5, five were selected for further investigation (Table 2.6). These were annexin 2 and HSP90B1 (also known as GRP94, endoplasmin and tumour rejection antigen), GAPDH and pyruvate kinase, which displayed increased expression in tumour tissue relative to normal. Gelsolin was also selected for further investigation, but this protein displayed reduced expression in tumour tissue relative to normal (Fig. 2.7 and Table 2.6).

Table 2.6: Summary of differentially expressed proteins selected for further investigation. Average ratio: Unless otherwise indicated, an increase in expression was observed in tumour tissue compared to normal, where (-) indicates protein is down-regulated in tumour compared to normal. HSP90B1, pyruvate kinase and gelsolin appear twice on Table 2.4 therefore have two average ratios.

Tumour/Normal	
Ave ratio	Name
3.11	Annexin 2
2.69 and 3.23	GP96
7.74	GAPDH
2.14 and 2.42	Pyruvate kinase
-2.3 and -2.71	Gelsolin

HSP90B1 (GP96 in Table 2.6), which belongs to the HSP90 family, was selected for further investigation because this protein has previously been associated with prostate and breast cancer (121,122). Altered gelsolin expression was previously observed in prostate and ovarian cancer

(123,124) and altered annexin A2 expression has been reported for human gliomas and pancreatic cancer (125,126).

Furthermore, both gelsolin and annexin 2 are involved in actin dynamics and could impact on important cellular processes such as cell motility and invasion (127-130). The other two proteins of interest, GAPDH and pyruvate kinase, both involved in the glycolytic pathway, displayed elevated expression in tumour tissue. The observation that tumour tissue displays elevated levels of glycolytic enzymes, and thus glycolysis, is a well documented phenomenon. The elevated glycolysis, and dependence of tumour tissue on glycolysis for energy is termed the Warburg effect (131). This observation will be explored in more detail in Chapter 4.

In Fig 2.7, the *Decyder* Software analysis depicts a 3-dimensional visualisation of the spots, reflecting the quantitation of the spots, (highlighted by arrows) illustrating that annexin 2 (Fig 2.7a), HSP90B1 (Fig 2.7c), GAPDH (Fig. 2.7g) and pyruvate kinase (Fig. 2.7i) expression is increased in tumour tissue compared to normal tissue. Gelsolin expression (Fig 2.5e), however, is decreased in tumour compared to normal tissue. This information is represented graphically in Fig. 2.7 b,d, f, h and j showing the standardized abundance of each protein in tumour tissue compared to normal tissue, where each point represents the protein spot obtained in triplicate gels. The data in panels b, d, f, h and j of Figure 2.7 shows the differences between the different gels, providing information about the spread, and therefore the consistency of data between the gels. The graphical representation further illustrates that the expression of annexin 2, HSP90B1, GAPDH and pyruvate kinase expression are significantly increased (> 2-fold) in tumour compared to normal tissue while the expression of gelsolin is significantly reduced (> 2-fold) in tumour compared to normal tissue (where $P< 0.05$). MALDI-MS generated mass spectra of each digested protein (Appendix B: Fig. B1 – Fig. B5) were internally calibrated with trypsin autolysis peaks and peptide mass fingerprints were analysed, as described in the methods section.

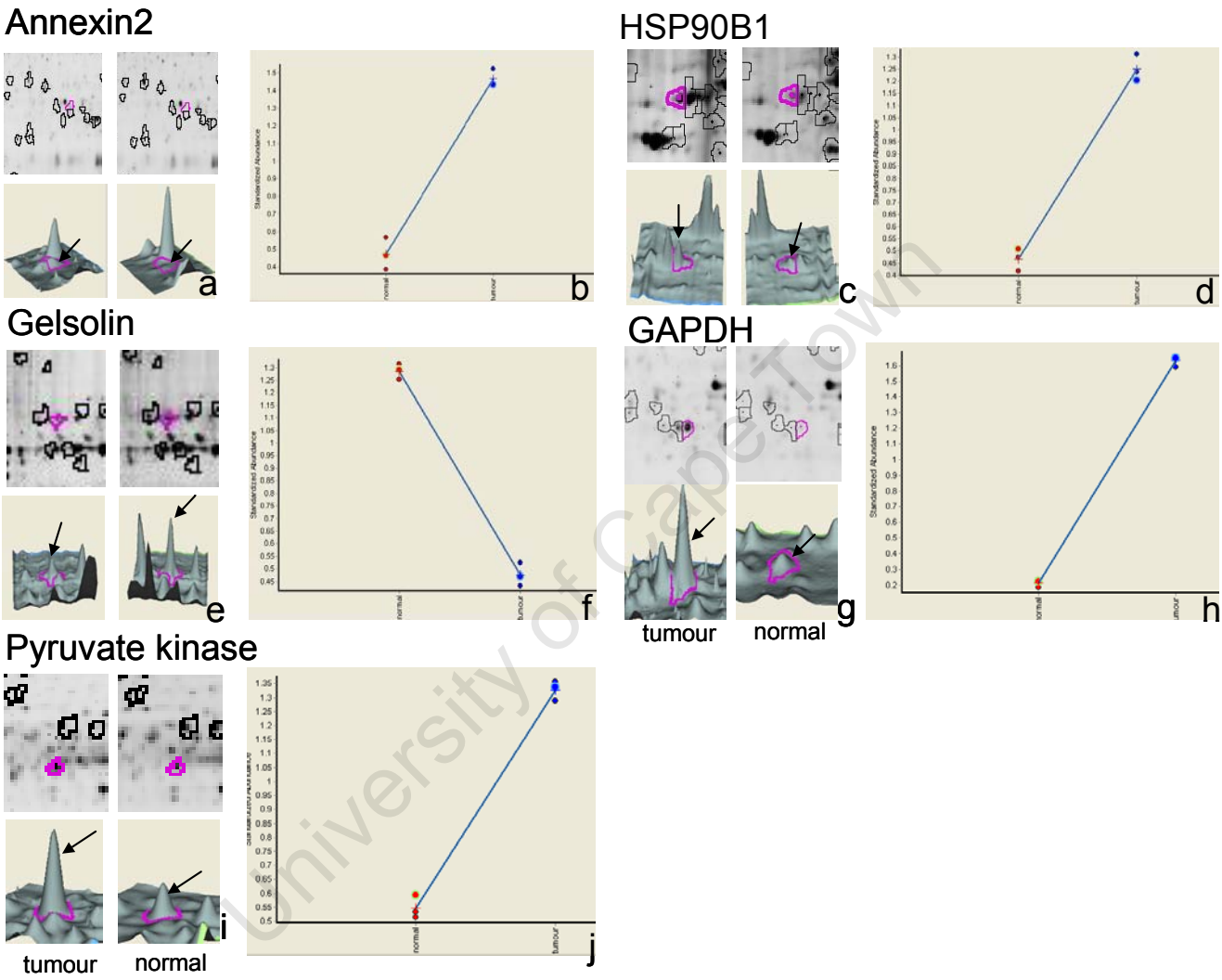

Figure 2.7: Depicts *Decyder* Software analysis of the following differentially expressed proteins: Annexin 2 (a and b), HSP90B1 (c and d), Gelsolin (e and f), GAPDH (g and h) and Pyruvate kinase (I and j). The top panels in a, c, e, g and i highlight the protein spot of interest in purple. The bottom panel in a, c, e, g and i; graphically represent the protein expression levels in tumour compared to normal (indicated by the arrows). The standardized abundance (*y*-axis) of the proteins' expression in tumour (blue points) compared to normal (red points) (*x*-axis) is shown in b, d, f, h and j. The points are representative of the protein spot in three separate gels and the difference in expression is

significant, where P<0.05 (see Table 2.4). The blue line connects the points representative of the protein spot in gel 2 (Table 2.1).

2.3.3

2.3.4 IHC of selected targets

IHC staining of archived paraffin-embedded tissue was used to assess the expression of annexin 2, HSP90B1 and gelsolin in oesophageal tumours and paired normal tissues from 18 patients. Annexin 2 expression was markedly elevated in tumour tissue compared to normal tissue (Fig. 2.8 a-c) in all 18 sections examined, confirming the results observed by 2D-DIGE analysis. Furthermore, the plasma membrane of dysplastic epithelial cells stained strongly for annexin2, relative to the weak annexin 2 staining observed in normal epithelial cells (Fig. 2.8 a and b). The strong increase in annexin 2 staining, observed in early dysplasia, prompted us to examine whether annexin 2 was linked to survival status (Fig. 2.8 b). However, no statistically significant correlation with survival status was observed in a larger cohort, of 59 patients (Fig 2.9). Examining a larger cohort of patients would have improved the power of the study; ideally at least 100 patients would have improved the power from 0.568 (for the 59 patients examined) to 0.793 (Table 2.7). This would allow us to draw a statistically significant conclusion either way, but unfortunately, no further patient samples were available.

HSP90B1 expression was relatively weak in both normal epithelium and tumour tissue (Fig. 2.8d, e and f). All sections displayed negative to weak membrane expression of HSP90B1 in the normal epithelia, whereas the tumour tissue displayed a weak cytoplasmic staining, suggesting a possible increase in expression, and a change in sub-cellular localisation, both of which require further investigation. No gelsolin staining was observed in normal epithelial cells, whereas a weak

cytoplasmic stain was observed for gelsolin in tumour tissue (Fig. 2.8g and h), which is contrary to the 2D-DIGE data observed (Table 2.6). Furthermore, the muscle and stromal tissue stained strongly positive for gelsolin in both normal and tumour tissue.

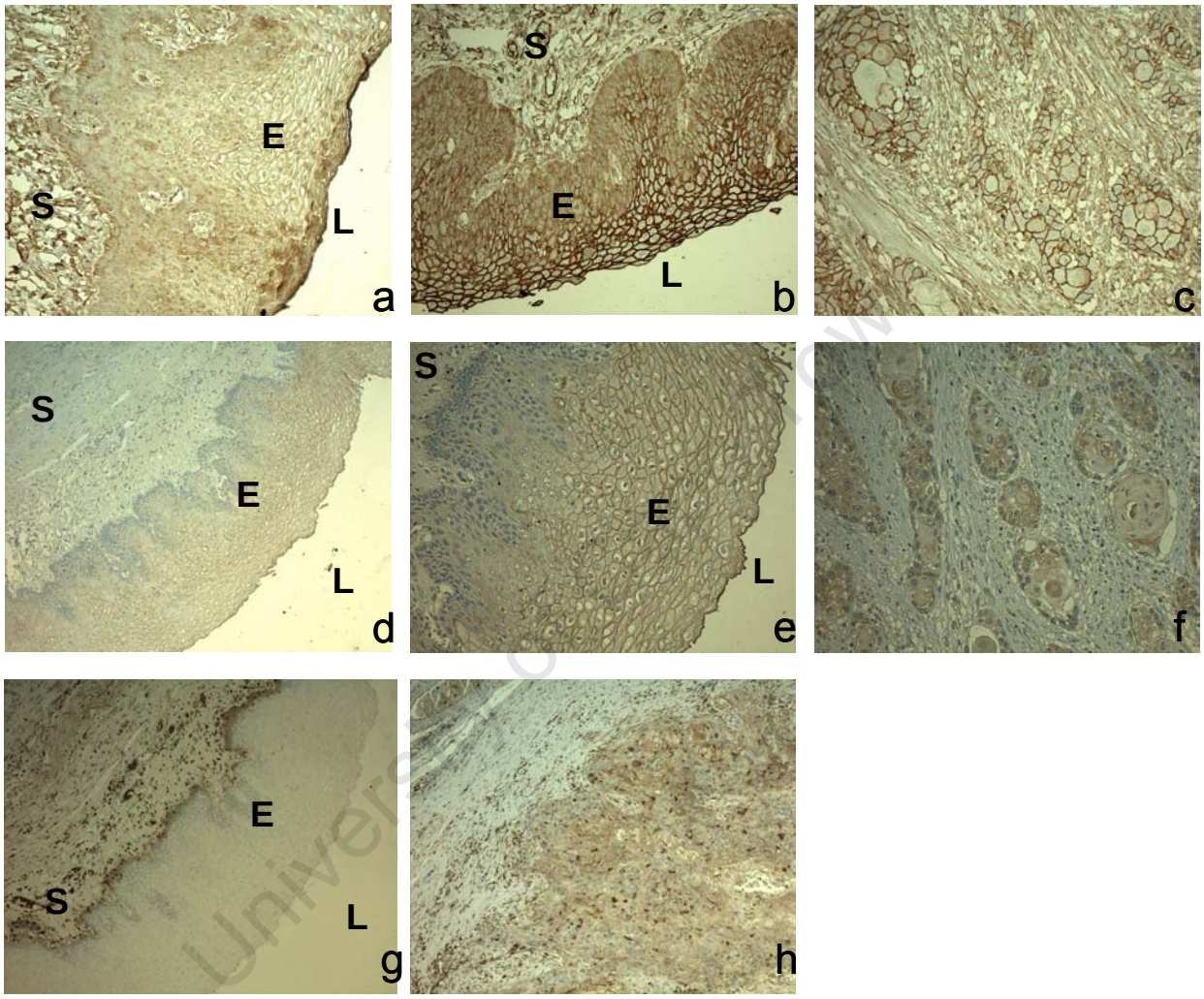

Figure 2.8: Immunohistochemical staining of annexin 2, HSP90B1 and gelsolin (a) Weak membrane staining of annexin 2 in normal epithelia [100X] (b) Strong membrane staining of annexin 2 in dysplastic epithelia [100X] (c) Intense membrane staining of Annexin 2 in invasive carcinoma characterized by "keratin pearls" [100X] (d) Weak membrane staining of HSP90B1 in normal epithelia [40X] (e) Magnification of (d) [100X] (f) Cytoplasmic blush of HSP90B1 in invasive carcinoma [100X] (g) Negative epithelial staining for gelsolin in normal epithelia [40X] (h) Cytoplasmic blush of gelsolin in invasive carcinoma [40X]. Where [ ] indicates total magnification, L indicates Lumen, E indicates epithelia and S indicates Stroma.

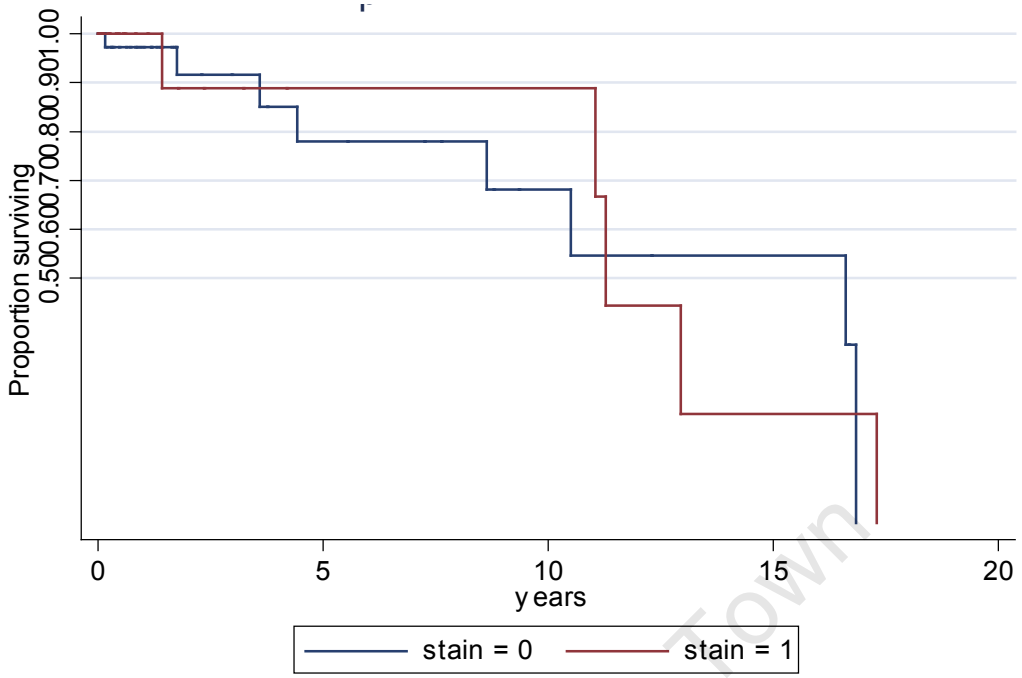

Figure 2.9: Kaplan Meier Survival curve illustrating the proportion of patients surviving in years based on annexin 2 status, where the blue line indicates patients negative for annexin 2 staining and the red line indicating patients with positive annexin 2 staining. Total number of events analysed were 59 (59 patients, details outlined in Table A4) from which no statistically significant correlation exists between annexin 2 staining and survival (p=0.38). This data indicates that annexin 2 over-expression, in OSCC patient tumour tissue does not correlate with a decrease in survival status.

Table 2.7: Calculated power and sample size. Hypothesis: increased annexin 2 expression is associated with poor patient survival. This study included 59 subjects/slides (n), an accrual interval (A) of 16.1 time units, and additional follow-up (F) after the accrual interval of 0 time units. Prior data indicate that the median survival time (m1 and m2) on the control treatment is 1.4 time units. If the true median survival times on the control and experimental treatments are 1.4 and 2 time units, respectively, we will be able to reject the null hypothesis that the experimental and control survival curves are equal with probability (power) of 0.568. The Type I error probability (α) associated with this test of this null hypothesis is 0.05. If the study included 100 subjects/slides (n) then we would have been able to reject the null hypothesis that the experimental and control survival curves are equal with probability (power) of 0.793.

α	n	m1	m2	A	F	M	Power
0.05	59	1.4	2	16.1	0	2.5	0.568
0.05	100	1.4	2	16.1	0	2.5	0.793

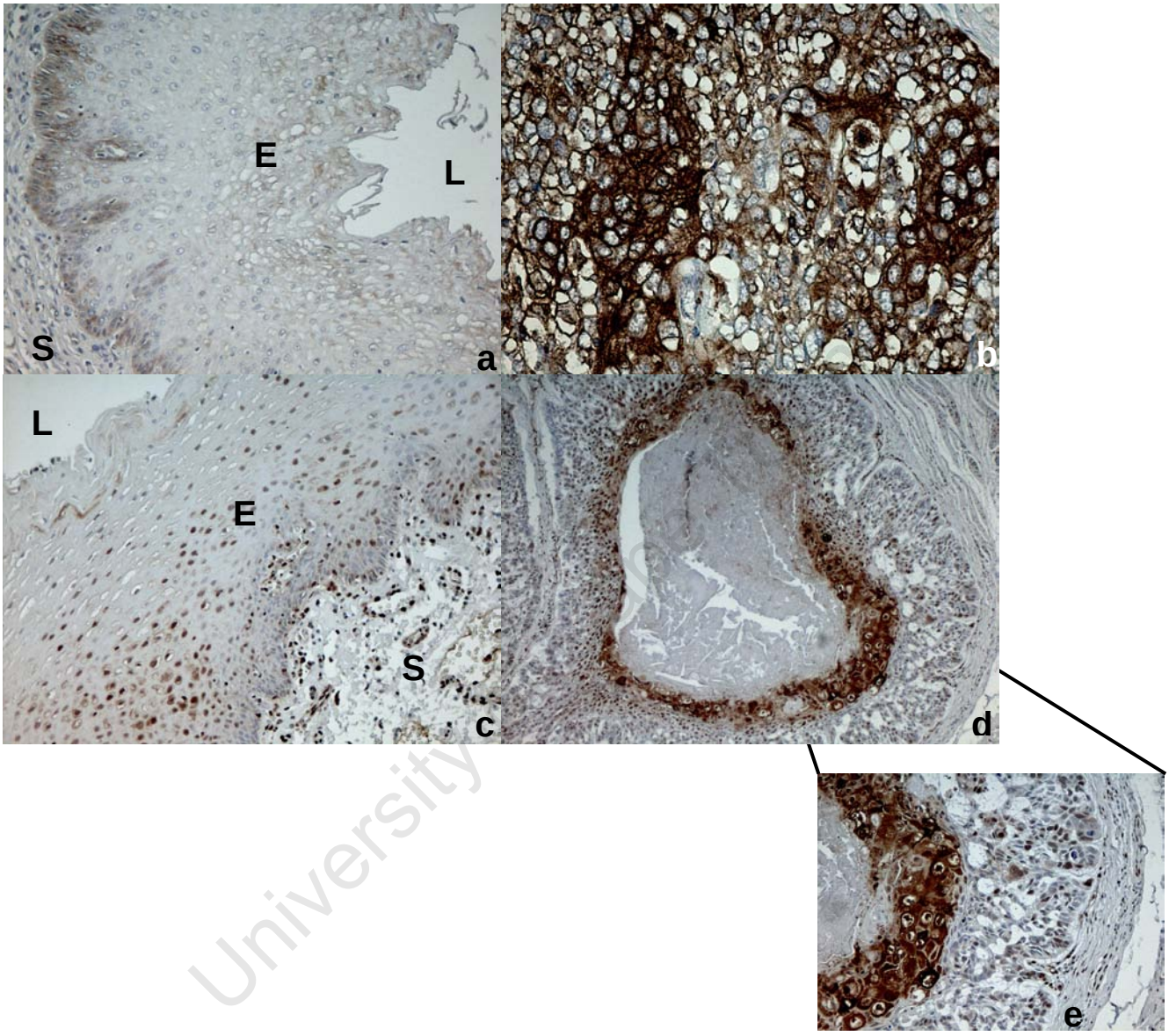

Figure 2.10: Immunohistochemical staining of pyruvate kinase (PK) and GAPDH: (a) Weak staining of PK in normal tissue [100X] (b) intense staining of PK in tumour tissue, characterized by the disorganized tissue architecture where boundaries for stroma and epithelia are not clearly defined [400X] (c) weak cytoplasmic GAPDH staining in normal tissue, with strong nuclear staining [100X], compared to (d) intense GAPDH staining [40X] in better differentiated tissue surrounding the keratin pearl in comparison to poor staining in less differentiated tissue, mimicking normal epithelial tissue architecture (e) Inset of the staining at the periphery of the keratin pearl [100X]. [ ] indicates total magnification, L indicates Lumen, E indicates epithelia and S indicates Stroma.

We also examined the expression levels of GAPDH and pyruvate kinase, which were both observed to show increased levels in tumour tissue in our 2D-DIGE analysis. Figure 2.10 shows both pyruvate kinase (PK2) (Fig. 2.10 a and b) and GAPDH (Fig. 2.10 c-e) display markedly increased levels in tumour tissue compared to normal tissue. All the sections examined displayed the same staining pattern.

The increase in GAPDH and PK2 levels were observed in early dysplasia. Furthermore, better differentiated cells displayed stronger staining than poorly differentiated cells. It was interesting to note that not only did GAPDH present with cytoplasmic staining, but a large proportion of the cells showed nuclear localisation (Fig. 2.10 c-e). Interestingly, as cells become less differentiated, the staining changed from cytoplasmic and nuclear to just nuclear.

Of the proteins identified, the increase in GAPDH and pyruvate kinase (enzymes involved in glycolysis) was of special interest and was further explored (see Chapter 4).

2.4 Discussion

Proteomic approaches such as 2D-DIGE promise to facilitate the identification of proteins that could potentially be exploited for diagnostic or therapeutic purposes, and compliment the information generated using more established genomic approaches. In this study 2D-DIGE was used to identify a group of proteins that are differentially expressed in oesophageal tumour versus paired normal tissue from the same patients.

Patient samples (biopsies) were exceptionally small (pinhead size), and not enough protein could be obtained from a single patient sample for use in 2D-DIGE. It was therefore necessary to pool samples, as outlined in Materials and Methods section. Although pooled samples yielded low statistical power, it still allowed within-group variability to be determined. An advantage is that the heterogeneous pools balance out inter-individual differences and highlight biological variation between normal and tumour tissue (132). Technical replicates revealed good reproducibility as displayed by the consistency of protein spots between replicate gels (Fig.2.7), illustrating the low variability inherent to the technique used.

Although the tissue samples in this study were separated into cytoplasmic and crude membrane fractions prior to 2D-DIGE, some proteins typically associated with the cytoplasm were identified in the membrane fraction, including pyruvate kinase and GAPDH (Table 2.4). We cannot exclude the possibility that the crude membrane fractions were contaminated with cytoplasmic cell components despite the extensive washing steps performed. However, it is also possible that the presence of these proteins in the membrane preparation may reflect their association with structures, which co-purify with the membrane fraction, as previously reported for pyruvate kinase (133,134) and GAPDH (135,136).

The increased levels of glycolytic enzymes in tumour tissue observed here has been observed before for other cancers (137-139). Presumably this reflects the shift from mitochondrial oxidative phosphorylation to aerobic glycolysis for glucose metabolism, as originally observed by Warburg (131). Our observation that oesophageal cancer cells display elevated levels of glycolytic enzymes suggest that this cancer also displays altered glucose metabolism, which presents unique therapeutic opportunities as reported elsewhere for lung and breast cancer (139). The opportunity to exploit this for therapeutic intervention in oesophageal cancer was investigated and will be reported in Chapter 4.

Proteins that displayed altered levels of expression in tumour compared to normal tissues, but were not further investigated in this study, included cytoskeletal/attachment/ extracellular matrix (ECM) elements and cell signalling molecules.

14-3-3 ζ plays a role in signal transduction, mitogenesis, cell survival and cell cycle control; however, recently it has also been shown that an increase in 14-3-3 ζ results in decreased apoptotic potential (117). These oncogenic characteristics have led to the suggestion that increased expression of 14-3-3 ζ is associated with tumour promotion. Increased levels of 14-3-3 ζ observed in the cytoplasmic fraction of tumour tissue in this study is consistent with reports of elevated expression of this protein in breast cancer, lung cancer and gastric cancer, although the exact role of 14-3-3 ζ in the development of these cancers is poorly understood (140-143).

Collagen alpha 2 (iv) (also type IV collagen) is the major structural component of basement membranes, in a complex network with laminins, proteoglycans and entactin/nidogen (144,145). Previously, collagen alpha 2 (iv) has been shown to display diminished expression in colorectal cancer as well as in prostate cancer (146). Ikeda *et al* showed that the decreased levels of type IV collagen in colon cancer is due to hypermethylation of the promoter region (147).

The cytoskeletal components of a cell play an important role in co-ordinated and directed movement displayed by many cell types. This complex network of proteins includes a number of the proteins identified in this study including actin, tubulin, desmin coronin, tropomyosin, gelsolin, T-complex protein ETA subunit and myosin (classes detailed in Table 2.4 and 2.5). Coronin, gelsolin and tropomyosin are actin binding proteins, whereas T-complex protein ETA subunit is a chaperonin facilitating actin and tubulin folding (148).

Winston *et al* showed that down-regulation of gelsolin correlates with the progression of breast carcinoma (149), whereas an adverse prognostic effect was observed for non-small cell lung cancer with increased and variable levels of gelsolin (150). In this study, we were unable to confirm the decreased level of gelsolin in tumour tissue, as observed by 2D-DIGE. This was due to the low level of gelsolin staining in normal oesophageal epithelium. While this could be due to an inactive antibody or poor quality sections, the strong, specific staining observed in muscle tissue of the same sections, ruled out these possibilties (151). The reason for the low levels of staining for gelsolin staining is unknown.

Actin, tubulin, desmin coronin, tropomyosin, gelsolin, T-complex protein ETA subunit and myosin all displayed a decreased level in tumour compared to normal. The expression of these cytoskeletal-associated proteins and intermediate filaments, reflect their role in morphologic and functional differentiation status (152). Although no consistent differences in cytoskeletal structure between normal and tumour cells have been identified, the possibilty that altered levels of these cytoskeletal elements contributes to the development of cancer, cannot be excluded (152).

Although annexin 2 can bind actin directly (thus forming part of the complex network that extends throughout the cytoplasm), it is not always associated with actin, and instead, is recruited to sites of actin assembly at cellular membranes (153,154). Annexin 2 is associated with dynamic actin

structures involved in phagocytosis, pinocytosis and migration (154). Annexin 2 (also known as p36 and calpactin 1) belongs to a family of calcium and lipid binding proteins that are expressed in a wide range of organisms from protists to vertebrates. Knockdown studies of annexin 2 in human glioma cells suggest that this protein plays an important role in cellular migration (125). The elevated expression of annexin 2 observed in tumour tissue by 2D-DIGE was validated in oesophageal tumour sections using IHC.

The elevated expression of annexin 2 observed in this study suggests that annexin 2 may play a similar role in oesophageal cancer. Furthermore, our results also suggest that alterations in annexin 2 gene expression may be an early event in the neoplastic process in oesophageal cancer. Of the 18 archived paraffin blocks that were analysed, 14 sections contained dysplastic tissue, all of which exhibited elevated annexin 2 levels. The elevated expression of annexin 2 at an early stage of oesophageal neoplasia suggests that this protein could be explored further as a potential early marker for the development of OSCC. Analysis of whether annexin 2 levels correlated with patient survival, showed that the correlation was not significant (Fig. 2.9). Unfortunately, only 59 sections were used in the statistical analysis, reducing the power of the study and decreasing the possibility of identifying a positive correlation. By increasing the number of patients in the cohort, it is possible that a statistically significant, positive correlation may be obtained (Table 2.6). Unfortunately, this study was limited by the patient sample available and increasing the number of patients in the cohort was not possible.

Keratins also form part of the intermediate filament family involved in the complex network of proteins that spread throughout the cytoplasm and play a role in maintaining cell architecture and structure (152). In an IHC study, Takahashi *et al* (155) reported that OSCC tissue displayed altered levels of keratin reactivity and distribution compared to normal oesophageal tissue. Our results support this finding, where several members of the keratin family displayed altered levels in tumour compared to

normal tissue in OSCC patients. It is well established that keratin 10 expression is associated with keratinising cells in squamous cell carcinomas of epidermis, lung, bladder, cervix and oesophagus (156,157). Another keratin identified in this study is keratin 6b, an isomer of keratin 6. Keratin 6 is unusual in that it is considered a marker for cell proliferation (158,159), consistent with the increased levels observed in tumour tissue compared to normal in OSCC patients. Keratin Type 2 cytoskeletal 5, also known as keratin 5, displayed decreased levels in tumour compared to normal tissue in OSCC patients, possibly reflecting differentiation status of the tissues used. In the neoplastic process, cells clearly change their profiles of keratins, reflected by the altered architecture.

Plasminogen precursor, human serum albumin precursor (albumin), fibrinogen and alpha-2-macroglobulin are found in the plasma, reflecting possible contaminating serum components in the membrane fraction. Levels of these proteins in tumour tissue compared to normal tissue were not of interest in this study as the altered levels were considered artefacts of serum contamination. Serum protein contamination was relatively inevitable, considering the amounts of blood attached to each biopsy used. Unfortunately, due to the method of biopsy collection, serum contamination could have been avoided if more washing steps were included prior to homogenisation. Due to the rapidity at which the samples thawed, care was taken minimise protein degradation, hence washing before homogenisation was not performed.

Glutaminyl-tRNA synthetase (glutaminyl-tRNA ligase) is responsible for charging tRNA with L-glutamine. Although this protein is primarily involved in protein synthesis, recent data reveals a regulatory role in apoptosis (160). Glutaminyl-tRNA synthetase is reported to have a pro-apoptotic role by interacting with, or blocking, its interaction with pro-apoptotic mediator, Daxx, the downstream kinase, ASK1 (apoptosis signal-regulating kinase) (160,161). One of the key molecular changes of a tumour cell is an ability to evade apoptosis (22). Reduced glutaminyl-tRNA synthetase

levels in tumour tissue compared to normal tissue, as observed in this study, would contribute to tumour cells' resistance to apoptosis.

Yagui-Beltran *et al* (115) demonstrated that normal squamous epithelia display a novel heat shock response, including changes in levels of protein-glutamine glutamyltransferase (transglutaminase-3) and cornulin. These proteins may regulate normal cellular integrity in squamous cell epithelia and a decrease in their levels may result in the development of cancer (115).

In this study, transglutaminase-3 displayed decreased levels in tumour tissue compared to normal in OSCC patients. This is in agreement with other studies reported by others, in which both proteomic and immunohistochemical data suggest transglutaminase-3 as a prognostic marker for OSCC (162,163).

Tumour related protein or cornulin (Chromosome 1 open reading frame 10 -C1orf10) is known to be down-regulated in OSCC compared to normal tissue (116), as confirmed in this study. It has been reported that exogenous expression of cornulin inhibits cell proliferation, therefore reduced expression of cornulin would facilitate the neoplastic process (116).

Multiple forms of creatine kinase exist (164). In our study a decrease in creatine kinase (B-chain-brain type) levels and an increase in creatine kinase (M-chain- muscle type) levels were observed in the cytoplasmic fraction. Creatine kinase is important in energy metabolism and generally found in high energy requiring tissues (165). Our study is not the first to describe decreased levels of brain type creatine kinase. Pretlow *et al* reported a decrease in creatine kinase in prostate cancer compared to benign prostatic hyperplasia (166).

Acetyl-coA acetyltransferase is located in the cytosol and is involved in cholesterol and steroid synthesis as well as ketogenesis (167,168). It is intriguing that acetyl-coA acetyltransferase levels

show reduced expression in tumour tissue compared to normal tissue our study, considering the importance of sterol synthesis for membrane biosynthesis in rapidly dividing cells.

Glutathione S transferase is an enzyme that is involved in xenobiotic metabolism (169). It is expressed in a wide range of tissues that includes the aorta, bone, breast, colon, oesophagus, foreskin, lung, ovary, pancreas, prostate, stomach, testis and uterus (170,171). Considering the broad spectrum of tissue expression, Board *et al* (170) suggested that it may have a significant housekeeping function, such as protection from oxidative stress. Considering the increased oxidative stress in tumour cells, the protective function of glutathione S transferase is consistent with the elevated expression of this protein in tumour tissue observed in this study.

Nicotinimide n-methyltransferase, like Glutathione S transferase is also involved in metabolism of foreign compounds (172). Nicotinimide n-methyltransferase has shown to be elevated levels in gastric cancer tissue compared to its normal counterpart (173). It has also been identified as a serum marker for the identification of colorectal cancer (174). Considering that it displayed increased levels in OSCC compared to normal tissue in this study, its diagnostic significance as a serum marker in OSCC should be considered.

Aldo-keto reductase family 1 B10 (AKR1B10), a member of the aldo-keto reductase superfamily. In addition to displaying an increased expression in OSCC in this study, it has also been shown to have elevated levels in lung squamous cell carcinoma and colorectal cancer (175,176). It functions mainly as part of the detoxification system and its overexpression has been associated with smoking in lung cancer (175). Furthermore, using a cultured colorectal cancer cell line as a model system, it was determined that AKR1B10 also plays a role in regulating cell proliferation (176). Knocking down this gene, using small interfering RNA technology, resulted in a 50% decrease in cell growth suggesting that this protein could represent a credible therapeutic target (176).

Although serotransferrin precursor or transferrin is a secreted protein located in the plasma, it is usually bound to its receptor on the cell membrane (177,178), probably accounting for the presence of transferrin in the membrane fraction in this study. Transferrin is responsible for carrying iron from the intestine, reticuloendothelial system, and liver parenchymal cells to all proliferating cells in the body (177,178). The elevated level of transferrin observed in this study is consistent with the need for transferrin in cellular proliferation (179).

The membrane protein VAT-1 (vesicular amine transporter 1) homolog, (also known as SLC18A1-solute carrier family 18) is located in membranes, but in this study, this protein was recovered from the cytoplasmic fraction. VAT-1 functions to accumulate cytosolic monoamines into vesicles, using the proton gradient maintained across the vesicular membrane (180). These vesicles could have fractionated with the cytoplasmic fraction in this study. Although no link to cancer development is known, it has been established that it can serve as a calcium-regulated activation marker for epithelial cells (181).

Serpins are a group of proteins with similar structures that were first identified as a set of proteins able to inhibit proteases. The name serpin is derived from this activity - **ser**ine **p**rotease **in**hibitors (120). In our study we showed serpin B13 and serpin B1 had decreased levels in OSCC compared to normal tissue.

Serpin B13 is responsible for inhibiting papain-like cysteine proteases (182) and is thought to play a role in cell proliferation and differentiation in keratinocytes (183,184). Our data is in agreement with literature reports as low levels of serpin B13 were observed in squamous cell carcinoma of the oral cavity compared with normal oral mucosa (184).

Serpin B1 is involved in regulating the activity of the neutrophil proteases elastase, cathepsin G, proteinase-3, chymase, chymotrypsin, and kallikrein-3 (185). Furthermore, it inhibits several intracellular proteases and displays anti-apoptotic activity (185).

HSP90B1, also known as GRP94, endoplasmin and tumour rejection antigen, is an endoplasmic reticulum chaperone that belongs to the HSP90 family (186). Increased HSP90B1 levels are correlated with hepatitis B virus (HBV)-induced disease progression, where HSP90B1 levels are highest in hepatocellular carcinoma (HCC) tissues (187). From these results, Zhu *et al* proposed HSP90B1 as a good candidate for a diagnostic or prognostic biomarker for HBV infection and HBV-induced diseases (187). HSP90B1 has been shown to be elevated in oesophageal cancer, however the validation of it's expression was performed via western blot analysis (70,105). This study used IHC, allowing visualisation of the sub-cellular localisation of HSP90B1 levels. Although weak staining was observed in our study, the IHC analysis showed that HSP90B1 was moderately elevated in the cytoplasm of tumour tissue, suggesting that it may have potential as a biomarker for oesophageal cancer; however, this will require further investigation.

Previous proteomic studies on oesophageal cancer have identified a number of proteins as differentially expressed. Methods used included Laser Capture Microdissection (LCM), to isolate proteins from whole cell lysates from one case (70,105,162). The proteins were then either subjected to conventional 2DE methods or 2D-DIGE linked to MS to identify the proteins (70,105,162,188).

In our study we pooled samples, as described above, in order to overcome the inter-individual heterogeneity between oesophageal cancer patients. We are, however, confident that the differences in expression patterns displayed for proteins were significant as they were representative of the protein of interest's expression in three separate gels and normalized with an internal standard (Figure 4b).

A total of 39 differentially expressed proteins were identified, which constituted a substantially different group of proteins to those in the studies reported by Qi *et al* (188), Zhou *et al (70,105)* and Uemura *et al* (162). HSP90B1 was common to our study, Qi *et al* (188) and Zhou *et al* (70,105). The identification of transglutaminase-3 was shared between our study and Uemura *et al* (162).

To our knowledge none of the previous studies identified annexin 2 and gelsolin to be differentially expressed. We validated annexin 2, HSP90B1, gelsolin, GAPDH and pyruvate kinase expression using immuno-histochemical analyses. Previous studies have utilized western blot analyses to confirm protein expression patterns (105,188). However, IHC has the added advantage that it also provides information regarding localization of the protein during the tumourigenic process (162).

In summary, this study has identified a number of proteins that are differentially expressed in tumour tissue compared to normal tissue from oesophageal cancer patients. Further functional studies of annexin 2 could validate its potential use as either an early diagnostic marker and/or prospective therapeutic target. Furthermore, this study highlights the importance of validating protein expression data obtained from proteomic studies using a method that permits the demonstration of the sub-cellular localization.

3 Altered glycoprotein profile in OSCC cell line compared to an immortalized normal oesophageal cell line

3.1 Introduction

Membrane proteins displaying elevated expression in tumour tissue relative to normal tissue have attracted considerable attention from cancer biologists recently as potential therapeutic targets or diagnostic markers. Unfortunately, membrane proteins are particularly difficult to separate in 2D gel systems and consequently other approaches, to profile the expression of membrane proteins, have been explored.

The work reported in this section exploits the observation that most proteins on the cell surface are glycosylated by the post-translational linkage of carbohydrate moieties to specific amino acid residues (189). Protein glycosylation facilitates protein folding and stability, and plays an important role in cell adhesion and recognition process (189,190). Two categories of glycosylation have been identified: N-

linked glycosylation and O-linked glycosylation (Fig 3.1). In N-linked glycosylation, the addition of carbohydrate moiety occurs at the amide nitrogen on the side chain of asparagine residues (Fig 3.1a). In O-linked glycosylation, the addition of the carbohydrate moiety occurs on the hydroxyl oxygen on the side chain of hydroxylysine, hydroxyproline, serine, or threonine residues (Fig 3.1b) (189).

In serine-and threonine -type *O*-linked glycoproteins, the carbohydrate moiety that is directly attached to the protein is GalNAc (N-acetylgalactosamine), whereas GlcNAc (N-acetylglucosamine) is directly linked to asparagine in N-linked glycoproteins. The carbohydrate chains in glycoproteins vary in length, composition and complexity (189,190). The carbohydrate chains typically include N-acetylgalactosamine, N-acetylglucosamine, galactose, mannose, fucose, glucose, glucuronic acid, sialic acid and xylose. These can be organized in either simple, linear or complex, branched structures with O-linked glycoproteins less complex in comparison to N-linked glycoproteins (189,190). Protein glycosylation contributes extraordinary diversity to the chemical structure of proteins, thereby extending their functional role.

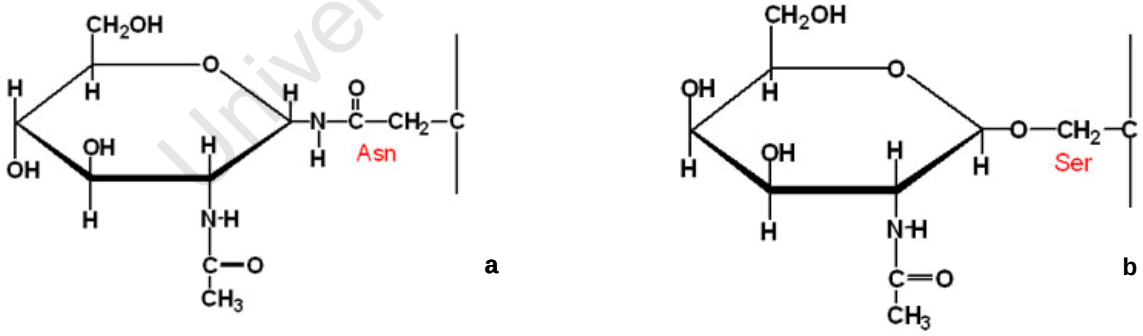

Figure 3.1: Types of glycosylation (a) N-linked glycosylation: N-acetylglucosamine linked to asparagine (b) O-linked glycosylation: N-acetylgalactosamine linked to serine (figure adapted from (191)

Glycosyltransferases are responsible for catalyzing the addition of these carbohydrate moieties to proteins via an assembly line in the endoplasmic reticulum and Golgi compartment (189,190). In contrast to glycoprotein assembly, the hydrolysis of glycoproteins occurs within lysosomes with various enzymes participating in the hydrolysis, depending on the complexity of the glycoprotein (189,190). Since most proteins on the cell surface are glycosylated, this provides an opportunity to target cell-surface proteins. The enzymatic reactions involved in the glycosylation and de-glycosylation reaction have been exploited in the development of the proteomic approach utilized in this study (96).

In this study, we targeted cell-surface glycoproteins with carbohydrate chains that terminate in galactose residues. Principally, the approach involves enzymatically replacing terminal galcatose residues with radio-labeled galactose, followed by the separation of membrane proteins on polyacrylamide gels. The enzyme used to hydrolyse the terminal galactose moiety in cell-surface glycoproteins is beta-galactosidase. Within the cell other substrates of beta-galactosidase include ganglioside GM1, lactosylceramides and lactose, but this method specifically targets cell-surface proteins (as described in Materials and Methods).

The galactose moieties that were enzymatically removed are replaced by ^{3}H or ^{14}C – galactose, which are enzymatically added by galactosyltransferase (a glycosyltransferase specific for the addition of galactose moieties). The novelty of this approach resides on our ability to label cells from two different conditions (e.g. normal and cancer cells) with either ^{3}H or ^{14}C – galactose, combining the samples followed by separation in the same lane by SDS-PAGE (as described in Materials and Methods).

Although the method used in this chapter does not have the same resolving capacity as 2D-DIGE, it allows the separation of membrane proteins that are difficult to resolve in the IEF steps of 2D-DIGE.

Furthermore, the availability and access to this particular method encouraged the use of this method as opposed to more cutting-edge methods currently available.

In this study, a labelling method exploiting de-glycosylation and glycosylation was used to determine altered protein expression in a cultured oesophageal cancer cell line in comparison to an immortalized normal cultured oesophageal cell line. Proteins with altered expression in tumour cell lines compared to normal were identified and their expression status confirmed by immunohistochemistry in tissue sections.

3.2 Materials and methods

3.2.1 Propagation of cell lines

Two cell lines, WHCO1 and EPC-2, were used in this section of the study. The WHCO1 cell line was derived from a squamous cell carcinoma of the oesophagus of moderate differentiation status, prepared at the University of Witwatersrand in South Africa and provided as a gift by Dr Rob Veale (University of Witwatersrand, South Africa).

The EPC-2 cell line was developed from squamous epithelial cells, derived from the morphologically normal proximal oesophagus of a 55 year old male who underwent an oesophagectomy for Barret's

oesophagus. The cell line was immortalized with telomerase and provided as a gift by Prof A. Rustgi (University of Pennsylvania, Philadelphia, USA).

WHCO1 cells were cultured and maintained in DMEM (Gibco-BRL, USA) containing 10% heat-inactivated FBS (Gibco-BRL, USA), 100 units/ml penicillin and 100µg/ml streptomycin. EPC-2 cells were grown in KSFM (Gibco-BRL, USA) supplemented with 50µg/ml bovine pituitary extract (Gibco-BRL, USA), 1ng/ml epidermal growth factor (Gibco-BRL, USA), 100 units/ml penicillin and 100µg/ml streptomycin. Both cell lines were incubated at 37ºC with 5% CO_2 humidity. On reaching confluency, the cells were rinsed and then removed from the substratum, with 0.05% trypsin in PBS containing 10 mM EDTA, by incubation at 37ºC for 3-5 minutes. In the case of WHCO1 cells, trypsinisation was inhibited by the addition of an equal amount of DMEM containing 10% FBS. However, in the case of the EPC-2 cells, trypsinisation was inhibited by the addition of 0.25ng/ml Soya Bean Trypsin Inhibitor (Sigma, USA). The cells were pelleted by centrifugation at 500 X g for 5 min, at 4°C (in a Beckman TJ-6), re-suspended in appropriate media and split at a ratio of 1:5 (to maintain cultures).

3.2.2 Labeling of plasma membrane glycoproteins, plasma membrane protein preparation and protein separation

Labelling of the plasma-membrane glycoproteins was performed according to a previously described method (96), with a few adaptations, courtesy of Dr Chris Maske (Division of Anatomical Pathology, University of Cape Town).

For each experiment, $0.5X10^6$ cells were plated per 60 mm dish and incubated at 37ºC with 5% CO_2 with humidity for up to 48 hours. Cells were subsequently placed on ice immediately prior to the labelling step and kept at 4°C for the duration of the experiment, in order to avoid membrane internalization.

Once the media was aspirated, the cells were washed twice with ice-cold HEPES buffered saline. Cells were then treated with 100 µl of 0.2U/ml beta-galactosidase (prepared from *Streptococcus pneumoniae* and provided as a gift from Prof Lutz Thilo - Division of Medical Biochemistry, University of Cape Town) for 10 minutes at 4°C, to remove terminal galactose on the cell surface proteins. This was done by placing the 100µl beta-galactosidase in the centre of the dish and placing a 60mm disks over the surface of the plate, to spread the beta-galactosidase evenly across the dish, as illustrated (Fig. 3.2). The, disks had been cut from overhead transparency film (Pelikan, UK), and washed in 0.1% detergent, rinsed twice in distilled water, rinsed with 70% ethanol and allowed to air-dry. After the 10 min β-galactosidase treatment, the disks were gently removed and the cells subsequently washed twice with ice-cold HEPES buffered saline, to remove the excess β-galactosidase. Cells were then labelled for 30 minutes at 4°C with a labelling/incubation mix (40µCi/ml UDP[6-^{3}H]Gal or UDP [U-^{14}C]Gal, 0.5 U/ml Galactosyltransferase and 5mM MnCl) in the same manner as described for the β-galactosidase treatment and subsequently washed twice with ice-cold HEPES buffered saline. Cells were collected in 300 – 500 µl homogenisation buffer (containing a protease inhibitors cocktail – c*O*mplete, Roche) per dish, by scraping with a sterile rubber policeman and mechanically sheared by passing the collected cell suspension through a cell cracker. The post-nuclear supernatant (PNS) was prepared by centrifuging the cell homogenate at 1000 X g in a Beckman GS-6R for 12 minutes at 4°C. A 20 µl aliquot of the PNS was placed in 3 ml scintillation fluid (Zinzer Analytic, UK) and counted in a Liquid Scintillation Analyzer 1900 CA (PACKARD, USA), to determine total dpm (disintegrations per minute) of labelled homogenate. This served as the first

checkpoint to determine if sufficient labelling had occurred. The experiment was terminated at this point if the total dpm of the labelled homogenate was less than 100 000 dpm.

A layer of 0.5 ml 80% sucrose was deposited at the bottom of a Beckman Polyallomer centrifuge tube (14 X 95 mm), above which a layer of 27% Percoll was placed, as illustrated (Fig. 3.2). The PNS (approximately 2ml) was then slowly layered onto the 27% Percoll ® (Sigma, USA) gradient (as described in Appendix A) and the tube was centrifuged at 30 000 X g at 4 °C for 90 min in an SW-40 rotor in a Beckman LM-8 ultra-centrifuge.

After centrifugation, the sample was fractionated and 20µl aliquots, from each fraction, was placed in 3ml scintillation fluid and counted in a Liquid Scintillation Analyzer 1900 CA (PACKARD, USA), to determine the amount of label in each fraction. Plasma membrane fractions corresponded to the fractions displaying peak dpm values. The fractions containing the plasma membrane fraction were collected, pooled and made up to 12 ml with ice-cold homogenisation buffer in a Beckman Polyallomer centrifuge tube (14 X 95 mm). The re-suspended membrane fraction was centrifuged at 130 000 X g for 2 hours at 4°C in an SW-40 rotor in a Beckman LM-8 ultra-centrifuge to pellet the membranes. The supernatant was discarded and the pellet was re-suspended in 2.5 ml 0.5M KCl and transferred to a thick-walled Beckman tube. The samples were sonicated 12 times for 5 seconds, whilst on ice. Sonication allowed the disruption of membranes that formed micelles, facilitating the release of the content of the micelles, thereby allowing the purification of membranous particulate only. The samples were then centrifuged at 70 000 X g at 4°C for 1 hour in a Beckman 70.1 Ti rotor in a Beckman LM-8 ultra-centrifuge to pellet the membrane fraction. The opaque membrane pellet was collected and the label quantitated by counting a series of aliquots (2µl, 4µl and 8µl) in a liquid scintillation analyzer. These values were used to calculate the yield of radioactively labelled membranes.

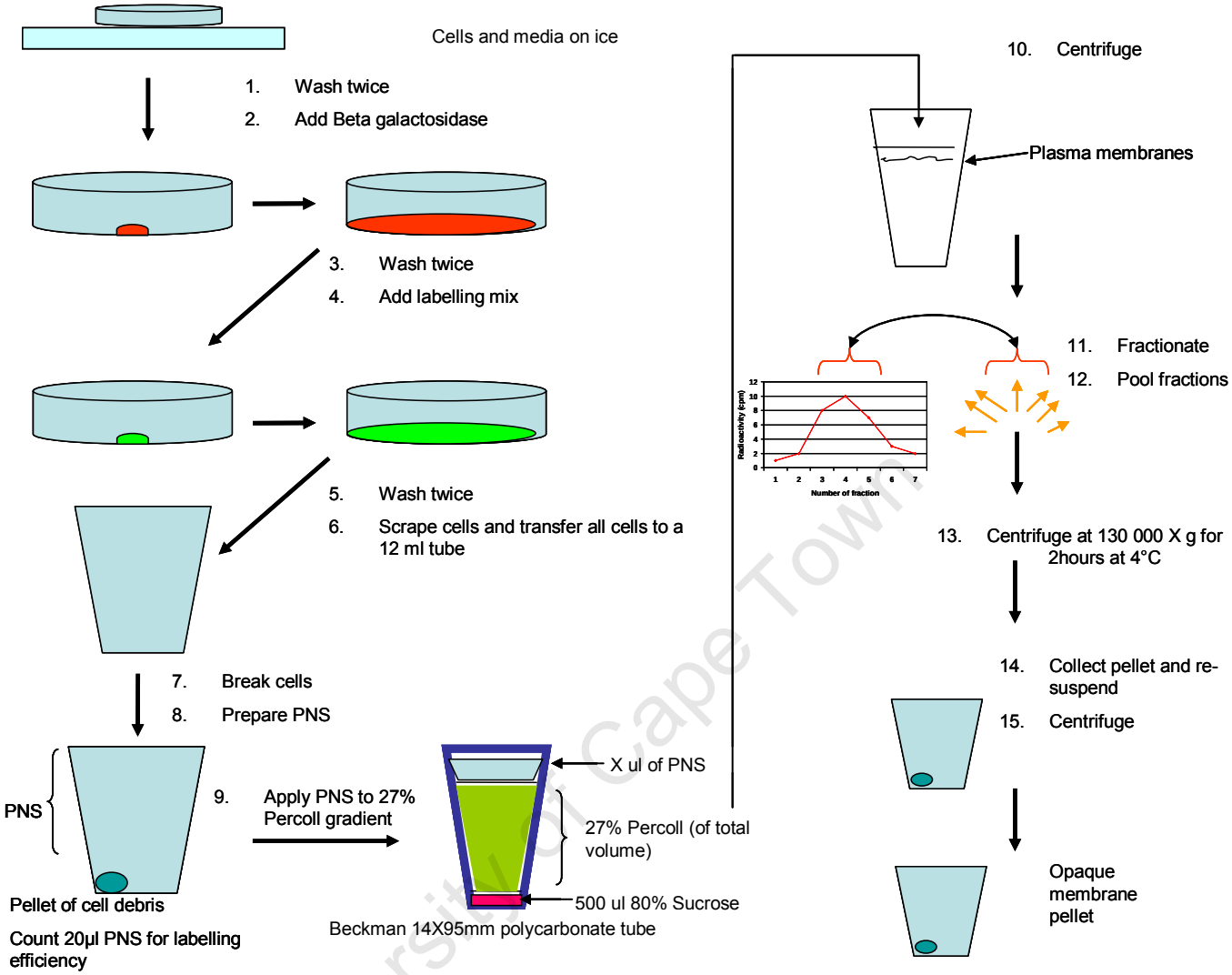

Figure 3.2: Labelling method: Flow diagram describing method of labelling plasma-membrane glycoproteins. (1) Remove media and wash twice with Hepes saline (2) Place 100 µl Beta galactosidase in centre of dish and gently overlay transparency disk to spread (3). After 10 min remove disk and wash twice with Hepes saline (4)Place 100 µl labelling mix (containing ^{3}H and ^{14}C) in centre of dish and gently overlay transparency disk to spread (5) After 30 min remove disk and wash twice with Hepes saline (6) Scrape cells with rubber policeman in up to 500µl homogenisation buffer and transfer all cells to a 12 ml tube (7) Mechanically shear cells with a cell cracker (8) Prepare PNS via centrifugation (500 X g for 12 minutes) (9) Apply PNS to 27%Percoll gradient (10) Centrifuge at 30 000 X g for 90 min at 4°C (11) Fractionate via mechanical fractionation (12) Pool fractions corresponding to radioactively labelled plasma membrane with homogenization buffer (13) Centrifuge at 130 000 X g for 2hours at 4°C (14) Collect opaque pellet, re-suspend in 0.5M KCl and sonicate (15) Centrifuge at 70 000 X g for 1 hour at 4°C to reveal the membrane pellet.

One part ^{14}C-labelled proteins were mixed with 4 parts ^{3}H-labelled proteins, re-suspended in loading buffer (see Appendix A) and separated on a gradient of 8% to 15% by SDS-PAGE (Fig 3.3 - lane 3)

(details in Appendix A). ^{14}C-labelled proteins were always loaded in excess to ^{3}H-labelled proteins in lane 3, as the energy emission spectra for ^{14}C and ^{3}H overlap. During subsequent dual counting of these radio-isotopes (via liquid scintillation counting), the ^{14}C energy emission that overlaps into the ^{3}H energy emission window is not included in ^{3}H counts. However, due to the overlap in energy emission spectra more ^{3}H label needs to be included to raise ^{3}H energy emission above background ^{14}C energy emission.

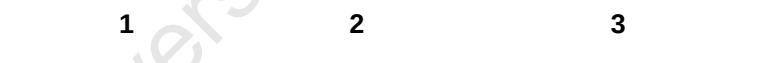

Figure 3.3: Sample Loading: Scheme illustrating sample loading for ^{14}C and ^{3}H- labelled membrane protein fraction. Lane 1: Molecular-weight marker, Lane 2: Two parts ^{14}C-labeled protein and Lane 3: Mixture of one part ^{14}C and four parts ^{3}H- labelled membrane protein. The vertical red line in Lane 2 indicates that the lane was cut into two parts and used for counting and MS analysis, respectively.

A molecular-weight marker was loaded in lane 1, and 2 parts ^{14}C-labelled protein was loaded in lane 2, for subsequent identification and analysis (Fig 3.3). ^{14}C-labelled proteins from half of lane 2 were used as an internal control. ^{14}C- labelled proteins from lane 2 should have approximately double the value of ^{14}C-labelled proteins in lane 3. Therefore ^{14}C- labelled proteins from half of lane 2 should have similar values compared to ^{14}C-labelled proteins in lane 3, assuming co-migration of proteins in

lanes 2 and 3 in the poly-acrylamide gel. In principle, this step provides a mechanism to check that the proteins in the gel slice of interest in lane 3 correspond to the same proteins in the gel slice in lane 2.

3.2.3 Post-staining, gel anlysis, slice excision and digestion

Gels were stained with Coomassie Blue; typically, gels were stained and fixed in coomassie blue staining solution for 12 minutes and subsequently de-stained overnight. The following steps were performed with gloves in a sterile area, free of contaminating proteins. All utensils and surface areas were washed with detergent and sprayed down with 70% ethanol. Gels were dried and a grid with slices 0.5 mm in height and 1.5 cm wide was drawn on the gel in order to excise slices for further analysis.

Half of the gel slices in lane 2 (indicated by the red line in Fig. 3.3) and the gel slices from lane 3 were subsequently processed as follows (Fig. 3.4). The proteins in the excised slices from the stained gel were in-gel digested in 1.5 ml Eppendorf tubes, with 1 ml trypsin-EDTA, pH 7.4 at 37°C overnight. The extracted peptides from the first round of extraction in the 1 ml trypsin was transferred to a scintillation vial with 3 ml scintillation fluid and stored O/N in the dark at room temperature. Another 1 ml trypsin-EDTA was added to the remaining gel slice O/N at 37°C, for a second round of peptide extraction (Fig. 3.4). The second round of extracted peptides in the 1 ml trypsin was added to the scintillation vial as from the first round. Label was measured on a dual counting protocol on the liquid scintillation analyzer, to separately give the dpm for each isotope as an indication of amount of labelled peptides of each type. In each O/N extraction, care was taken to ensure that no gel slice residue was transferred to the scintillation fluid.

The data obtained were normalized and represented graphically (Graphpad Prism version 5 and Microsoft Excel Software ©). The data were plotted as a profile of radioactivity against the slice

number. For direct comparison of two profiles (^{3}H or ^{14}C), the relative areas under each profile were normalized to the same/similar values.

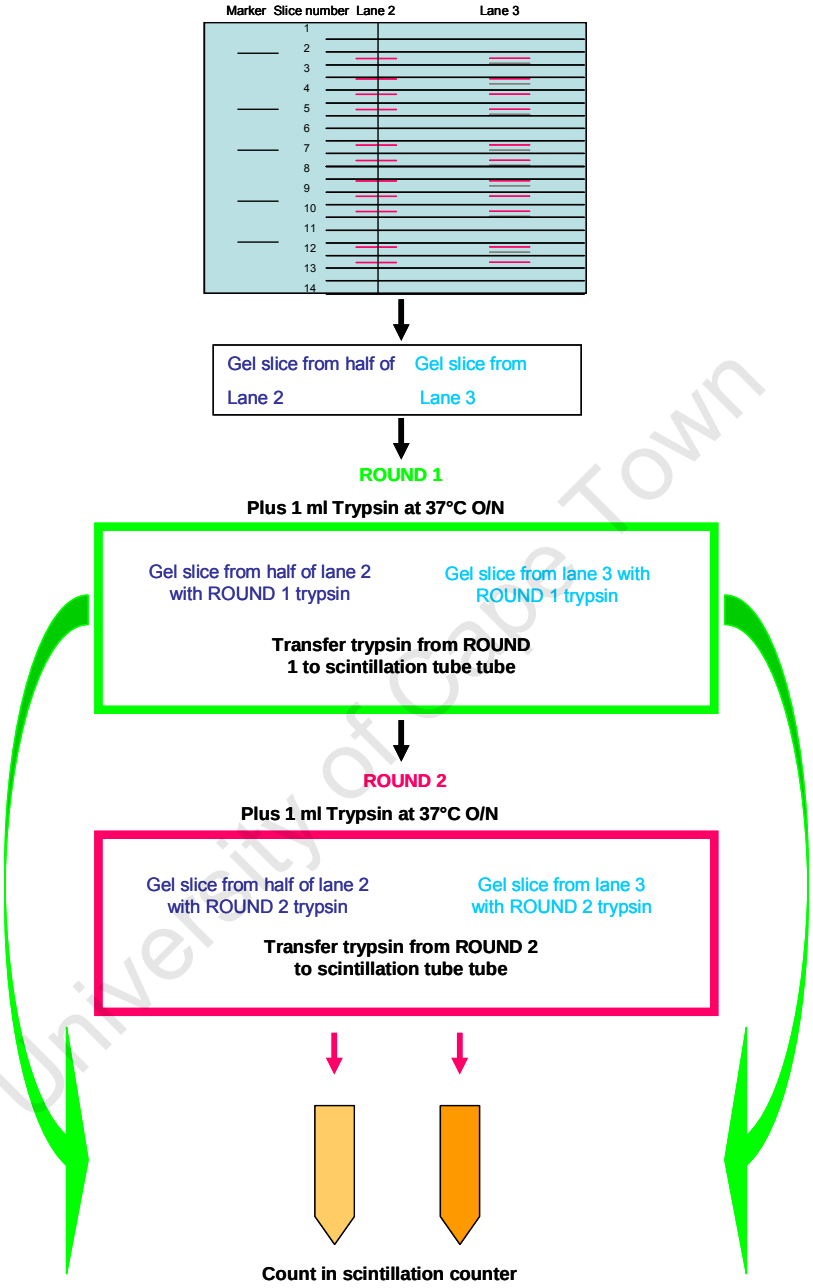

Figure 3.4: Gel trypsinisation: Scheme illustrating procedure for trypsinisation of gel slices, to release radioactively labelled peptides for counting in a liquid scintillation analyzer.

In order to observe differences in protein expression in tumour compared to normal cells, ratios of the two labels in each slice were calculated and compared.

Slices that displayed reproducible differences between all three experiments were further investigated. Slices of interest from lane 3 were targeted for further investigation and the corresponding gel slice from the remaining half of lane 2 was sent for identification.

3.2.4 ESI-QUAD-TOF MS and identification of proteins

Gel slices from lane 2 were stored at RT, until further use. Digested peptide extracts were subjected to electron-spray ionisation linked to a quadrupole-time-of-flight mass analyser (ESI-QUAD-TOF). Proteins were subsequently identified using Mascot Daemon (Matrix Science, UK). Identifications were accepted when percentage protein coverage exceeded 25% and MOWSE scores were higher than the threshold value (P=0.05), the predicted protein mass agreed with the gel-based mass and the proteins identified were human. Once proteins were identified, the expression levels of the protein in tumour tissue were compared to normal tissue using immunohistochemical staining on tissue sections.

3.2.5 Confirmation of protein expression by IHC

Frozen sections of tumour and normal tissue from 10 oesophageal cancer patients were used. Sections were blocked for endogenous peroxidase activity by submerging the slides in 3% hydrogen peroxide for 20 minutes. The slides were then incubated at room temperature with a 1/20 dilution of goat serum (Dako, California) for 30 minutes. The mouse antibody to CD98 (heavy chain) (C2443-81, Unites States Biological) was used at a dilution of 1/250 for 1 hr at RT. The omission of the primary antibody served as a negative control in each case. The Envision-polyallomer detection system (DAKO, California) was used according to manufacturer's instructions to visualise the location of the antibody. Sections were visualized by staining with DAB chromagen as previously described in

Chapter 2. Sections were counterstained with haemotoxylin and subsequently dehydrated. The slides were independently evaluated by a qualified anatomical pathologist.

The criteria used to score IHC staining are outlined in Table 3.1. CD98 is expressed on the plasma membrane and therefore membrane staining in cells was evaluated when scoring IHC staining.

Table 3.1: Criteria used by independent pathologist for scoring IHC slides. Slides were assigned a score of 0 to 4+ based on the percentage membrane staining observed in a tissue section.

Intensity	Percentage membrane staining in field of view
0	less than 5% stained
1+	between 5 and 25% stained
2+	between 26 and 50% stained
3+	between 51 and 75% stained
4+	more than 75% stained

3.3 Results

3.3.1 Radioactive labeling of plasma membrane glycoproteins

Checkpoints were included at various steps in the radioactive labelling method in order to determine the efficiency of the labelling procedure. Essentially, aliquots were taken at these checkpoints for measuring labelling efficiency. The results that follow are representative of 3 experiments performed, but only the details of one are presented here.

The first checkpoint was taken subsequent to preparing the PNS. On average the total counts in the PNS exceeded 100 000 dpm for both ^{3}H and ^{14}C labelling. Counts above this threshold indicated that there was sufficient labelling to continue with the experiment. In all cases labelling efficiency was higher in WHCO1 cell lines (^{14}C labelled) compared to EPC-2 hTERT (^{3}H labelled). The total dpm of the PNS from each were 845 716 dpm and 532 800 dpm, respectively.

Once the PNS was fractionated, the bulk of the label was concentrated in the fraction, which contained the membrane proteins (Fig. 3.5). The elution profile of the labelled protein reflected the volume of the PNS loaded on the Percoll gradient. Fractions 14 to 18 (from ^{14}C labelled proteins) and fractions 12 to 18 (from the ^{3}H labelled proteins) (Fig. 3.5) were pooled and membrane proteins were collected by centrifugation, followed by washing proteins as described in Materials and Methods.

Subsequent to washing, aliquots of the purified plasma membrane protein preparation were counted on a liquid scintillation analyzer, in order to calculate the amount of radioactively labelled proteins in the sample. For efficient analysis by SDS-PAGE, the protein samples had to fulfil two criteria. First, the intensity of labelling should be sufficient so that more than about 3000 dpm could be loaded on a lane. This was required so that sufficient counting accuracy was obtained. Second, at least 4-fold

more radioactivity must be loaded for the ^{3}H-labelled samples, in order to minimise the effects of ^{14}C-spillover with the ^{3}H counting channel during dual isotope scintillation counting.

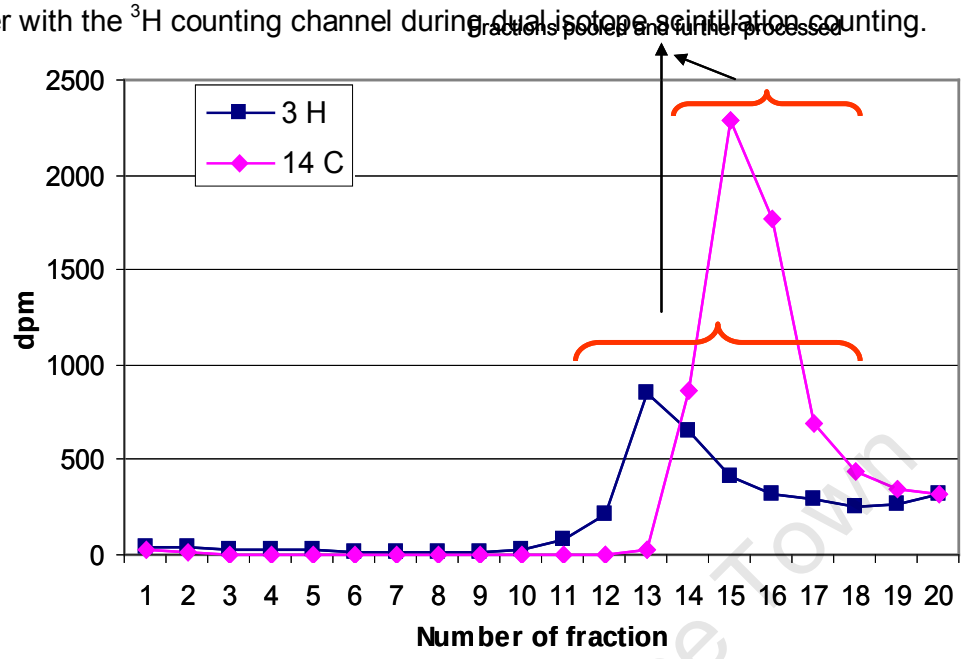

Figure 3.5: Elution profile of labelled PNS after density centrifugation on a 27% Percoll gradient. PNS's were prepared from WHCO1 cells (^{14}C, total 845 716 dpm ▲) and from EPC-2 cells (^{3}H, total 532 800 dpm ◆). Fractions that contained labelled membrane proteins (indicated by the red brackets) were collected for further analysis)

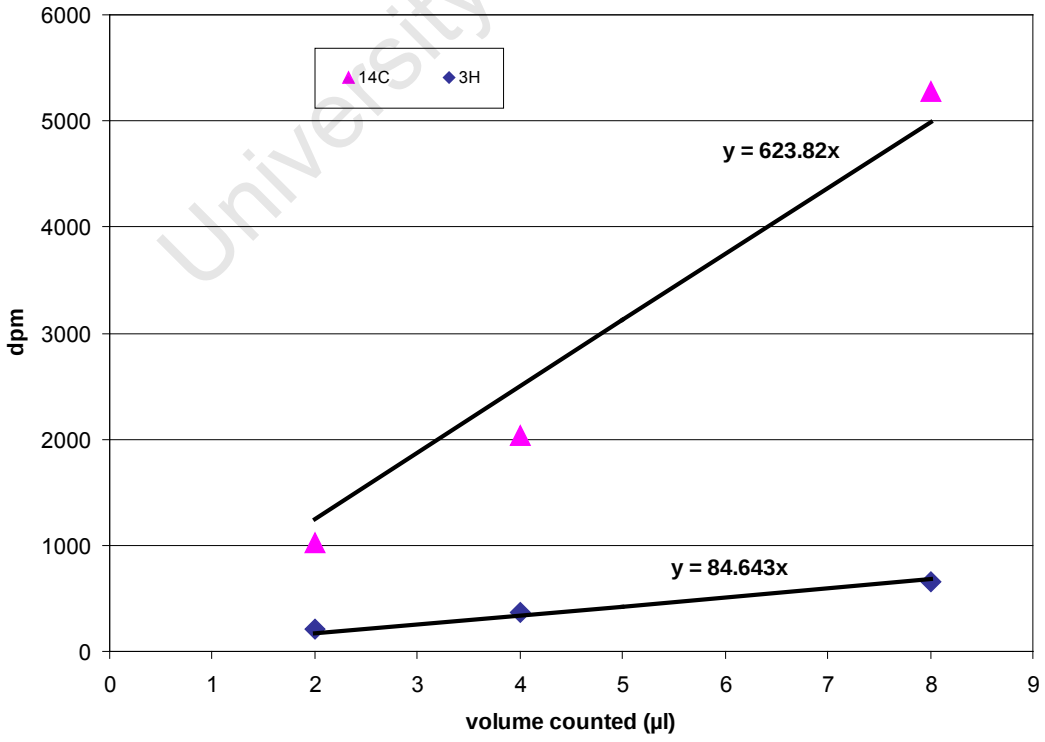

Figure 3.6: Data representative of method used to calculate concentration of radioactively labelled sample: Aliquots of 2, 4 and 8µl were counted on a liquid scintillation analyzer and the corresponding dpm plotted, as shown. The concentration of label (dpm/µl) was obtained from the slope of a linear regression line. ^{3}H-labelled protein profile in blue (—◆—) and the ^{14}C- labelled profile in pink (—▲—).

The data presented here are indicative of a typical labelling efficiency (Fig. 3.6). The concentration calculated for the ^{14}C-labeled protein sample is 623.82 dpm/µl and the concentration for ^{3}H-labelled protein sample is 84.64 dpm/µl (Fig. 3.6). Concentrations of samples were calculated as described in Materials and Methods.

3.3.2 Profile pattern of proteins showing altered levels of expression

Separation of proteins on large format 1-dimensional SDS polyacrylamide gels allowed the excision of 60-100 slices per lane. As described in Materials and Methods, these slices were trypsinized and the radioactivity of eluted peptides were quantitated by scintillation counting.

Representative data are summarized in Table 3.2. In this experiment, the sum of the dpm of ^{3}H-labelled proteins from lane 3 (as in Fig 3.3) was 6152.31 dpm, the sum of the dpm of ^{14}C-labelled proteins from lane 2 (as in Fig. 3.3) was 6609.9 dpm and the sum of the dpm of ^{14}C-labelled proteins from lane 3 (as in Fig. 3.3) was 4975.31 dpm. For a direct comparison of the radioactivity profiles, the areas under the curve were normalised to the same value, as outlined in Materials and Methods (Table 3.2). Normalized dpm values were then plotted versus slice number, to yield data as represented in Figure 3.7.

Figure 3.7 is a representative image of 3 independent experiments. Different levels of expression in the tumour cell line compared to the normal cell line, were observed (Top panel in Fig.3.7). The four slices corresponding to slices 15, 17, 24 and 27, highlighted as pink, blue, orange and green respective bands running vertically through the graph (Fig 3.7), were reproducibly found to display elevated levels in the tumour cell line compared to the normal cell line. Furthermore, the average

ratios of peptides from these gel slices displayed at least 1.5–fold increased levels in tumour compared to normal cells (Table 3.3).

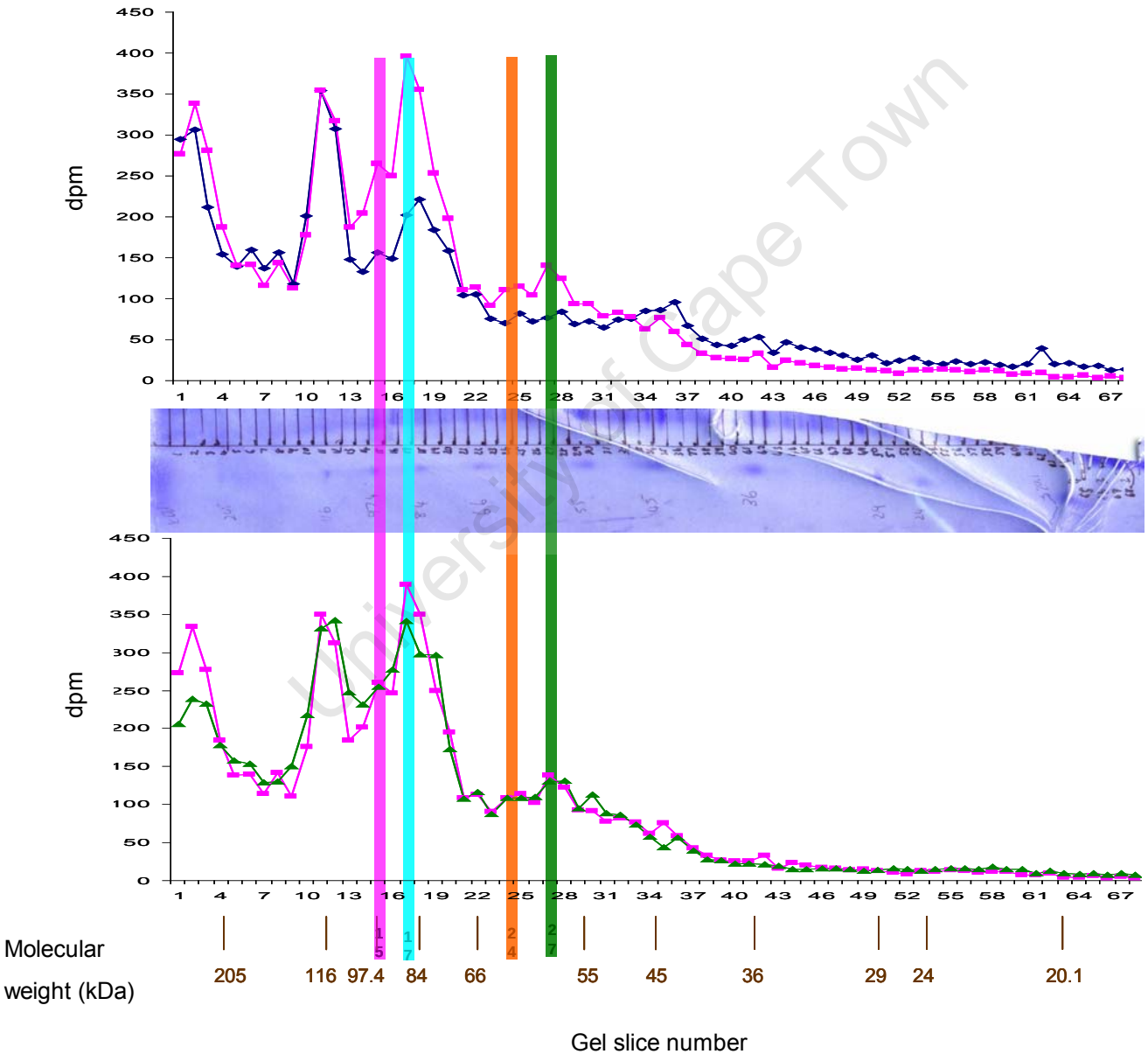

Figure 3.7: Radioactive profiles: Radioactive profile of glycosylated proteins on the surface of WHCO1 cells, labelled with ^{14}C, and glycosylated proteins on the surface of EPC-2 cells, labelled with ^{3}H. The top panel displays the ^{3}H-labelled protein profile in blue (—◆—) and the ^{14}C- labelled profile in pink (—■—) from the lane in which the labelled samples were mixed (Lane 3 in Figure 3.3). The middle panel shows half of the lane (Lane 2 in Figure 3.3) containing ^{14}C-labelled protein only (used to identify proteins of interest via ESI-QUAD-TOF-MS). The other half of this lane (Lane 2 in Figure 3.3) was prepared (as described in Materials and Methods) to yield the profile of ^{14}C-labelled proteins (—▲—), as seen in the bottom panel, in comparison to the ^{14}C-labelled proteins from the lane in which the labelled samples were mixed (Lane 3 in Figure 3.3). The brown lines indicate the position of the molecular weight markers. The pink (slice 15), blue (slice 17), orange (slice 24) and green (slice 27) elongated boxes across the image highlight the proteins of interest that were picked and sent for identification via ESI-QUAD-TOF-MS analysis.

	Original values			Normalized values	
Slice number	^{14}C counts from lane 3 (dpm)	^{3}H counts from lane 3 (dpm)	^{14}C counts from lane 2 (dpm)	^{14}C counts from lane 3 (dpm) normalized to ^{3}H counts in lane 3	^{14}C counts from lane 3 (dpm) normalized to ^{14}C counts lane 2
1	205.0867	295.03	205.4	254.30747	272.76527
2	250.7	305.8867	238.37	310.868	333.431
3	208.16	211.37	231.95	258.1184	276.8528
4	138.46	153.9633	177.66	171.6904	184.1518
5	104.28	139.2	158.06	129.3072	138.6924
6	104.8933	159.31	153.52	130.06773	139.50813
7	85.56333	137.6767	129.33	106.09853	113.79923
8	106.4867	156.6933	130.13	132.04347	141.62727
9	83.45	117.9833	150.59	103.478	110.9885
10	131.9033	201.5233	217.78	163.56013	175.43143
11	262.75	353.86	331.28	325.81	349.4575
12	234.9833	307.7367	342.54	291.37933	312.52783
13	138.91	147.5367	247.03	172.2484	184.7503
14	151.3133	132.7667	231.76	187.62853	201.24673
15	195.9733	156.6467	255.11	243.00693	260.64453
16	185.4267	149.2333	277	229.92907	246.61747
17	292.87	202.6433	341	363.1588	389.5171
18	263.19	221.6233	297.75	326.3556	350.0427
19	187.5733	184.5267	296.69	232.59093	249.47253
20	146.6633	158.76	172.38	181.86253	195.06223
21	81.83	103.79	107.64	101.4692	108.8339
22	84.66	104.9167	116.38	104.9784	112.5978
23	68.16	75.15667	87.66	84.5184	90.6528
24	81.98	70.25	109	101.6552	109.0334
25	85.42	82.16	108.24	105.9208	113.6086
26	76.98	71.89	109.7	95.4552	102.3834
27	104.3867	76.77667	129.67	129.43947	138.83427
28	92.4	83.51667	130.71	114.576	122.892
29	69.43333	68.75667	94.99	86.097333	92.346333
30	69.24667	72.39	113.22	85.865867	92.098067
31	58.52333	64.77667	88.92	72.568933	77.836033
32	61.41333	73.98667	86.28	76.152533	81.679733
33	57.63	75.61667	73.36	71.4612	76.6479
34	46.13333	84.7	57.11	57.205333	61.357333
35	56.57	85.95667	43.61	70.1468	75.2381
36	43.76	95.4	56.01	54.2624	58.2008
37	32.31333	67.53333	39.88	40.068533	42.976733
38	24.76333	51.5	27.94	30.706533	32.935233
39	20.42	43.55	26.99	25.3208	27.1586
40	19.50667	42.47	22.59	24.188267	25.943867
41	18.92667	49.66	22.82	23.469067	25.172467
42	24.45667	53.49	20.88	30.326267	32.527367
43	11.66667	33.64333	18.86	14.466667	15.516667
44	17.73667	47.22	14.71	21.993467	23.589767
45	15.43667	40.50667	15.06	19.141467	20.530767
46	13.22667	37.97	15.86	16.401067	17.591467
47	11.73333	33.95667	16.46	14.549333	15.605333
48	10.20667	30.5	15.37	12.656267	13.574867
49	11.16333	25.56667	12.92	13.842533	14.847233
50	9.23	30.7	14.26	11.4452	12.2759
51	8.4	21.67333	16.31	10.416	11.172
52	6.556667	23.98333	15.12	8.1302667	8.7203667
53	9.25	27.58	13.13	11.47	12.3025
54	9.193333	21.46667	15.05	11.399733	12.227133
55	10.21	20.39333	16.09	12.6604	13.5793
56	9.603333	23.46	15.55	11.908133	12.772433
57	8.12	20.05667	14.41	10.0688	10.7996
58	9.213333	22.46667	18.09	11.424533	12.253733
59	8.65	19.49333	15.36	10.726	11.5045
60	5.536667	17.44333	14.86	6.8654667	7.3637667
61	5.996667	20.66667	9.11	7.4358667	7.9755667
62	7.093333	38.94667	12.85	8.7957333	9.4341333
63	3.403333	19.79333	10.01	4.2201333	4.5264333
64	3.253333	21.51	8.1	4.0341333	4.3269333
65	4.596667	16.52667	9.44	5.6998667	6.1135667
66	2.283333	17.84667	7.16	2.8313333	3.0368333
67	3.966667	12.38667	9.3	4.9186667	5.2756667
68	2.033333	14.34	7.53	2.5213333	2.7043333
Sum of counts (dpm) or area under the curve	**4975.31**	**6152.31**	**6609.9**	**6169.3844**	**6617.1623**

Table 3.2: Data of counts obtained for gel slices containing radiolabeled proteins (dpm): In this experime 68 slices (0.5 mm X 1.5 cm) were excised from lanes 2 and 3 (see Fig. 3.4). Gel slices were trypsinized and peptides eluted, as described. Radioactivity of eluted peptides were counted on a liquid scintillation counter. Counts were normalized to give the same area under radioactivity profile, as described in Materials and Metho

The matched gel slices from lane 2 were subsequently digested and subjected to ESI-QUAD-TOF MS for identification.

3.3.3 Identification of proteins

Staining of gels revealed that protein levels were too low for Coomassie Blue detection and possibly, for successful MS-based identification. Of the four slices subjected to ESI-QUAD-TOF-MS analysis, only one slice was successfully identified (Gel slice 17 in Fig. 3.7 and).

The scoring system used here is based on the MOWSE scoring algorithm (used in Mascot searches). Probability-based MOWSE scores for peptides obtained from gel slices 15, 24 and 27 indicated that no significant hits were identified (Fig. 3.8 a, c and d). The probability-based MOWSE scores obtained for peptides from gel slice 17 indicated a number of hits that exceeded the significance threshold ($p < 0.05$) (Fig. 3.8 c and f). Although the percentage coverage of the protein identified is only 12% (lower than the limits outlined in Materials and Methods i.e. 25%), the probability that this identification is correct is significantly high, as the top 10 significant hits indicate the same protein (i.e. member of the solute carrier 3 protein family) with varying percentage protein coverage (Fig. 3.8 e and f).

The protein identified is a member of the solute carrier 3 protein family of amino acid transporters and will be referred to as CD98 hc from this point. According to its location on the gel, it corresponds to approximately 85 kDa (Fig. 3.8). However, bioinformatics search engines predict its molecular weight at approximately 57.9 kDa, (accession number: P08195). However, the predicted mass generated by the search engines does not take into account glycosylation status, which would affect the electrophoretic mobility of this protein in an SDS-PAGE gel. Reports in the literature confirm that the molecular mass, based on SDS-PAGE analysis of CD98 hc, is indeed approximately 80kDa (192).

Figure 3.8: Images reproduced from Mascot search results (www.matrixscience.com): (a), (b), (c) and (d) indicate probability based MOWSE score for gel slices 15, 17, 24 and 27, respectively. Each red bar indicates a hit observed for the peptide of interest, however, only red bars NOT in green shaded areas are considered significant as in (b) where the probability-based MOWSE score for gel slice 17 indicates that all scores above 70 are significant ($p < 0.05$). Score is -10*Log(P), where P is the probability that the observed match is a random event. (e) The green box highlights the top 10 significant protein identifications that displayed the highest score for peptides from gel slice 17. The red box outlines the most significant hit as being a member of solute carrier family 3 and (f) displays amino acid sequence of solute carrier 3 protein where red highlighted amino acids are those that matched amino acid sequences from peptides obtained from gel slice 17, amounting to a 12% protein coverage.

Table 3.3: Results of proteins sent for identification: Av. Ratio = Average ratio: indicates fold-difference of the protein in tumour cells compared to normal cells, IPI number = International protein index reference number, pI = pH at which protein's charge is zero according to protein database, Mw (pred) Da = Molecular weight in Daltons according to protein database, Mw (gel) Da = Molecular weight in Daltons according to observed migration, Score = Number of peptides matching the top hit from Mascot Daemon programme versus the total number of masses submitted, % Cov = Amino acid sequence coverage for the identified protein

Gel slice	Av. Ratio (Tumour/Normal)	Name	IPI number	pI (pred)	Mw (pred) Da	Mw (gel) Da	Score	%Cov
15	1.7	No significant hits	See Fig. 3.9 a					
17	1.5	solute carrier family 3, CD98 hc, 4F2 heavy chain, MDU1	IPI00027493	4.93	57944	85 000	91	12%
24	1.5	No significant hits	See Fig. 3.9 b					
27	1.9	No significant hits	See Fig. 3.9 c					

The identification of the peptides from gel slice b to match CD98/SLC3A2 with a score of 91 exceeded the threshold for significance (70). In order to validate the expression of CD98 hc, by an alternative independent method, IHC was applied.

3.3.4 Confirmation of protein expression by IHC

IHC staining of frozen tissue was used to assess the expression of CD98 hc in oesophageal tumours and paired normal tissues from 10 patients. In normal epithelia, the basal cells (or less differentiated tissue) stained exclusively in comparison to the rest of the tissue (Fig. 3.9a and b). The staining was confined to the plasma membrane. The upper or more differentiated layers in normal epithelia stained very weakly. Due to the type of staining pattern observed in the normal epithelia, scoring the level of staining could not be executed.

Scoring criteria was successfully applied to the corresponding tumour tissue for all 10 patients (Table 3.4). Of the patient tissue evaluated, 90% of tumour tissue displayed more than 75% staining of CD98 hc (Table 3.4 and Fig. 3.9 c-f). An intense staining pattern was observed for CD98 hc as early as dysplasia (Fig. 3.9 c and d).

Table 3.4: IHC staining score for patient cohort: Observations are based on percentage membrane staining in tissue section. T indicates tumour section. Scoring for normal tissue was not included as basal cells stained exclusively in comparison to rest of the tissue. Scoring criteria: 0 indicates less than 5% stained, 1+ indicates between 5 and 25% stained, 2+ indicates between 26 and 50% stained, 3+ indicates between 51 and 75% stained and 4+ indicates more than 75% stained.

Patient number	T
1	4+
2	4+
3	4+
4	4+
5	4+
6	4+
7	2+
8	4+
9	4+
10	4+

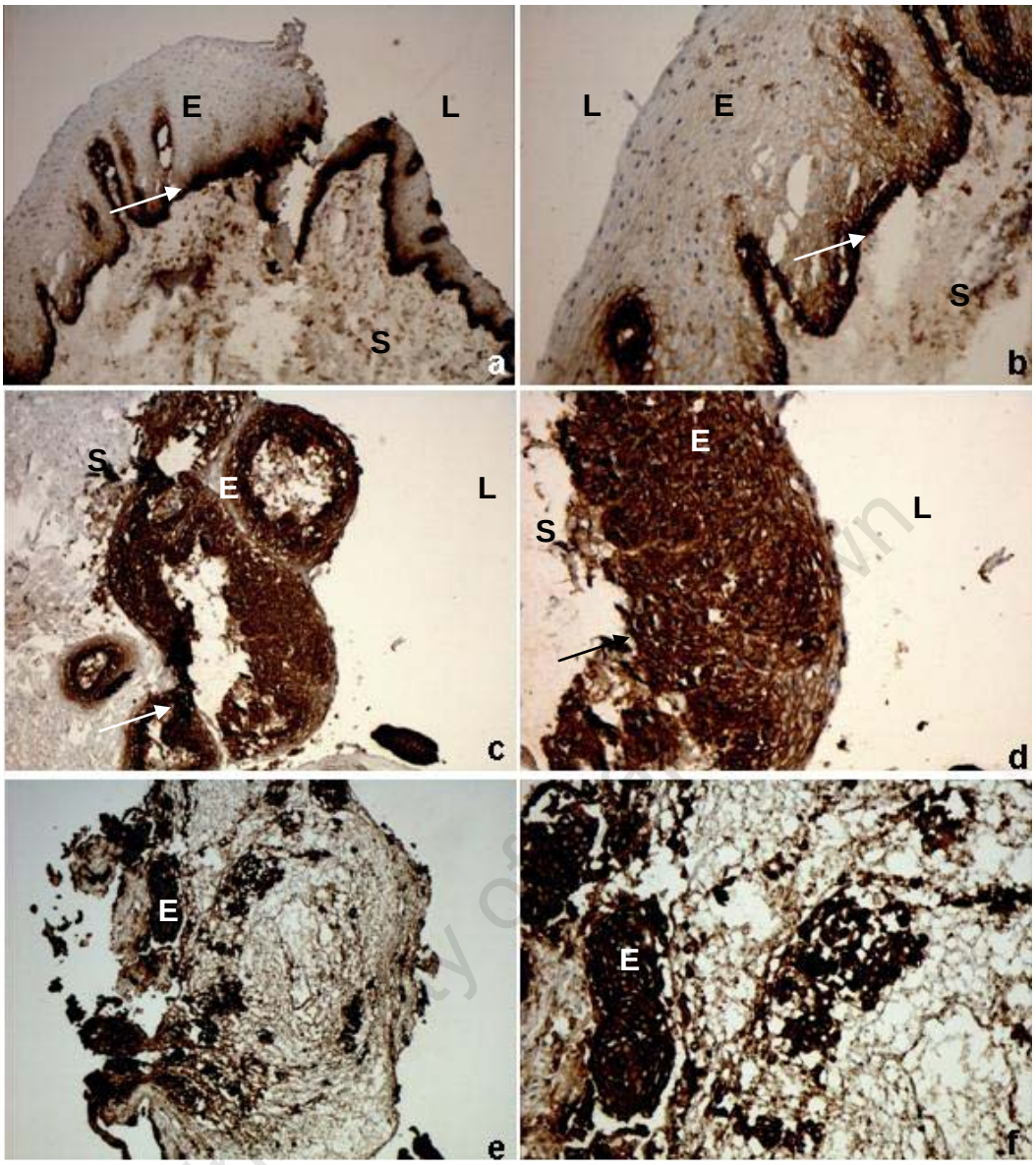

Figure 3.9 : Immunohistochemical staining of CD98 hc: (a) and (b) indicates weak membrane staining of in normal epithelia in suprabasal layers and intense staining in the basal layer where (a) is [40X] and (b) is [100X], (c) and (d) indicates strong membrane staining in dysplastic epithelia where (c) is [40X] and (d) is [100X], (e) and (f) displays intense staining in invasive carcinoma but not in stroma where (e) is [40X] and (f) is [100X]. [ ] indicates strength of magnification, L indicates Lumen, E indicates epithelia, indicates Basal cells and S indicates Stroma.

Although normal epithelial staining for CD98 hc could not be scored because staining was confined to basal and suprabasal cells, CD98 hc expression was markedly elevated in tumour tissue compared to normal tissue (Fig. 3.9 a, b, e and f) in all 10 sections examined, confirming the results observed by REQUA linked to ESI-QUAD-TOF-MS analysis. Furthermore, the plasma membrane of dysplastic epithelial cells (Fig. 3.9 c and d) stained strongly for CD98 hc, relative to the weak CD98 staining observed in the maturing cells from the normal epithelia (Fig. 3.9 a-d). The enhanced expression of CD98 hc in dysplasia earmarks CD98 hc expression as a possible early diagnostic marker for the development of OSCC.

3.4 Discussion

REQUA (relative quantification of glycosylated proteins) offers the opportunity to decrease the complexity of a sample, by allowing the analysis of a subset of proteins on the surface of cells. This method was previously used to aid in the molecular characterisation and interactions of phagosomes in *Mycobacterium tuberculosis* and *Mycobacterium avium* (193,194). We report the first use of REQUA to identify glycosylated surface proteins that display altered expression in tumour cells compared to normal cells.

The type of cell line used makes a significant impact on labelling efficiencies of the method used. Cells of *Dictyostelium discoideum* showed a high labelling efficiency (96,97), in contrast to the cells used in this study that displayed a relatively low labelling efficiency, despite the use of same labelling parameters. The low percentage of labelling observed in this study could be due to the losses incurred in the extensive washing steps, required to yield a plasma membrane protein preparation, or the number of cells used during labelling.

Because REQUA allows reduction in sample complexity, it is possible to avoid using iso-electric focusing as a primary separation approach followed by SDS-PAGE. Hydrophobic proteins are notorious for not separating well during iso-electric focusing, therefore affecting the ability of 2D gel electrophoresis to identify proteins of a hydrophobic nature. REQUA does not include an iso-electric focusing step, thereby allowing the identification of hydrophobic proteins on the surface of the cell.

REQUA, however, like most proteomic methods does have its drawbacks. The method is time consuming and some of the reagents are relatively expensive. Furthermore, REQUA can only be

applied to cells in culture. Like all other proteomic methods, the levels of proteins of interest must be validated using an alternative method, such as IHC. REQUA is also unfortunately not ideal for use as a high-throughput method. Although REQUA has previously been used successfully (193) to identify a number of glycosylated proteins, in this study we were only able to identify one of the four membrane bound glycosylated proteins of interest. The reason for the low rate of identification is related to the amount of protein available in each slice. The use of radioactivity allows for increased sensitivity, thereby allowing the identification of proteins displaying altered expression. Unfortunately, the amount of radioactivity does not necessarily translate to the quantity of protein in the slice of interest, considering multiple proteins would be in present in one gel slice. Furthermore, we also observed degradation of proteins that were stored. MALDI-MS analysis was performed in Germany. Possibly the long-term storage of samples (prior to analysis) led to degradation of proteins thereby translating to a low extraction yield from the gel slice of interest.

The protein identified was CD98 heavy chain (hc). CD98hc is an 80 kDA transmembrane protein, with the C-terminus presenting outside the cell. CD98 hc is also known as 4F2, Lymphocyte activation antigen 4F2 large subunit, MDU1 and NACAE (195). CD98 hc is part of the solute carrier 3 protein family and is commonly referred to as SLC3A2 (195). The glycosylated CD98 hc forms part of a heterodimer with the non-glycosylated CD98 light chains 1, 2 and 3 (LAT-1: L-amino acid transporters) to form the CD98 protein or Heteromeric Amino acid Transporter (HAT) complex that represents several of the classical mammalian amino acid transporters (196,197). Haynes *et al* first characterised CD98 protein in 1981 as a T-cell activation antigen comprising of an 80kDa heavy chain and a 40 kDa light chain (192,198). Later it was determined that CD98 protein is responsible for the transport of neutral amino acids (199). However, CD98 protein has also been shown to play a role in cell fusion, cell adhesion, cell survival, integrin and adhesive signalling and cell proliferation

(200-207), although the exact mechanism by which CD98 hc contributes these processes is not known (208-210).

An increase in cell proliferation is associated with an increase in metabolic requirements, reflected by the increased level of CD98 hc observed in both the basal and suprabasal cells of normal epithelia and the increased expression in tumour tissue (211). For growth, proliferation and maintenance of the tumour cells, protein biosynthesis is required and therefore transport of amino acids (from outside of the cells to inside of the cells) becomes important.

Increased levels of CD98 hc have been observed in other cancers, such as breast cancer, ovarian cancer and gliomas (212-214). In this study, we observed a marked increased of CD98 hc levels in oesophageal cancer tissue compared to normal tissue. The involvement of CD98 hc in proliferation suggests that this protein may be a good target for cancer therapy. However, it is ubiquitously expressed in all tissues with high levels in certain tissues such as the kidney, placenta and testis (197,215). Despite the ubiquitous expression of this protein, a humanized antibody to CD98hc has been developed and is currently being investigated as a potential means of therapeutic intervention (216). Furthermore, CD98 hc has been patented as an early diagnostic marker for cancer (215).

In addition to the potential of CD98 hc as a means of therapeutic intervention, Xiao *et al* (217) demonstrated reduced levels of CD98 in the plasma of individuals with lung cancer. CD98 levels in plasma have been included in a panel with other proteins to have good predictive value in lung cancer staging, with a high degree of specificity and sensitivity. The study by Xiao et *al* (217) suggests that CD98 can be included in a cohort of proteins to serve as a prognostic marker for lung cancer.

Although our study did not explore whether CD98 hc is shed into the extracellular milieu of oesophageal tissue, our study does highlight CD98 hc as a potential prognostic marker for early

diagnosis of OSCC. Furthermore, based on developments in the literature regarding the humanizing of CD98 hc antibodies, it is conceivable that CD98 hc could be a credible target for treatment of OSCC in the future.

4 DCA as a potential therapeutic drug in OSCC

4.1 Introduction

Comparative 2D-DIGE analysis of proteins from tumour and normal tissue from OSCC patients showed elevated levels of glycolytic enzymes in tumour tissue compared to normal tissue. Subsequent immunohistochemical analysis of paraffin-embedded tissue confirmed that levels of glycolytic enzymes (PK and GPDH) were indeed elevated in OSCC patients (Fig. 2.10).

The increase in glycolytic enzymes in tumour cells compared to normal cells, reflecting an increased dependence of tumour cells on glycolysis as an energy source, is a well-described phenomenon, referred to as the Warburg effect. Otto Warburg first described this phenomenon in the late 1920's and since then it has been recognised as a phenomenon typifying cancer cells (131). In cancer cells, elevated levels of glycolytic enzymes occur since glycolysis is utilised as the primary source of ATP production, despite the availability of oxygen. It is thought that this increase in aerobic glycolysis is due to mitochondrial dysfunction, conferring apoptotic resistance, as a result of increased mitochondrial membrane potential. The latter increase in membrane potential has been reported in

many cancers and it has been shown that decreasing membrane potential, results in the induction of apoptosis (139,218,219).

Targeting cells displaying increased glycolytic pathway activity therefore represents a novel means of therapeutic intervention. A recent publication by Bonnet et al, describes the use of dichloro acetic acid (DCA) as a potential therapeutic agent for glioblastoma cells, which also displayed elevated glycolytic pathway activity (139). DCA can shift cellular metabolism from primarily glycolysis to include the Kreb's cycle and oxidative phosphorylation as key energy sources. DCA inhibits pyruvate dehydrogenase kinase (PDK), which in turn inhibits pyruvate dehydrogenase (PDH) (Fig. 4.1) (220). PDH controls the link between glycolysis and the Krebs cycle, if PDH is inhibited, pyruvate is not shuttled to the Krebs cycle, which results in reduced levels of oxidative phosphorylation (220,221).

DCA allows PDH to remain activated, by inhibiting PDK, and in so doing enables oxidative phosphorylation to take place with the associated generation of reactive oxygen species (ROS). ROS generation leads to decreased mitochondrial membrane potential, resulting in the generation of apoptotic inducing factors (Fig. 4.1.), which would normally facilitate the induction of apoptosis in stressed cells. In cancer cells, this ability to induce apoptosis in response to abnormal stress is by-passed (139,222).

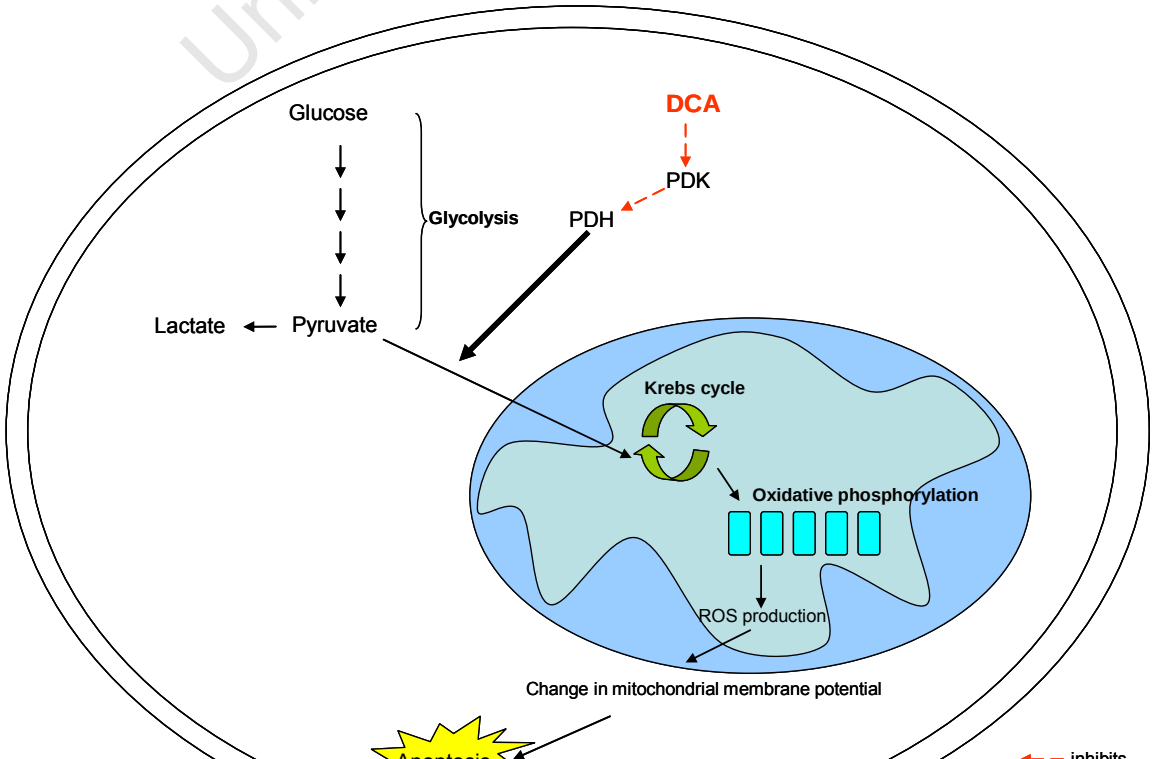

Figure 4.1: Schematic diagram illustrating mechanism by which DCA triggers apoptosis in tumour cells (adapted from (139)).

The significance of Bonnet's study is, however, that DCA only affects tumour cells and not normal cells, by targeting the glycolytic pathway. DCA treatment exploits the inability of tumour cells to commit pyruvate to the metabolic processes in mitochondria, whereas normal cells display normal mitochondrial activity and are not susceptible to DCA treatment (139,220). Others have subsequently shown that by targeting the glycolytic pathway with DCA, in cultured cells, apoptosis is induced in cancer cells with no effect on normal cells (218). In this chapter we investigated whether targeting the glycolytic pathway of OSCC cells, with DCA, would be an effective therapeutic treatment in OSCC, using cell culture as a model system.

4.2 Materials and Methods

4.2.1 Propagation of cell lines

The cell lines used included WHCO1 (obtained as a gift from Dr R. Veale, University of Witwatersrand, South Africa), KYSE 30 and KYSE 450 (obtained as a gift from Prof Y. Shimada, Kyoto University, Kyoto, Japan) (223). DMB's are a primary fibroblast culture prepared from human skin (kindly developed and donated by Sheena Jones in the laboratory of Dr D. Marais, University of Cape Town, South Africa) and EPC-2 –hTERT (EPC-2) (obtained as gift from Prof A. Rustgi, University of Pennsylvania, Philadelphia, USA.) are derived from squamous epithelial cells isolated from the morphologically normal proximal oesophagus of a 55 year old male who underwent an

oesophagectomy for Barret's oesophagus. The cell line was immortalized with human telomerase (224).

WHCO1, KYSE 30, KYSE 450 and DMB cells were cultured and maintained in Dulbecco's Modified Eagle's Medium (DMEM) (Gibco-BRL, USA) containing 10% heat-inactivated foetal bovine serum (FBS) (Gibco-BRL, USA), 100 units penicillin and 100µg/ml streptomycin. EPC-2 cells were grown in Keratinocyte Serum Free Medium (KSFM) (Gibco-BRL, USA) supplemented with 50µg/ml bovine pituitary extract (Gibco-BRL, USA), 1ng/ml epidermal growth factor (Gibco-BRL, USA), 100 units penicillin and 100µg/ml streptomycin. All cell lines were incubated at 37ºC with 5% CO_2 humidity. On reaching confluency, the cells were rinsed and then harvested with 0.05% trypsin in PBS containing 10 mM EDTA, by incubation at 37ºC for 3-5 minutes. In the case of WHCO1 cells, trypsinisation was inhibited with the addition of an equal amount DMEM containing 10% FBS. In the case of the EPC-2 cells, trypsinisation was inhibited by the addition of 0.25ng/ml Soya bean trypsin inhibitor (Sigma, USA). The cells were pelleted by brief centrifugation at 1000 rpm for 5 min, re-suspended in their respective media and split at a ratio of 1:5.

4.2.2 Growth assays

Cells were seeded at 1500 cells per well, in quadruplicate, in 7 separate 96- well dishes. After each day, 10µl MTT (Sigma, USA) reagent was added to appropriate wells. Subsequently, 100µl solubilization reagent (10% w/v SDS, 0.01M HCl) was added after 4hrs incubation with MTT, at 37ºC with 5% CO_2 humidity. Cells were allowed to solubilize overnight at 37ºC with 5% CO_2 humidity. Absorbance was read at 595nm using a Biotek EL800 96-well plate reader. This process was repeated over seven days. Doubling time was calculated by plating an exponential growth curve on Graphpad Prism version 4.03 (Graphpad Software ©)

4.2.3 Cell counting assays

Cells were seeded at $5X10^4$ in a 6-well dish (35 mm plate), in triplicate. The cells were allowed to settle overnight and subsequently treated with 0, 0.5, 5, 10, 50 and 100mM DCA (Sigma, USA) for 48 hrs. Both media and cells were collected and the amount of cells was counted, using trypan blue in order to calculate cell viability and the concentration at which 50% cell death occurs (EC_{50}). These experiments were performed in triplicate.

Similarly, $2X10^4$ cells were seeded in a 24-well dish, in triplicate. The cells were allowed to settle overnight and subsequently treated with 0, 10, 50 and 100mM DCA for 0, 12, 24 and 48 hours. Cells were counted, using trypan blue, at each time point in order to determine the time at which DCA causes cell death at various concentrations.

4.2.4 Cell cycle analysis

Cells were seeded at $0.5X10^6$ per 60 mm dish and allowed to settle overnight. WHCO1 were treated with 0 and 10 mM DCA for 48 hrs, whilst KYSE 450's were treated with 0 and 50 mM DCA for 48 hours. The cells were harvested using 0.05% trypsin and fixed in ice-cold 70% ethanol. Cells were stored at -20°C until further use. For cell cycle analysis, $0.8X10^6$ cells were washed in a phospho-citrate buffer and to ensure that only DNA stained with propidium iodide, cells were treated with RNase A at a final concentration of 50 µg/ml. Cells were then stained for 20 min with a staining solution and subjected to flow cytometry on the BD FACSCalibur™ flow cytometer system (BD Biosciences, USA). Cell cycle analysis was performed using ModFit LT™ Software program (Verity Software House, USA).

4.2.5 Apoptosis assays (Caspase 3/7 activity)

Cells were seeded at 5000 cells per well in a 96-well plates and allowed to settle overnight. Cells were treated with 0, 20, 50 and 100 mM DCA for 6, 12, 24 and 48 hours. Each treatment was

performed in quadruplicate. Cells treated with 5µg/ml Doxyrubicin, for the indicated times, were used as a positive control. Apoptosis assays were performed using the commercially available Caspase-Glo ® assay (Promega, USA), according to manufacturers' instructions, with the following modifications. An amount of 60µl of Caspase-Glo ® reagent was added to cells with 60µl media and allowed to incubate at room temperature for 30 minutes. Thereafter, 100µl were transferred to an opaque plate and allowed to stand at room temperature for a further 30 minutes. Luminescent readings were performed using the Glomax 96-plate luminometer (Promega, USA).

4.2.6 Western Blot analysis (PARP cleavage)

Cells were seeded at $1X10^6$ per 60mm dish and allowed to settle overnight. The cells were then treated with 0, 10 and 20 mM DCA for 48 hours. Cells treated with 5 µM Doxorubicin for 48 hrs served as a positive control for the induction of apoptosis. Protein was prepared by the addition of a lysis buffer containing a cocktail of protease inhibitors (cOmplete, Roche) as well as phosphatase inhibitors (1M NaF and 0.1 M PMSF). Protein was then subjected to a 10 % SDS-PAGE and transferred to nitrocellulose membrane (GE Healthcare, UK). Membranes were blocked with 7% milk in TBST for 1 hour at room temperature, and primary antibody (1/1000 dilution in 5% milk for PARP) [Santa Cruz, USA], overnight at 4°C, both whilst shaking. Membranes were subsequently shaken at room temperature for 1 hour in secondary antibody (anti-rabbit: 1/5000 dilution in 5% milk in TBST) [Bio-rad, UK] and detected using SuperSignal ® (Pierce, USA). Images were converted to black and white in Microsoft Powerpoint ©.

4.2.7 Necrosis assay

Cells were seeded at $1X10^5$ per well (in triplicate) in a 96-well dish an allowed to settle overnight. Cells were then treated with 0 and 100mM DCA for 12 hours. In order to determine whether cell death involved necrosis, the Cytotox ONE assay was used as per manufacturer's instructions, with

the following modifications. An amount of 60µl of media from each well was transferred to an opaque 96-well dish and allowed to equilibrate to room temperature. An equivalent amount of Cytotox reagent was added to each well for 10 minutes. The reaction was then stopped by the addition of 30µl stop solution. Cells treated with lysis buffer (provided by the manufacturer) were used as a positive control. The plates were kept in the dark and read immediately by exciting the reagent at 560nm and recording fluorescence emission at 590 nm on the Carey Eclipse Fluorescence spectrometer (Varian Inc, UK) using slit widths of 10 nm.

4.2.8 PDH and lactate assays

Cells were seeded at $0.5X10^6$ in 35 mm dishes, in triplicate. The cells were allowed to settle overnight and subsequently treated with up to 10 mM DCA for 48 hrs. Concentration of lactate was determined by removing a 300 µl aliquot of media from each dish and placing on on ice. The media aliquot was centrifuged at 1000 rpm for 5 min at 4°C, to pellet any cell debris. The supernatant was subsequently placed back on ice and lactate concentration was determined via the Beckman Synchron CX9 Clinical System (Beckman Coulter, USA) at Chemical Pathology, National Health Laboratory Services, Red Cross Hospital in Cape Town.

PDH activity was determined as previously described (225), with a few modifications. Briefly, total cell activity was measured in triplicate, using [1-^{14}C]pyruvate (PerkinElmer Life Science Products, Boston,MA, U.S.A.) as a substrate, after maximal activation of PDK by treatment of the cells for 15 min with 5 mM DCA before PDK extraction. The cells were pre-incubated in 0.5 mM $CaCl_2$ and 10 mM $MgCl_2$ for 10 min at 37°C as previously described (226). Citrate synthase was determined as previously described (227). Protein concentration was determined according to the method of Bradford, with BSA as the standard (228).

Lactate levels and PDH activity was corrected for cell number by using the concentration of protein for each dish.

4.2.9 Statistical evaluations

For all data comparisons the statistical significance of the differences was determined by the two-tailed Student's t-test. Statistical analysis was performed in either Microsoft Excel © or Graphpad prism version 5 Software (Graphpad software, San Diego, USA). A *p*-value of <0.05 was considered statistically significant.

4.3 Results

4.3.1 Oesophageal cell lines display various levels of sensitivity to DCA treatment

We investigated various methods to determine the sensitivity of the cell lines to DCA treatment. DCA interfered with the MTT reagent resulting in increased absorbance values, unrelated to cell number. Although the crystal violet assay displayed the expected decrease in cell viability in response to treatment with DCA, the high levels of background observed using this assay, led to the use of cell counting assays via trypan blue staining as the method of choice to determine cell viability.

Table 4.1 outlines the average EC_{50} for DCA in each cell line calculated from three independent experiments. WHCO1 was the most sensitive to DCA with an EC_{50} of 9mM (CI 8.98-9.03) followed by DMB with 11.72 mM (CI 11.42-12.03), EPC-2 with 15.96 mM (CI 15.92-15.99), KYSE 30 with 32.7mM (CI 32.37-33.05) and KYSE 450 with 41.43 mM (CI 41.02-41.85).

Table 4.1: Calculated EC_{50}'s for DCA and corresponding 95% CI for the panel of cell lines tested.

Cell line	**EC_{50} (mM)**	95% Confidence Interval (CI)
WHCO1	9.00	8.98-9.03
KYSE 30	32.7	32.37-33.05
KYSE 450	41.43	41.02-41.85
EPC-2	15.96	15.92-15.99
DMB	11.72	11.42-12.03

.

The morphological appearance of the cells, in response to DCA treatment, corresponded to the EC_{50} for DCA. Although the number of fields of view were not documented, the images (Fig 4.2 -4.6) best illustrate that at concentrations below the EC_{50}, cells appeared normal whereas abnormal cell morphology (rounded cells) were present at DCA concentrations greater than EC_{50} (Fig 4.2 to 4.6).

Cells treated with DCA displayed a combination of morphological changes including increase in cell size, membrane blebbing and in some cases an increased number of vacuoles.

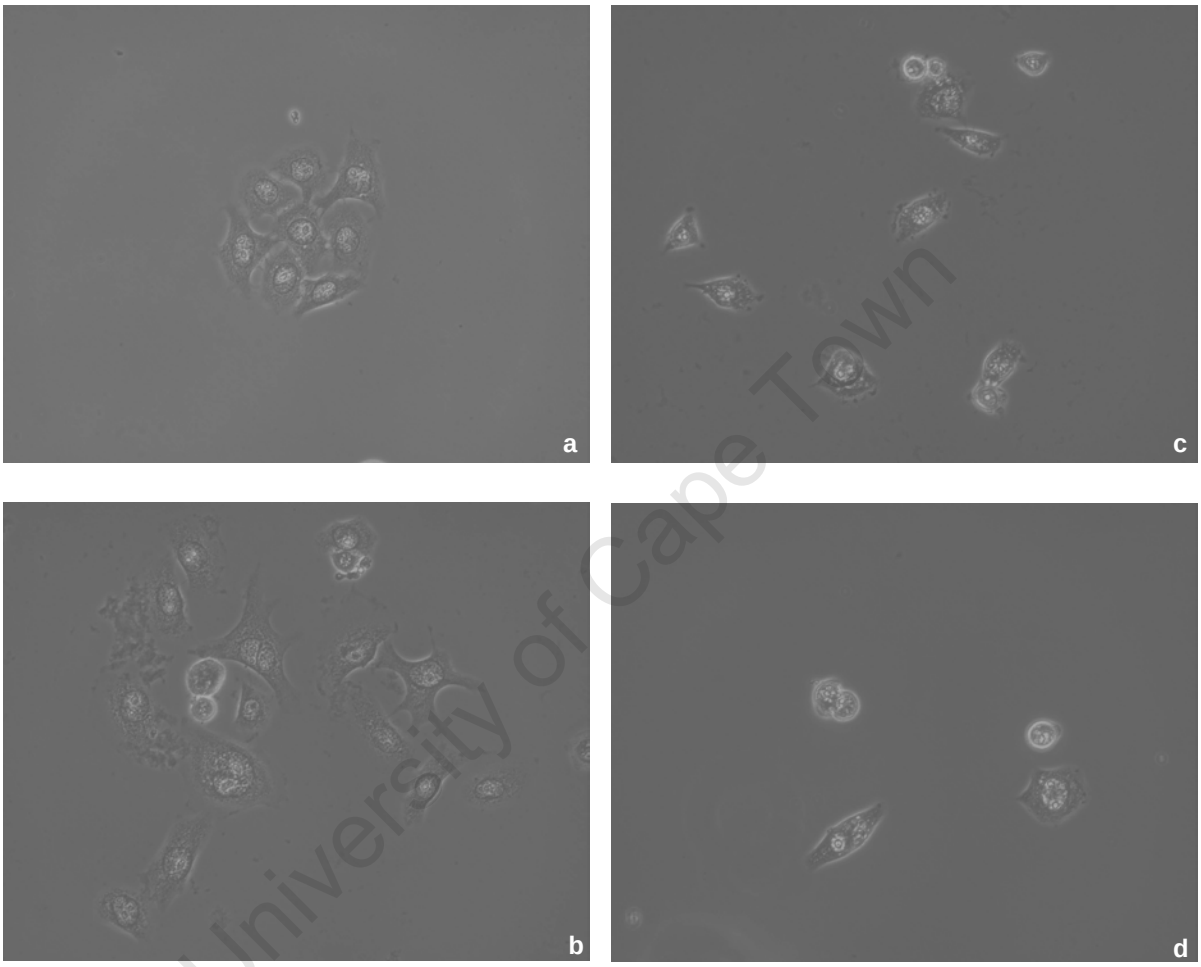

Figure 4.2: Phase-contrast images of WHCO1 cells treated with (a) 0, (b) 10, (c) 50 and (d) 100 mM of DCA for 48hrs. Magnification: 400X

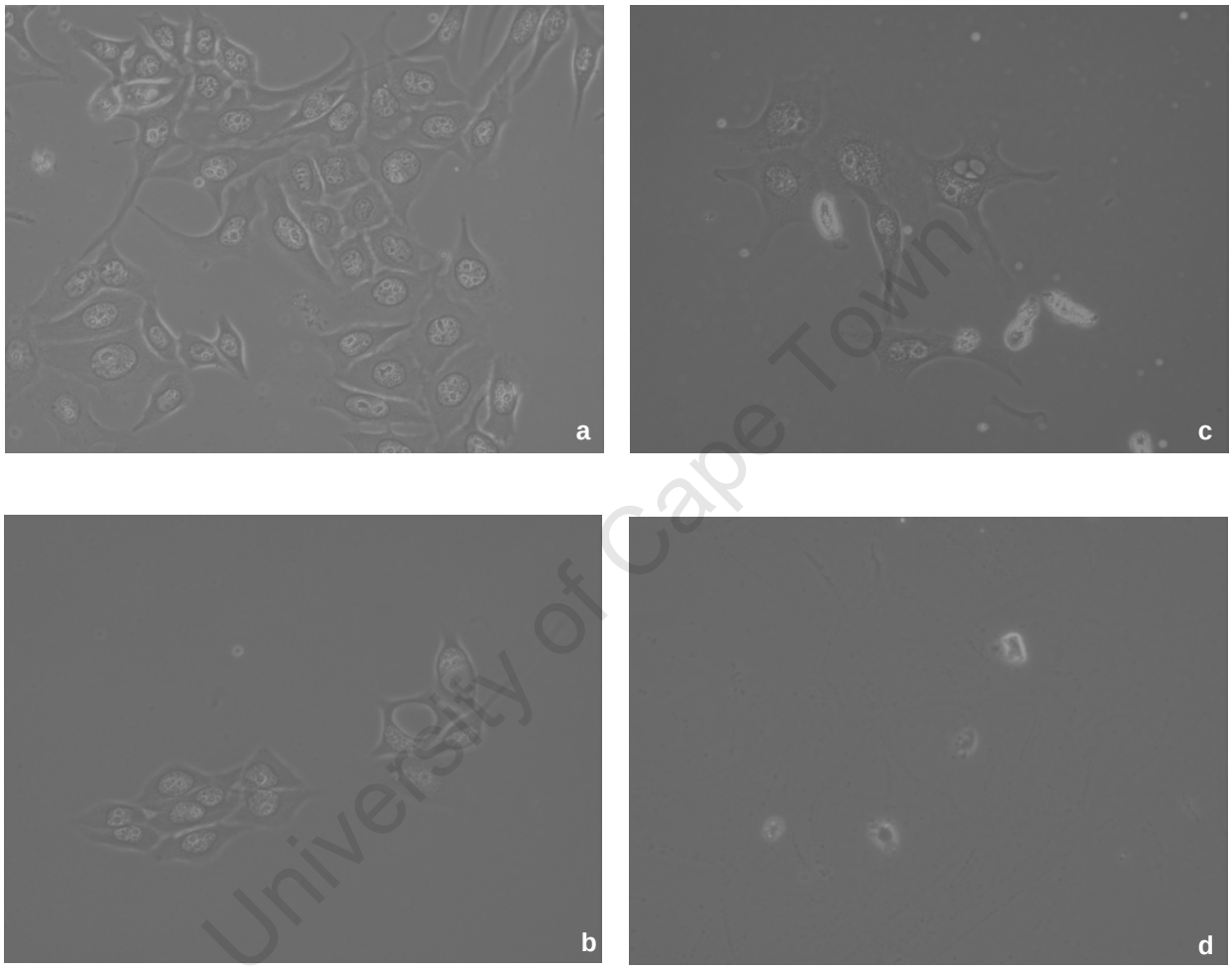

Figure 4.3: Phase-contrast images of KYSE 30 cells treated with (a) 0, (b) 10, (c) 50 and (d) 100 mM of DCA for 48hrs. Magnification : 400X

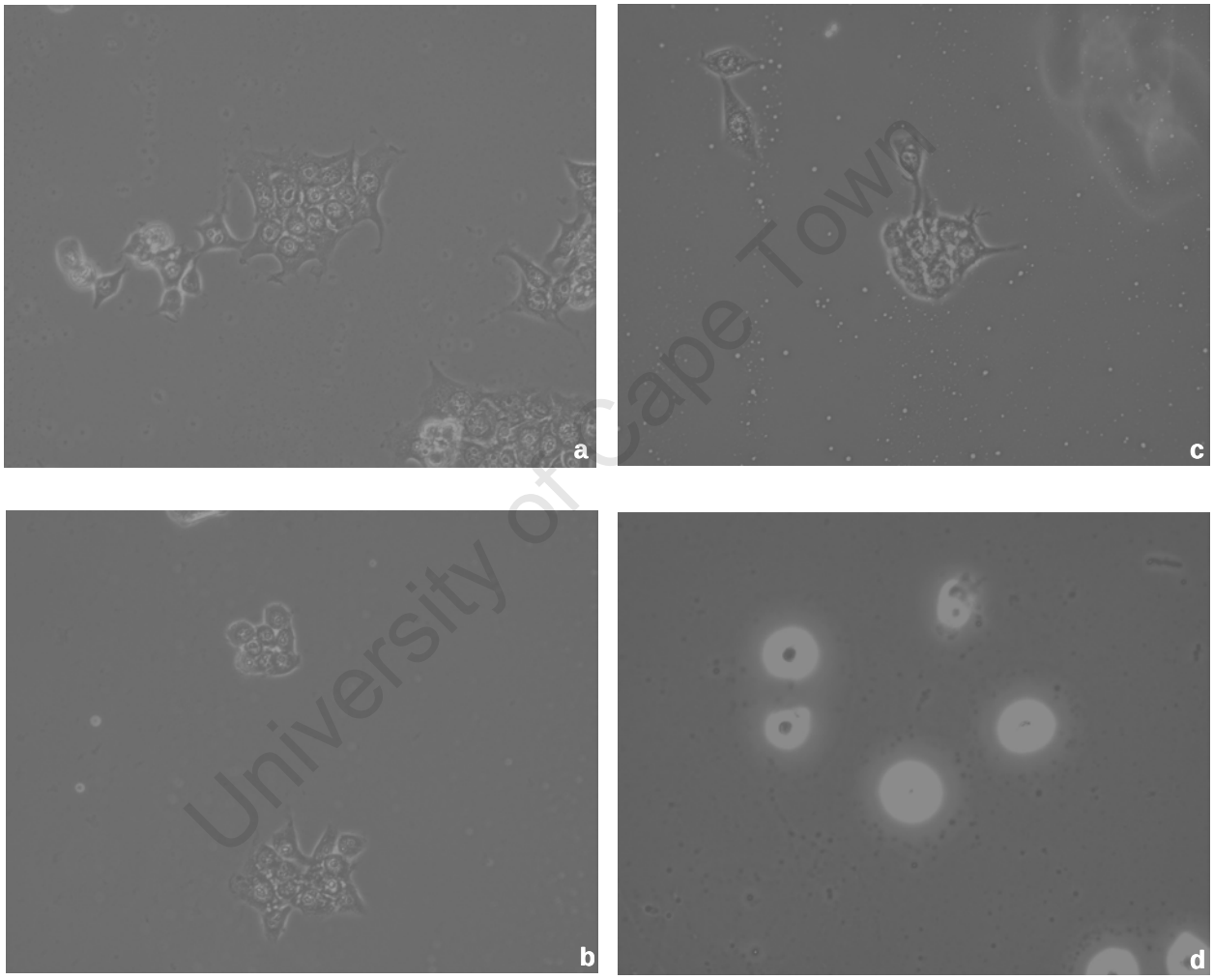

Figure 4.4: Phase-contrast images of KYSE 450 cells treated with (a) 0, (b) 10, (c) 50 and (d) 100 mM of DCA for 48hrs. Magnification : 400X

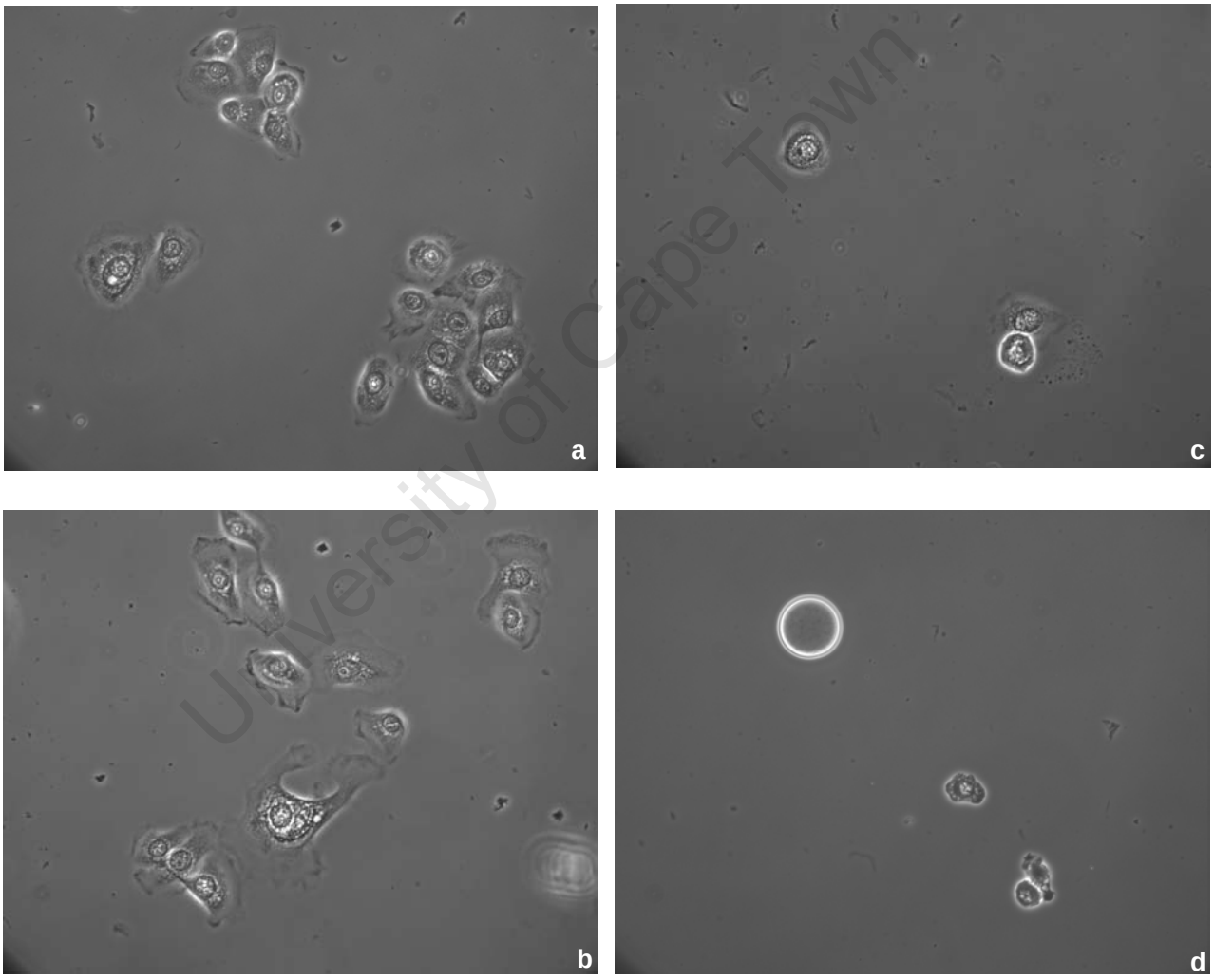

Figure 4.5: Phase-contrast images of EPC-2 cells treated with (a) 0, (b) 10, (c) 50 and (d) 100 mM of DCA for 48hrs. Magnification : 400X

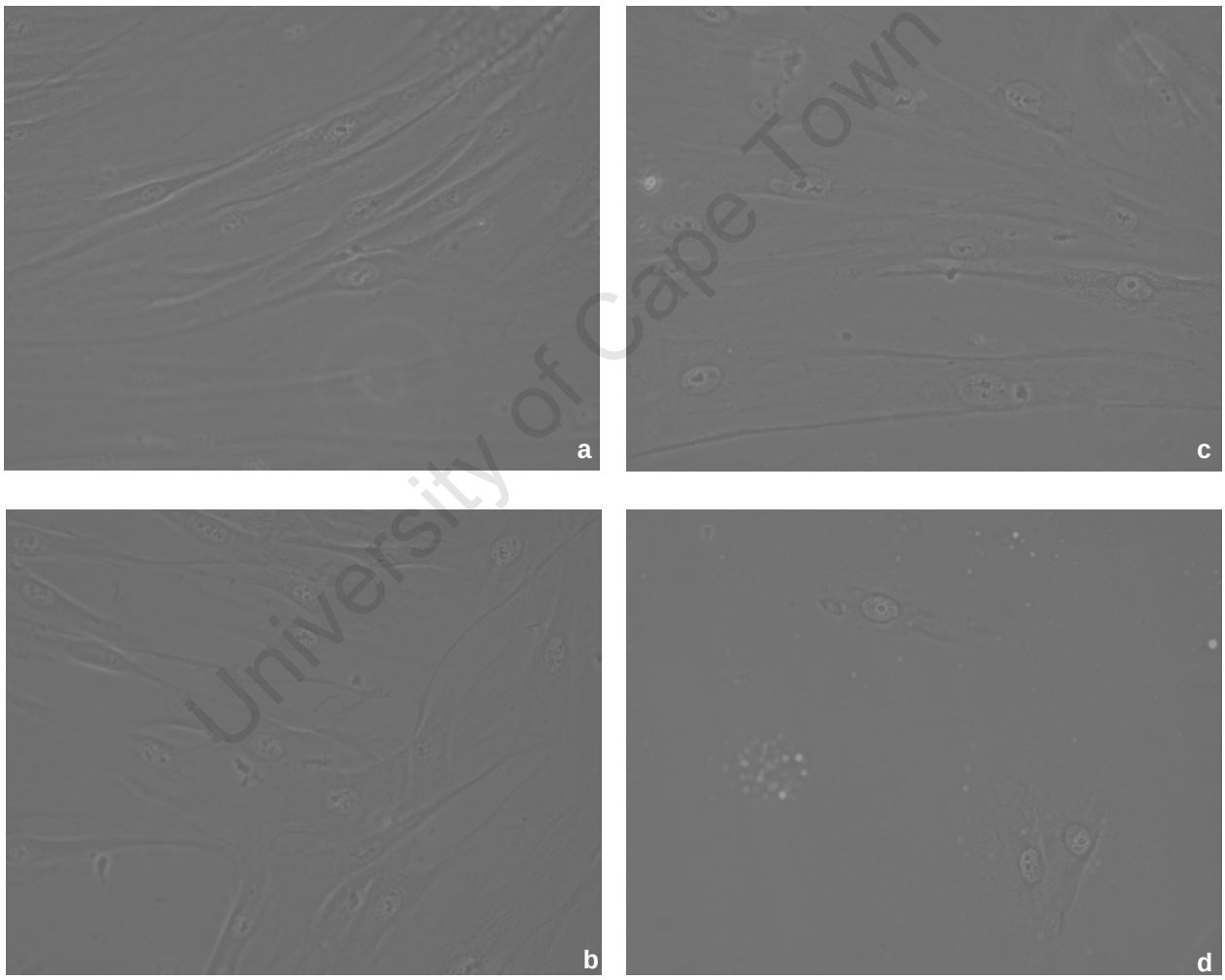

Figure 4.6: Phase-contrast images of DMB cells treated with (a) 0, (b) 10, (c) 50 and (d) 100 mM of DCA for 48hrs. Magnification : 400X

Generally the panel of cell lines were not sensitive to DCA as is highlighted by the observation that high doses were required for cell death to occur. The panel of cell lines used in this study displayed EC_{50} values for DCA that were 10 to 50-fold higher than those used in non-small-lung cancer, glioblastoma and breast cancer cell lines (139). It should be noted that the cell lines used in this study displayed sensitivities to DCA, similar to those reported for endometrial cancer cell lines (218).

Despite the high doses of DCA required for cell death to occur in the panel of cell lines used here, we investigated whether the mode of cell death was similar to that previously reported. We selected the cell line most sensitive to DCA treatment (WHCO1) and the one least sensitive to DCA treatment (Kyse 450) for further investigations.

4.3.2 Time-course of cell death

Both WHCO1 and Kyse 450 cells display approximately 50% decrease in cell number after 48hrs treatment with DCA at concentrations close to their calculated EC_{50} - 10mM for WHCO1 (Fig. 4.7a) and 50mM for KYSE 450 (Fig. 4.7b). However, when using a concentration that is more than double their calculated EC_{50}, both cell lines show an increase in cell death as early as 12 hours post-treatment with DCA; 50 and 100mM in WHCO1 (Fig. 4.7a) and 100mM in KYSE 450 (Fig. 4.7b), respectively.

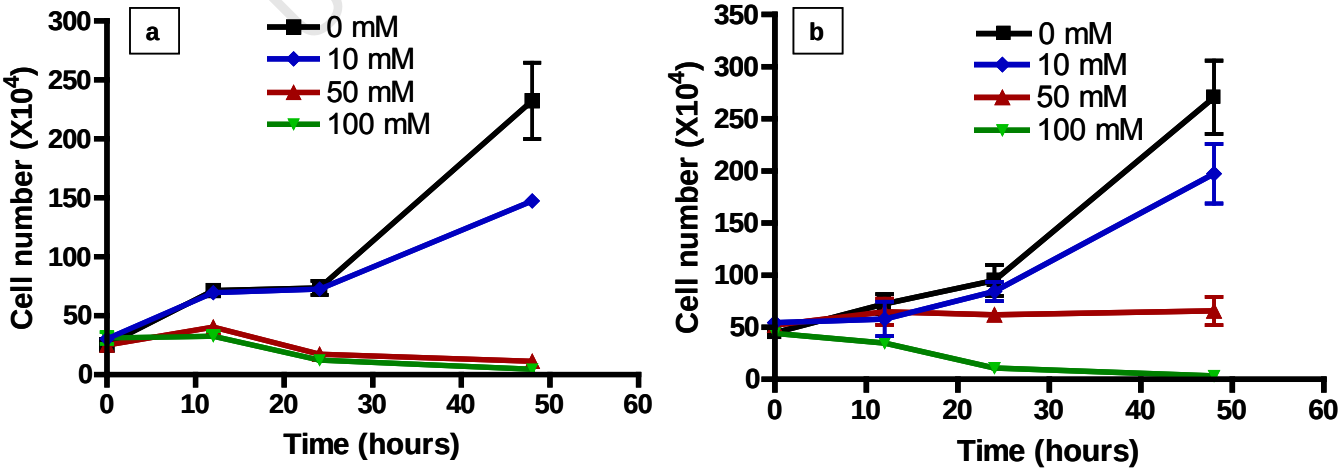

Figure 4.7: Time-course of DCA treatment for (a) WHCO1 and (b) KYSE 450 cells. Cells were counted at 0, 12, 24 and 48 hours treatment with 0, 10, 50 and 100 mM DCA. All data points were done in triplicate and error bars represent standard deviation.

Since DCA caused inhibition of cell proliferation after 48 hours, a period of 48 hours treatment with DCA was subsequently used in all experiments and in the case where the period of DCA treatment was shortened, DCA concentration was adjusted accordingly.

Considering the effects of DCA on cell proliferation, we proceeded to determine the impact of DCA on the cell cycle profile of treated cells.

4.3.3 Effects of DCA treatment on the cell cycle profile of OSCC cell lines

Since the time-course data showed that cell death occurred after 48 hours with 10mM and 50 mM DCA treatment, for WHCO1 and Kyse 450 cells, respectively, these were the concentrations used for cell cycle analysis.

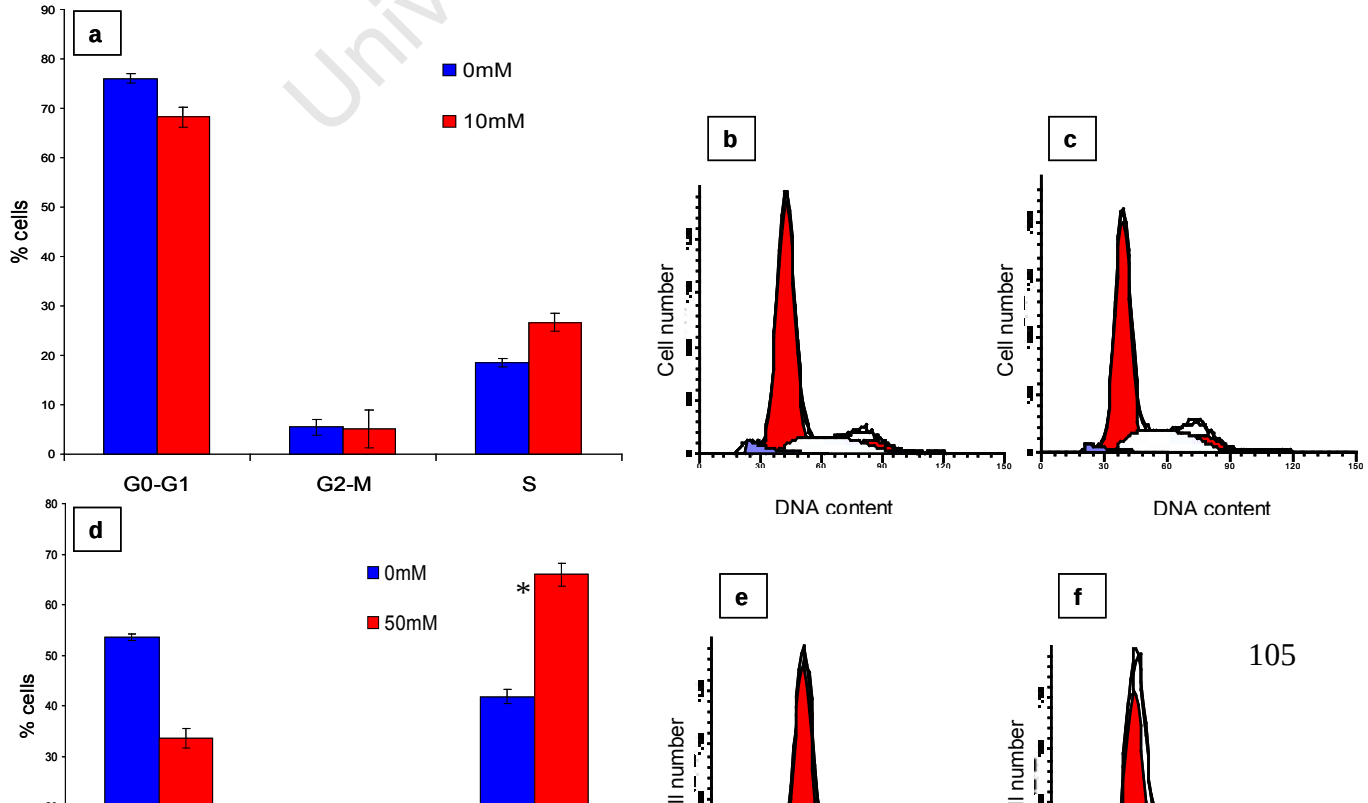

Figure 4.8: Cell cycle analysis of WHCO1 and KYSE 450 cells: (a) Graphical representation of average cell cycle profile of WHCO1 displaying no significant changes in cell cycle profile after treatment with DCA (b) Cell cycle profile of untreated WHCO1 (c) Cell cycle profile of WHCO1 treated with 10mM DCA for 48 hrs. (d) Graphical representation of average cell cycle profile of KYSE 450 where * indicates a significant S-phase arrest ($p < 0.05$) (e) Cell cycle profile of untreated KYSE 450 (f) Cell cycle profile of KYSE 450 treated with 50mM DCA for 48 hrs. Data points [in (a) and (d)] were done in triplicate and error bars represent standard error from three independent experiments.

Interestingly, both WHCO1 and Kyse 450 cells displayed an increase in S-phase arrest in response to DCA treatment; however, this S-phase arrest was only significant in Kyse 450 cells (Fig 4.8). To our knowledge, this is the first time that an S-phase arrest, in response to DCA treatment, has been observed. Previous studies observed no change in cell cycle profile in response to DCA treatment (218,229).

The S-phase arrest observed in Kyse 450 cells compared to WHCO1 cells could be due to a faster doubling time in Kyse 450 cells compared to WHCO1 cells, since this could allow more cells to accumulate in the S-phase. However, further investigation revealed no difference in doubling time between WHCO1 and Kyse 450 cell lines (Fig. 4.9).

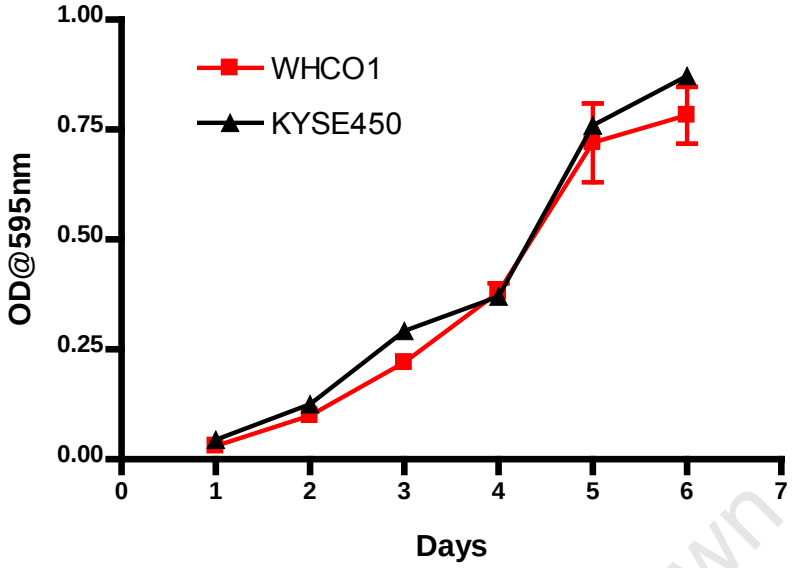

Figure 4.9: Growth curve for WHCO1 (in red) and KYSE 450 (in black), where the doubling time for WHCO1 is 1.646 days and KYSE 450 is 1.659 days. All data points were done in triplicate and error bars represent standard deviation.

Although, a significant S-phase arrest was only observed in KYSE 450 cells and not in WHCO1 cells, cell death occurred in both cell lines when treated with DCA. The method of cell death was further investigated.

4.3.4 Apoptosis or necrosis?

Firstly, based on the morphological observation of membrane blebbing in some cells treated with DCA, we set out to determine whether apoptosis was induced in response to DCA treatment. PARP cleavage was first used to determine whether apoptosis was occurring post-treatment with DCA (Fig. 4.10). Although no PARP cleavage was observed, an alternative method was used to confirm the lack of apoptosis. Caspase assays, using a luminogenic substrate, confirmed that no apoptosis was observed in either WHCO1 or K450 cells in response to DCA treatment, in comparison to the positive control (Fig. 4.11). Unexpectedly, a dose-dependant decrease in caspase activity was

observed in cells treated with DCA. A 77% decrease in caspase activity was observed in response to 20mM DCA treatment for 12 hours for both WHCO1 and Kyse 450 cells, in comparison to the 82% and 75% increase in caspase activity for WHCO1 and Kyse 450 cells, respectively, in response to doxorubicin treatment (where $p<0.005$). A more than 90% decrease in caspase activity was observed, for both WHCO1 and Kyse 450 cells, in response to 100mM DCA for 12 hours (where $p<0.0005$). The significant error observed in the positive control for WHCO1 is because of one particular well, which displayed decreased caspase activity due to possible pipetting error. All other data display marginally small error. Furthermore, this decrease in caspase activity was observed as early as 6 hours and as late as 48 hours post-treatment with DCA, thereby corroborating the PARP cleavage data. In summary, no measurable increase in apoptosis was observed on both WHCO1 and Kyse 450 cells treated with DCA, despite using two different approaches.

Figure 4.10: PARP cleavage assay for WHCO1 and KYSE 450 cells. PARP cleavage was determined after 48 hours with increasing concentrations of DCA, as indicated. Cells treated with 5μM doxorubicin for 48 hours were used as a positive control (+).

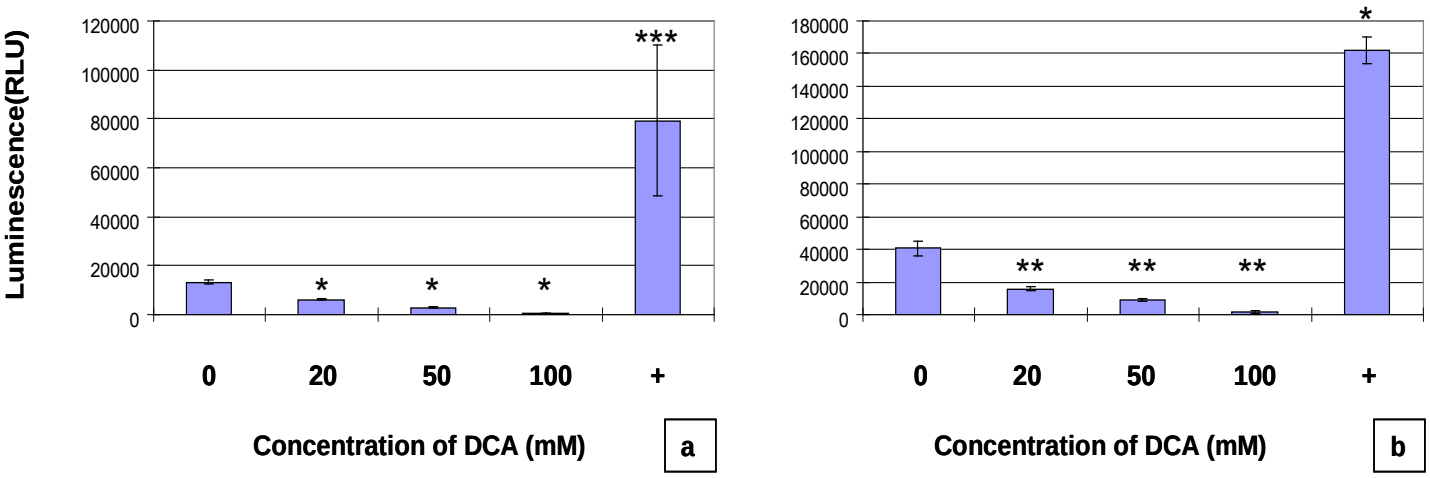

Figure 4.11: Caspase activity assay in WHCO1 and KYSE 450 cells. Caspase 3/7 activity was determined after 12 hours after treatment with increasing concentrations of DCA in (a) WHCO1 and (b) Kyse 450 cells, as indicated. Cells treated with 5μM doxorubicin for 48 hours were used as a positive control (+). All data points were done in quadruplicate and error bars represent standard deviation. The decrease, and or increase, in caspase 3/7 activity observed (in comparison to 0 mM) are all statistically significant (where * indicates $p<0.00005$ and ** indicates $p<0.005$ and *** indicates $p<0.05$)

Since these results suggested that DCA-treated cells were not dying via apoptosis, necrosis was investigated as a possible mode of cell death. The necrosis assay is a fluorescent measure of the release of lactate dehydrogenase (LDH) from cells with a damaged membrane. The half-life of LDH that has been released from cells into the surrounding medium is approximately 9 hours. When the assay was performed for longer than 12 hours treatment with DCA, erratic results were obtained. Due to the nature of the assay, cells could only be treated for 12 hours. Since our previous time-course data (Fig. 4.7) indicated that 100 mM DCA treatment for 12 hours resulted in cell death for both WHCO1 and Kyse 450 cells, this concentration of DCA was selected to determine whether necrosis played a role.

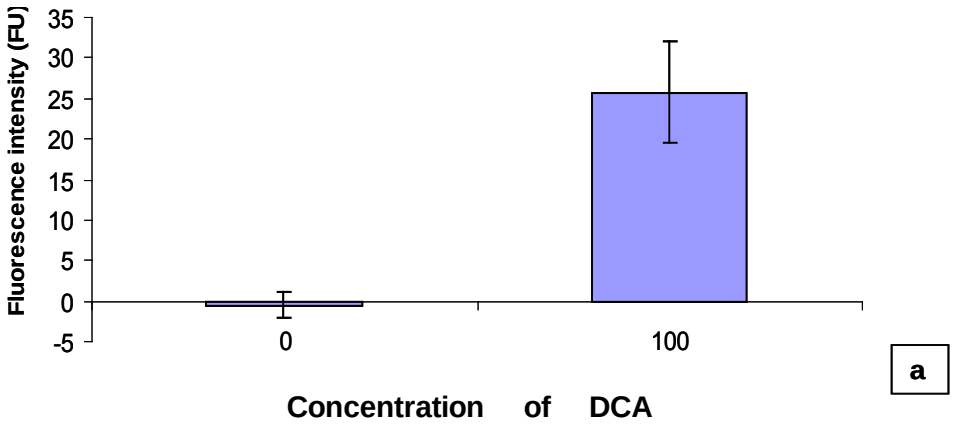

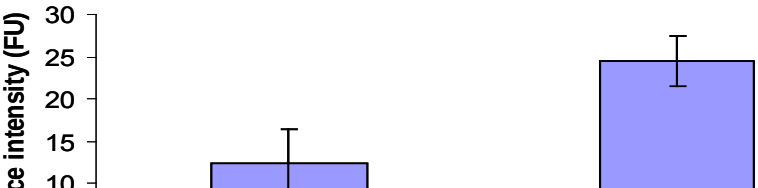

Figure 4.12: Necrosis assay after 12 hrs with 0 and 100mM DCA treatment for: (a) WHCO1 and (b) KYSE 450 cells. The difference between treated and untreated for both cell lines is significant (where $P<0.05$). All data points were done in triplicate and error bars represent standard deviation.

We observed a significant increase in necrosis in both WHCO1 and Kyse 450 cells in response to DCA treatment (Fig. 4. 12). The difference in necrosis observed in the absence of DCA could reflect the status of the cells during the experiment (Fig. 4.12). Although every effort was taken to ensure constant conditions for both cell lines, Kye 450's were possibly more stressed in this particular experiment, prior to treating with DCA. This does not deter from the fact that both cell lines display a significant amount of necrosis is response to DCA treatment.

4.3.5 DCA does not affect PDH activity and lactate levels in OSCC cell lines

The mode of action previously described for DCA, as reported for glioblastoma cells, involves the inhibition of PDK by DCA; allowing an increase in PDH activity followed by elevated mitochondrial

activity (Fig. 4.1). We would predict that this would be associated with decreased production of lactate (230). However, even though WHCO1 was shown to be the most sensitive cell line to DCA treatment in our panel of cell lines, no difference in PDH activity and an increase in lactate levels were observed in cells treated with DCA (data not shown).

Furthermore, no significant change in PDH activity and lactate levels were observed in any of the cell lines treated with DCA (data not shown). The lack of increased PDH activity and decreased lactate production after treatment with DCA suggests that DCA is not inducing cell death in oesophageal cancer cell lines by the same processes reported by Bonnet *et al* for glioblastoma cell lines.

The evidence presented here suggests that DCA causes cell death in our panel of cell lines, via necrosis and that the glycolytic pathway does not seem to be targeted.

4.4 Discussion

The finding that tumor cells, unlike their normal counterparts, primarily depend on glycolysis instead of mitochondrial oxidative phosphorylation as a source of glucose derived energy, despite the availability of oxygen, is known as the "Warburg effect" (131). This property of cancer

cells has been exploited in a clinical setting, in the form of positron-emission (PET) scanning, allowing earlier detection of tumours. PET scanning takes advantage of the increased uptake of glucose of tumour cells, to image tumors in patients, via the use of labelled glucose tracers (231). However, the dependence of cancer cells on glycolysis, and reduced mitochondrial metabolism also presents as an opportunity for chemotherapeutic targeting. One such chemotherapeutic agent that has shown promise in this field is DCA. A recent study by Bonnet *et al* (139) suggested that treatment of cancer cells with DCA could specifically induce apoptosis in cancer cells, leaving normal cells unaffected. The premise of this study is based on the observation that DCA inhibits the activity of PDK, thus increasing the flux of pyruvate into mitochondria, shunting glucose metabolism from aerobic glycolysis to complete glucose oxidation in mitochondria, thus exposing cancer cells to pro-apoptotic factors generated in functioning mitochondria. Our observation (in Chapter 2) that oesophageal cancer cells also display elevated levels of glycolytic pathway enzymes, suggested that oesophageal cancer cells may also be responsive to DCA treatment in this way. If this were the case, it could potentially alter the face of oesophageal cancer chemotherapy, and in this context, certainly warranted further investigation.

However, the results in this chapter indicate that the panel of oesophageal cancer cell lines investigated here, displayed lower sensitivities to DCA treatment than originally reported by Bonnet *et al* for glioblastoma and breast cancer cells and Wong *et al* for endometrial cancer cell lines (139,218). In the present study, DCA treatment induced cell death in a panel of oesophageal cancer cells with an EC_{50} that ranged from 9 – 40 mM. The cell proliferation assays were carried out by counting cells (using trypan blue), rather than MTT assays, since DCA interfered with the MTT reagent. The experiments reported here were repeated at least three times for each cell line, suggesting that the results obtained were reproducible, and

multiple batches of DCA were tested, to exclude the possibility that the apparent resistance of cells was due to the quality of the DCA tested. It should be recognised that the Bonnet *et al* article does not specifically report DCA EC_{50} values for any of the cell lines examined, which makes it rather difficult to compare the sensitivities of the cell lines reported. Instead, Bonnet *et al* comments on the substantial alterations in mitochondrial membrane potentials observed at 0.5mM DCA, indicating that apoptosis was induced at low DCA levels. Although the recent article by Wong *at a*l (218) that explored the sensitivity of a panel of endometrial cancer cell lines to DCA, suggested that DCA sensitized endometrial cells to apoptosis, a careful evaluation of the cell growth data is less convincing. In that study 10 mM DCA failed to decrease cell growth in 3 of the 7 cell lines examined, and only reduced cell growth by 10 – 20% in 3 of the other cell lines. Only 1 of 7 cell lines displayed a 50 – 60% decrease in cell number after treatment with 10 mM DCA. The effect of DCA on growth of oesophageal cancer cells observed in the present study, is very similar to the results reported by Wong *et al* for endometrial cancer cell lines.

DCA treatment failed to induce apoptosis in any of the oesophageal cancer cell lines studied here, (using two methods to assess apoptosis), unlike the reports for breast cancer, glioblastoma, non-small cell lung cancer (139) and endometrial cancer cells (218), where induction of apoptosis was readily observed. Instead, the decrease in cell number observed in oesophageal cancer cell lines in response to DCA treatment was due to necrotic processes, and not apoptosis. Furthermore, direct measurement of PDH activity and lactate levels in DCA treated oesophageal cancer cell lines indicated that DCA did not have the anticipated effect on these glycolytic pathway components. Given the observations reported by Bonnet *et al*, it was expected that DCA treatment of oesophageal cancer cell lines would result in increased levels of PDH activity, and decreased levels of lactate, reflecting the shift to complete oxidation of glucose

in mitochondria. However, 10 mM DCA had no effect on PDH activity in WHCO1 cells, even though these cells were the most sensitive to DCA, with an EC_{50} of 9 mM. In addition, treatment of WHCO1 cells with 10 mM DCA did not decrease lactate levels, suggesting that glucose was not shunted for complete mitochondrial oxidation. These results are consistent with the lack of apoptosis observed in oesophageal cancer cells in response to DCA treatment.

In this study we used EPC-2 cells (primary human oesophageal epithelial cells immortalised with hTERT) and DMB cells (primary human fibroblasts) as models of "normal" cells, so that the effect of DCA can be compared in cancer and normal cells. Considering that our results show that EPC-2 and DMB cells display EC_{50} values similar to that observed for the oesophageal cancer cells lines, we would suggest that DCA was unable to selectively target oesophageal cancer cell lines for destruction, above normal cells. We cannot exclude the possibility that the DCA treatment was unable to selectively target oesophageal cancer cells because the "normal cells" that we used here was inappropriate for this comparison. Perhaps a more appropriate "normal" cell model would have displayed much more resistance to DCA treatment than observed here. However, it is also equally possible that not all cancer cells respond to DCA treatment by activating apoptosis. This is highlighted by the observation that 2 of the 7 endometrial cancer cell lines tested for sensitivity to DCA were very resistant to the apoptosis-inducing effects of DCA (218).

Furthermore, the concentration range required for cell death to occur in our panel of cell lines was more that 10-fold the concentrations required for cell death to occur in other cell lines of the breast, lung. endometrial and prostate cancer origin (139,218,229). Interestingly, DCA treatment of prostate cancer cell lines resulted in an increased sensitivity of these cells to radiation therapy (229), suggesting that DCA may have some utility in combination therapy. Although it was reported that DCA has low toxicity in animals, the extrapolation of its effects in humans is problematic (232). The

results from our study together with the concerns of DCA's irreparable neurotoxic effects, identified from a randomized clinical trial of the effects of DCA (233), highlights that the use of DCA as a potential cancer therapeutic agent is still in its infancy and requires meticulous pre-clinical and clinical evaluation (220,234).

5 Conclusion

OSCC occurs at a high frequency in SA and is associated with a high mortality rate, making a South African cohort of OSCC patients a good model to study the development of the disease. Few studies have reported on molecular events leading to the development on OSCC in a South African cohort (101,235). Diagnosing the disease earlier or identifying better therapeutic targets remain a challenge. The aim of this study was to identify potential diagnostic markers and/or therapeutic targets using proteomic approaches. The objectives of both proteomic approaches was to identify altered protein expression in tumour compared to normal cells, validate altered protein expression and explore the potential of altered protein levels as markers for OSCC or as targets for therapeutic intervention.

Two proteomic techniques were applied to investigate the potential of membrane or membrane associated proteins as targets for therapy or for earlier diagnosis of the disease.

Although the application of 2D-DIGE to proteins from tumour and normal tissue identified a number of membrane and membrane-associated proteins, only Annexin 2, PK2 and GAPDH were subsequently validated and explored further.

We cannot conclusively state that the increase in annexin 2 expression was not related to the survival status of patients with OSCC, as the statistical power of the study is not significant. Unfortunately, due to limited patient sample, an IHC study of a larger cohort was not possible. Nevertheless, the increased levels of annexin 2 in OSCC tissue compared normal tissue, renders it as a potential therapeutic target. Future studies should include further molecular investigation as to contribution of annexin 2 in the development of OSCC, to determine its value as a potential therapeutic target in OSCC.

The increased level of glycolytic enzymes (PK2 and GAPDH) in tumour tissue was explored as a target for therapeutic intervention in OSCC. According to previous reports, OSCC was expected to be an ideal candidate for DCA treatment, based on its increased levels of glycolytic enzymes compared to normal tissue. Bonnet *et al* (139) neglected to report dose response curves (to calculate EC_{50}) for treatment with DCA, however, their murine models convincingly showed a reduction in tumour size post-treatment with DCA. Our model revealed that the concentrations of DCA required for cell death to occur was 10-fold more than concentrations required to cause cell death in other cancers (139,218). Furthermore, DCA caused cell death via a different pathway than previously reported. The significance of this study, based on these results, is that DCA will not be effective in the therapeutic intervention of patients with OSCC. However, further investigations, perhaps using in vivo mouse models (as Bonnet et al showed (139)) would be able to determine the potential of DCA as a therapeutic strategy in OSCC.

REQUA identified one glycosylated membrane protein, namely, CD98 hc. One of the significant findings of this study is that it marks CD98 hc as a good candidate as an early diagnostic marker and potential therapeutic target in OSCC. CD98 hc's potential as an early diagnostic marker and a potential therapeutic target is currently being explored in other cancers (215,216) and we recommend, based on our results, that OSCC be included in these trials. Furthermore, future studies should include an immunohistochemical study of CD98 hc in a larger cohort of OSCC patient (and corresponding normal) material, to determine CD98 hc's potential as a marker of survival, as was performed with annexin 2 in this study.

In summary this study achieved all its objectives, as we identified a number of membrane and membrane-associated proteins that displayed altered protein patterns in tumour cells compared

to normal cells. The proteins' of interest expression levels were validated. Finally, the potential of some of these proteins were explored further.

Appendix A:

Chapter 2

Plasma membrane preparation

HEPES Buffer (ph 7.4):10 mM HEPES and 1 mM EDTA

Cocktail of protease inhibitors (cOmplete, Roche):

> Stock solution : 1 tablet dissolved in 2ml dist water and separated into 100µl aliquots, results in a 10X stock solution, which is diluted to 1X with HEPES buffer, for every 200µl used 20µl of stock was included e.g. 180µl buffer plus 20µl stock

phenylmethanesulphonylfluoride or phenylmethylsulphonyl fluoride (PMSF) : Stock solution = 50 mM, final concentration in homogenate should be 1mM therefore need a 1/50 dilution from stock. E.g. if final volume is 3ml homogenate, include 60µl stock solution.

2D-DIGE and CCB staining

CyDyes (NHS-Cy2, -Cy3, -Cy5): from lyophilized powder (stored at -20ºC), reconstitute to 1 mM stock by dissolving in the appropriate volume of anhydrous DMF. Keep stock solutions in dark at -20ºC. Stable for up to 4 months.

Lysis buffer (pH 8.3): 8 M urea, 2 M thiourea, 4% (w/v) CHAPS, 0.5% NP-40 (w/v), 10 mM Tris-HCl pH 8.3. To make 100 mL, dissolve 48 g of urea and 15.2 g of thiourea in 50 mL of distilled H_2O. Add

4 g CHAPS, 0.5 g NP-40 and 0.67 mL of 1.5 M Tris pH 8.8 solution. *40% (w/v) CHAPS*: For 50 mL, dissolve 20 g CHAPS in H_2O and adjust to 50 mL.

10% (w/v) NP-40: For 50 mL, dilute 5 g of 100% NP-40 in H_2O and adjust to 50 mL.

L-lysine solution: 10 mM L-lysine in H_2O. Dissolve 9.1 mg in 5 mL distilled H_2O.

DTT solution: 1.3 M DTT in H_2O. To make 10 mL, dissolve 2 g DTT in distilled H_2O and complete to 10 mL. Aliquot and store at -20ºC.

Ampholines/Pharmalyte mix: Mix equal volumes of ampholines (pH 3.5-10) and Pharmalyte (pH 3-10). Store at 4ºC. These broad pH range IPG buffers can be replaced with narrow range buffers depending on the 1st dimension pH range.

Bromophenol blue: 0.2% (w/v) bromophenol blue in H_2O. To make 10 mL, weigh 20 mg bromophenol blue and complete to 10 mL with distilled H_2O. Filter and store at room temperature.

Bind Saline solution: For twelve 24 cm x 20 cm plates, mix 16 □L of Plus One Bind Saline, 400 □L glacial acetic acid, 16 mL ethanol and 3.6 mL distilled H_2O.

Equilibration buffer: 6 M urea, 30% (v/v) glycerol, 50 mM Tris-HCl pH 6.8, 2% (w/v) SDS. To make 200 mL, dissolve 72 g urea in 100 mL distilled H_2O. Add 60 mL of 100% glycerol, 10 mL of 1 M Tris pH 6.8 solution and 4 g SDS. Dissolve all powders and adjust volume to 200 mL with distilled H_2O. Aliquot and store at -20ºC.

Agarose overlay: 0.5% (w/v) low-melting point agarose in 1x SDS electrophoresis buffer. To make 200 mL, melt 1 g of agarose in 200 mL of 1x SDS electrophoresis buffer in a microwave on low heat. Add bromophenol blue solution to give a pale blue colour

Fixing solution: 35% (v/v) methanol, 7.5% (v/v) acetic acid in distilled H_2O.

Colloidal CBB fixing solution: For colloidal Coomassie brilliant blue staining, fix gels in 35% (v/v) ethanol, 2% (v/v) phosphoric acid in distilled H_2O.

Colloidal CBB staining solution: 34% (v/v) methanol, 17% (w/v) ammonium sulphate, 3% (v/v) phosphoric acid in distilled H_2O.

Calmix Standards

Peptide	MW	Final Conc pmol	Stock Conc/☐L	Stock Vol/☐L
Bradykinin	757.3	0.500	576 pmol	8.68 (1/10)
Angiotensin I	1296.6	0.500	650 pmol	7.69 (1/10)
Angiotensin II	1046.5	0.500	450 pmol	11.10 (1/10)
Bombesin	1619.8	1.00	1 nmol	10.00 (1/10)
Renin	1758.9	1.00	230 pmol	4.35
ACTH (1-17)	2093.08	1.00	132 pmol	7.58
ACTH 918-39)	2465.19	2.00	200 pmol	58.80
Insulin B Chain	3494.65	3.00	184 pmol	16.35
			Total vol	134.55

IHC images

Magnification was represented as *magnification of objective X 10* (magnification of ocular)

Chapter 3

Cell culture

Trypsin-EDTA: 0.05 % (w/v) trypsin, 0.8 % (w/v) NaCl, 0.15% (w/v) $Na_2HPO_4.2H_2O$, 0.02% (w/v) KCl, 0.02% (w/v) KH_2PO_4 and 10 mM EDTA (pH 8.0)

PBS: 137 mM NaCl, 2.7 mM KCl, 4.3 mM $Na_2HPO_4.7H_2O$ (pH 7.4) and 1.4 mM KH_2PO_4

Penicillin/streptomycin solution: 5X10^6 U Penicillin G Sodium (supplied by Highveld Biological) to 5 ml PBS plus 5 g 214S Streptomycin Sulphate (Highveld Biological) to 15 ml PBS. Combine the two and make volume up to 500 ml with PBS. Aliquots of 5 ml volumes are added to each 500 ml volume of media.

REQUA, gel electrophoresis and staining

Labeling/Incubation mix (Table A1)

HEPES saline buffer: 10 mM HEPES and 140 mM NaCl

UDP[6-^{3}H]Gal : (supplied by GE Healthcare as an ammonium salt in 50% aqueous ethanol at a specific activity of 5-20 Ci/mmol or 1 mCi/ml) is diluted to 40µCi/ml in the labeling mix.

UDP [U-^{14}C]Gal :(supplied by GE Healthcare as an ammonium salt in an aqueous solution containing 2% ethanol at a specific activity of 200mCi/mmol or 25 µCi/ml) is diluted to a concentration of 40µCi/ml in the labeling mix

Galactosyltransferase: (supplied by Sigma: G5507, obtained from bovine milk as a lyophilized powder, 3-15 U/mg protein in the presence of adequate α-lactalbumin) is diluted to a final concentration of 0.5 U/ml in the labeling mix

MnCl: 50mM stock diluted to 5mM in labeling mix

Table A 1: Illustrating guidelines for volumes of labeling mix constituents. **Because ^{3}H is in 50% ethanol and cells are sensitive to ethanol (whereas ^{14}C is in an ammonium salt buffer hence more compatible with cells), hence at least 50% of the ethanol's volume needs to be evaporated with nitrogen at 4°C. e.g. if you have 4 plates: you require 200µl labeling mix per plate therefore need

800ul of total labeling mix. The amounts one will use is therefore 80 ul GT, 80ul MnCl, 40ul Radiolabelled galactose and make up to 800ul with 600 ul HeS

HEPES Saline	**^{3}H** or ^{14}C**	**Galactosyltransferase**	**MnCl (50mM stock)**	**Total volume**
x-depends on amount required to make up total volume	100ul/2ml total volume	$1/10^{th}$ of total volume	$1/10^{th}$ of total volume	x- depends on amount required

Homogenisation Buffer (pH 7)*:* 0.25M Sucrose, 2mM EDTA and 10mM HEPES

Protease inhibitor: 1 c*O*mplete tablet was dissolved in 5 ml dH_2O to make a 10x solution. Aliquots were stored at -20°C.

Percoll: (supplied by Sigma: P1644) diluted to 27% of total volume (Table A2)

Table A 2: Illustrating an example of typical volumes in the Percoll ® gradient

Sucrose	Percoll	HB	PNS
500ul	5.67	15.33	2ml

80% sucrose: 80% (w/v) in H_2O

30% Acrylamide: 30% (w/v) acrylamide, 0.8% (w/v) bis-acrylamide and 0.1 g (w/v) SDS

Stacking Buffer (pH 6.3): 0.5 M Tris, 0.4% (w/v) SDS pH to 8.0

Resolving buffer (pH 8.8): 1.5 M Tris and 0.4% (w/v) SDS

Large format 8% to 15 % gradient SDS-PAGE: Table A3

Table A 3: Indicating volumes used to make up 8% to 15% gradient gels

	8%	15%
H_2O (ml)	17.4	4.8
Resolving buffer (ml)	9	9
30% Acrylamide (ml)	9.6	15.6

10X Electrophoresis buffer: 4% (w/v) glycine, 6.32% (w/v) Tris and 1% SDS. Dilute 1 in 10 for 1x running buffer

Coomassie Blue staining solution: 50% (v/v) methanol, 10% (v/v) acetic acid and 0.25% (w/v)

De-staining solution: 10% (v/v) methanol and 7.5% (v/v) acetic acid

IHC images

Magnification was represented as *magnification of objective X 10* (magnification of ocular)

Patient number	DATE DIAGNOSED/registration date	SURVstatus	Stage	Last follow up/death	Survival in years
1	4/28/1986	DEAD	2	1/1/2003	16.69041096
2	7/14/1986	DEAD	3	2/27/1994	7.630136986
3	1/19/1989	ALIVE	2	10/13/2006	17.74246575
4	6/29/1989	DEAD	3	7/7/1989	0.021917808
5	7/6/1989	ALIVE	2	11/13/2006	17.36712329
6	8/17/1989	DEAD	3	11/30/2001	12.29589041
7	9/28/1989	ALIVE	2	2/17/2006	16.4
8	1/25/1990	DEAD	3	5/17/1991	1.306849315
9	4/5/1990	DEAD	2	12/23/1990	0.717808219
10	5/17/1990	DEAD	2	12/5/1990	0.553424658
11	6/7/1990	DEAD	3	2/17/1992	1.698630137
12	1/3/1991	DEAD	2	2/11/1991	0.106849315
13	3/28/1991	DEAD	2	6/10/1991	0.202739726
14	5/7/1991	DEAD	3	6/11/1992	1.098630137
15	11/18/1991	DEAD	3	12/14/1991	0.071232877
16	1/23/1992	DEAD	2	11/8/2000	8.8
17	4/16/1992	DEAD	3	8/22/1994	2.350684932
18	5/21/1992	DEAD	2	2/16/1994	1.742465753
19	7/2/1992	DEAD	2	9/25/1995	3.232876712
20	7/16/1992	DEAD	2	8/30/1992	0.123287671
21	8/20/1992	DEAD	3	6/3/1994	1.78630137
22	9/10/1992	DEAD	2	9/29/1992	0.052054795
23	1/14/1993	DEAD	2	1/30/1993	0.043835616
24	1/21/1993	DEAD	3	6/1/1993	0.35890411
25	1/21/1993	DEAD	2	10/28/1996	3.769863014
26	3/4/1993	DEAD	3	3/20/1993	0.043835616
27	3/25/1993	DEAD	3	7/15/1993	0.306849315
28	4/2/1993	DEAD	3	6/26/1993	0.232876712
29	5/25/1993	ALIVE	2	6/30/2006	13.10684932
30	8/20/1993	DEAD	3	9/25/1993	0.098630137
31	2/4/1994	DEAD	3	7/2/1994	0.405479452
32	4/23/1994	DEAD	3	10/5/1994	0.452054795
33	12/4/1994	DEAD	3	12/11/1995	1.019178082
34	1/13/1995	DEAD	1	2/21/1995	0.106849315
35	1/27/1995	ALIVE	2	5/5/2006	11.27671233
36	4/21/1995	DEAD	3	12/9/1996	1.638356164
37	8/4/1995	DEAD	2	9/28/1995	0.150684932
38	8/25/1995	DEAD	3	6/22/1996	0.82739726
39	10/20/1995	DEAD	3	9/2/1996	0.871232877
40	11/3/1995	ALIVE	2	11/6/2006	11.01643836
41	1/19/1996	DEAD	2	1/1/1997	0.953424658
42	1/13/1997	DEAD	2	4/17/2004	7.263013699
43	2/14/1997	DEAD	2	7/19/1998	1.424657534
44	4/11/1997	DEAD	2	6/18/1998	1.18630137
45	9/19/1997	ALIVE	1	11/15/2006	9.161643836
46	11/6/1997	DEAD	2	4/30/1998	0.479452055
47	3/3/1998	DEAD	2	6/6/1999	1.260273973
48	4/17/1998	DEAD	3	8/21/1998	0.345205479
49	5/7/1998	DEAD	3	8/7/1998	0.252054795
50	6/18/1998	DEAD	2	1/1/2004	5.542465753
51	7/7/1998	DEAD	2	10/17/1998	0.279452055
52	12/11/1998	DEAD	2	12/1/2001	2.975342466
53	2000-02-14	DEAD	2	10/3/2000	0.635616438
54	5/22/2000	DEAD	2	7/30/2004	4.191780822
55	3/10/2006	ALIVE	3	8/18/2006	0.44109589
56	10/1/2002	ALIVE	2	6/30/2006	3.747945205
57	8/6/2004	ALIVE	2	7/14/2006	1.936986301
58	12/3/2004	ALIVE	3	10/20/2006	1.879452055
59	11/30/2001	ALIVE	2	10/27/2006	4.909589041

Table A 4: Status of 59 patients used in statistical evaluations at the time of analysis Note: the 18 patients used for confirmation of protein expression were included in the 59 patients used.

Chapter 4

DCA: (supplied by Sigma: 34, 779-5) diluted in PBS to desired concentration

Phase contrast images

Magnification was represented as *magnification of objective X 10* (magnification of ocular)

Growth assay

MTT: (supplied from sigma: M2128) diluted 5mg/ml in Sterile 1 x PBS solution, pH 7.4 (sterile filtered)

Solubilisation reagent: 10% SDS in 0.01M HCl, non sterile.

Cell cycle

Staining solution: 0.1 % Triton X100, 2 mM $MgCl_2$, 100 mM NaCl, 0.01 M PIPES buffer and 10 µg/ml propidium iodide

Western blotting

Lysis buffer: 150 mM NaCl, 1% (v/v) Triton X-100, 0.1% (w/v) SDS, 10 mM Tris at pH 7.5 and 1% (w/v) Na-deoxycholate

Protease inhibitor: 1 c*O*mplete tablet was dissolved in 5 ml dH_2O to make a 10x solution. Aliquots were stored at -20°C.

Lysis buffer plus protease and phosphatase inhibitors: 1µM Na_3VO_4, 20 µM NaF and 10% protease inhibitor

30% Acrylamide: 30% (w/v) acrylamide, 0.8% (w/v) bis-acrylamide and 0.1 g (w/v) SDS

Stacking Buffer (pH 8): 5.9% (w/v) Tris, 0.4% (w/v) SDS pH to 8.0

Resolving Buffer (pH 8.9): 36.2% (w/v) Tris and 0.8% (w/v) SDS

5x Loading Buffer (pH 6.8): 3.5% (w/v) Tris, 60% (v/v) glycine and 5% (w/v) SDS

Loading Dye: 200 µl 5x loading buffer, 100 µl β-mercaptoethanol, 100 µl saturated, filtered bromophenol blue

10X Electrophoresis buffer: 4% (w/v) glycine, 6.32% (w/v) Tris and 1% SDS. Dilute 1 in 10 for 1x running buffer

10x Transfer Buffer: 14.4% (w/v) glycine and 3.8 % (w/v) Tris

1x Transfer Buffer: 100 ml 10x transfer buffer, 200 ml isopropanol and 700 ml H_2O

Coomassie Blue staining solution: 50% (v/v) methanol, 10% (v/v) acetic acid and 0.25% (w/v)

De-staining solution: 10% (v/v) methanol and 7.5% (v/v) acetic acid

Ponceau-S stain solution: 0.1% (w/v) Ponceau S and 1% (v/v) glacial acetic acid

10x Tris buffered saline (pH 7.5): 6.05 % (w/v) Tris, 8.76% (w/v) NaCl

TBS plus 0.1 % Tween: 100 ml 10x TBS, 900 ml dH_2O and 1 ml Tween 20

Fixer (AGFA G333C): Dilute 100 ml stock solution with 400 ml H_2O

Developer (AGFA G128): Dilute 100 ml stock solution with 400 ml H_2O

RNA gel electrophoresis

10x MOPS: 0.4 M MOPS pH 7.0, 0.1 M sodium acetate and 0.01 M EDTA

Formaldehyde loading buffer: 5.3% (v/v) saturated bromophenol blue, 6.66% (v/v) glycerol, 10.7% (v/v) 10X MOPS, 17.3% (v/v) 12.3M formaldehyde and 47% (v/v) formamide.

Appendix B:

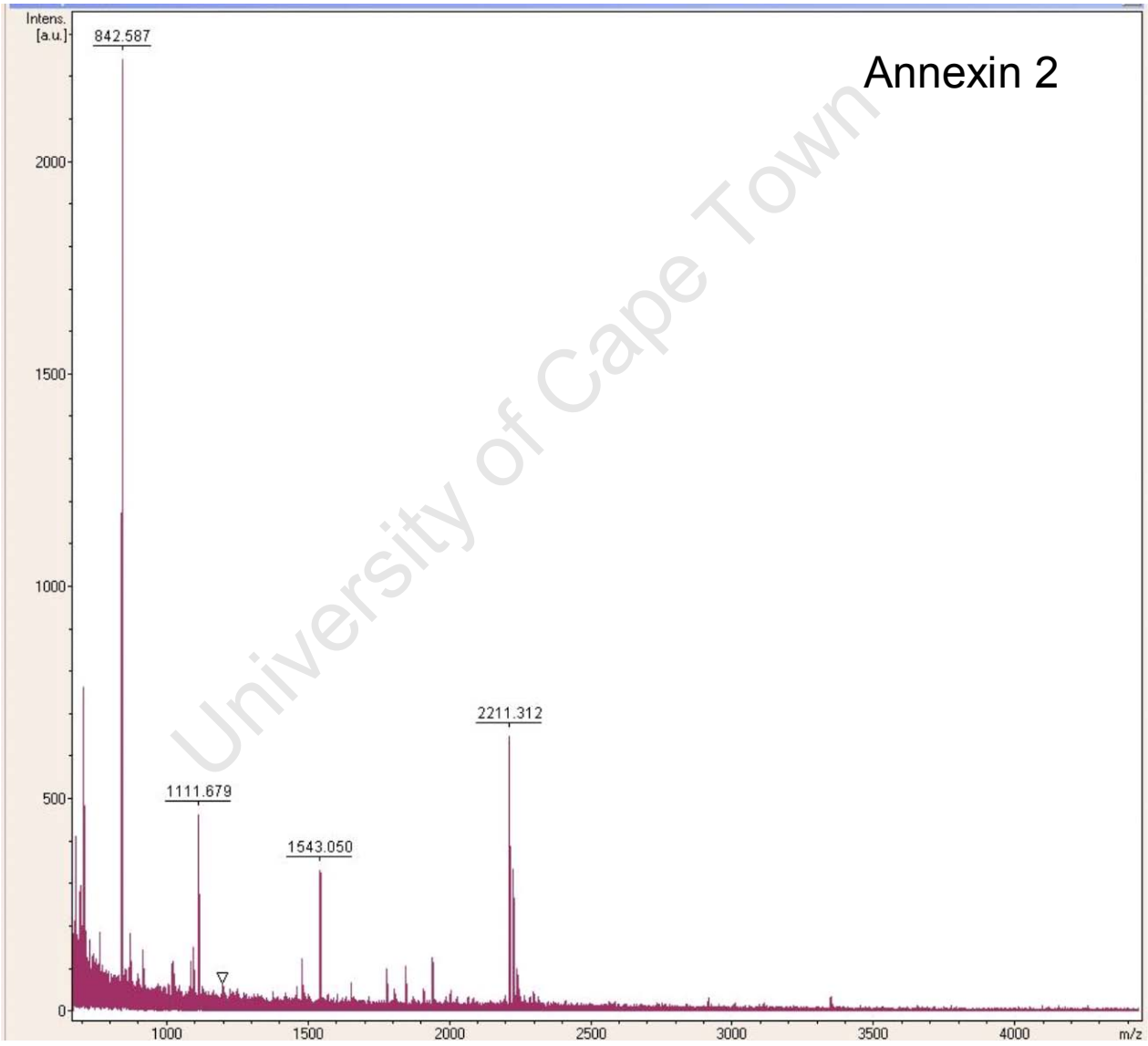

Annexin 2

Figure B 1: Mass spectrum for annexin 2. The mass-to-charge ratio (*m/z)* is on the *x*-axis and signal intensity is represented on the *y*-axis. MS data was generated as described in materials and methods, and internally calibrated using trypsin autolysis peaks.

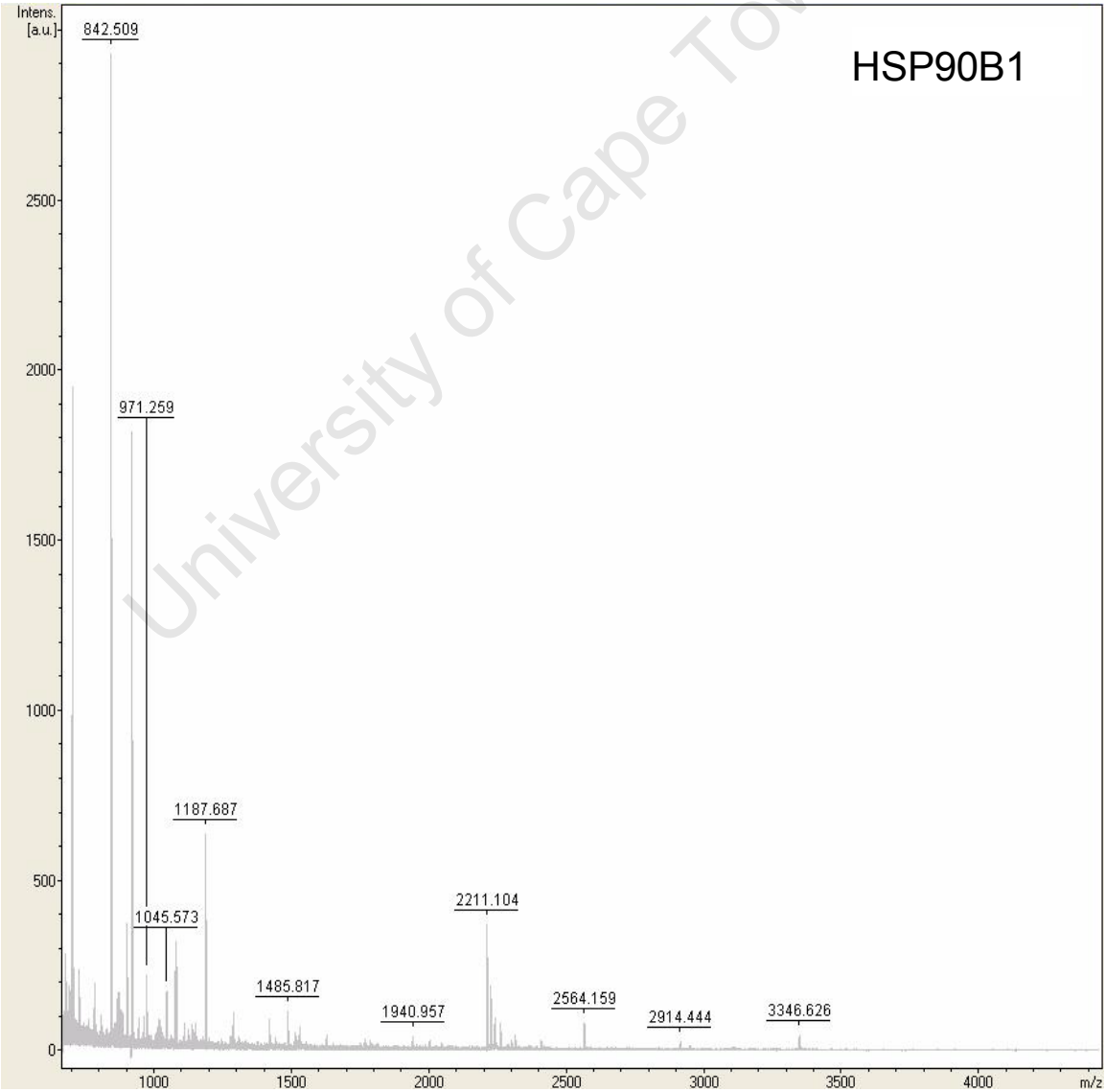

Figure B 2: Mass spectrum for HSP90B1. The mass-to-charge ratio (*m/z)* is on the *x*-axis and signal intensity is represented on the *y*-axis. MS data was generated as described in materials and methods, and internally calibrated using trypsin autolysis peaks.

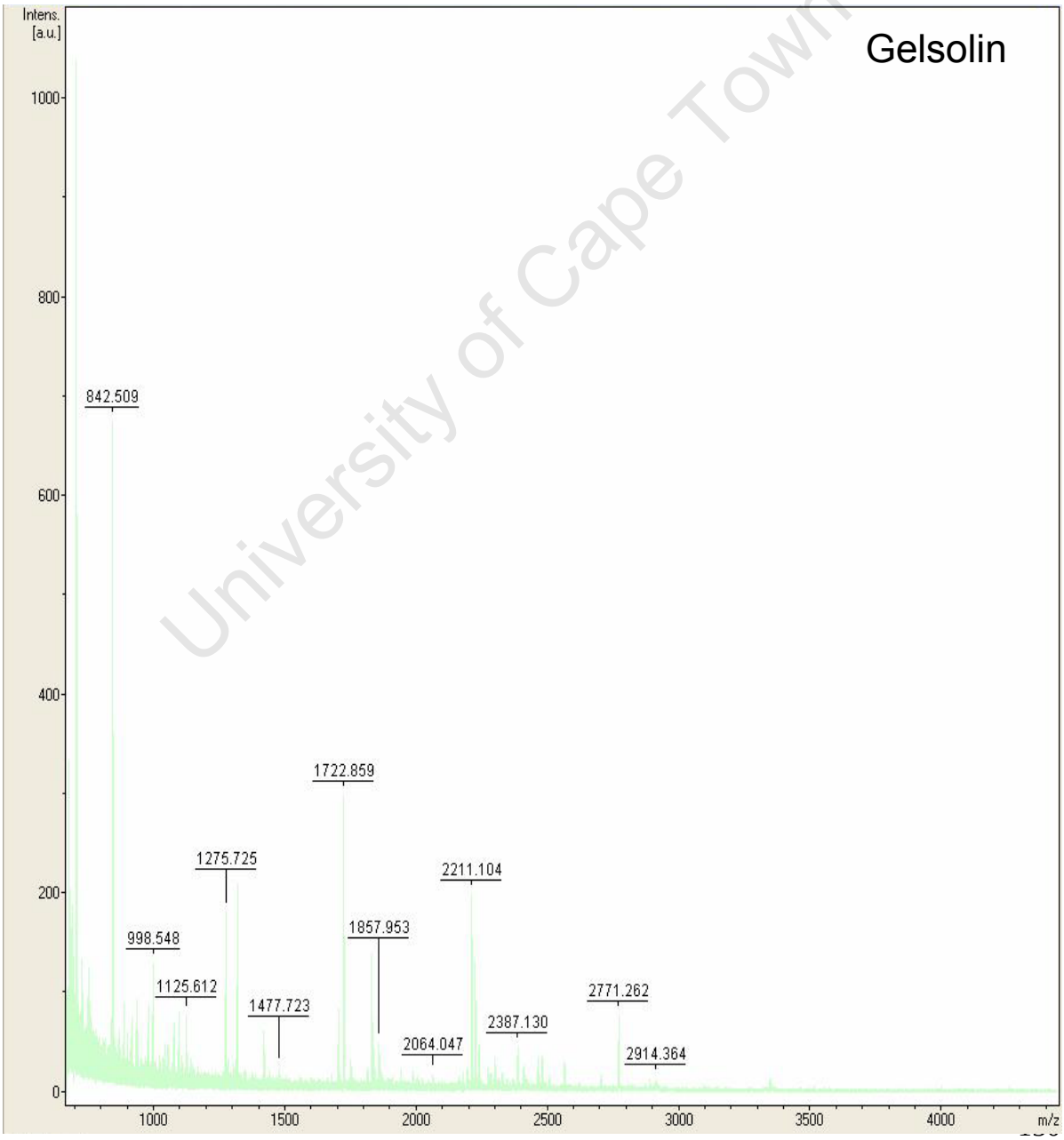

Figure B 3: Mass spectrum for gelsolin. The mass-to-charge ratio (*m/z)* is on the *x*-axis and signal intensity is represented on the *y*-axis. MS data was generated as described in materials and methods, and internally calibrated using trypsin autolysis peaks.

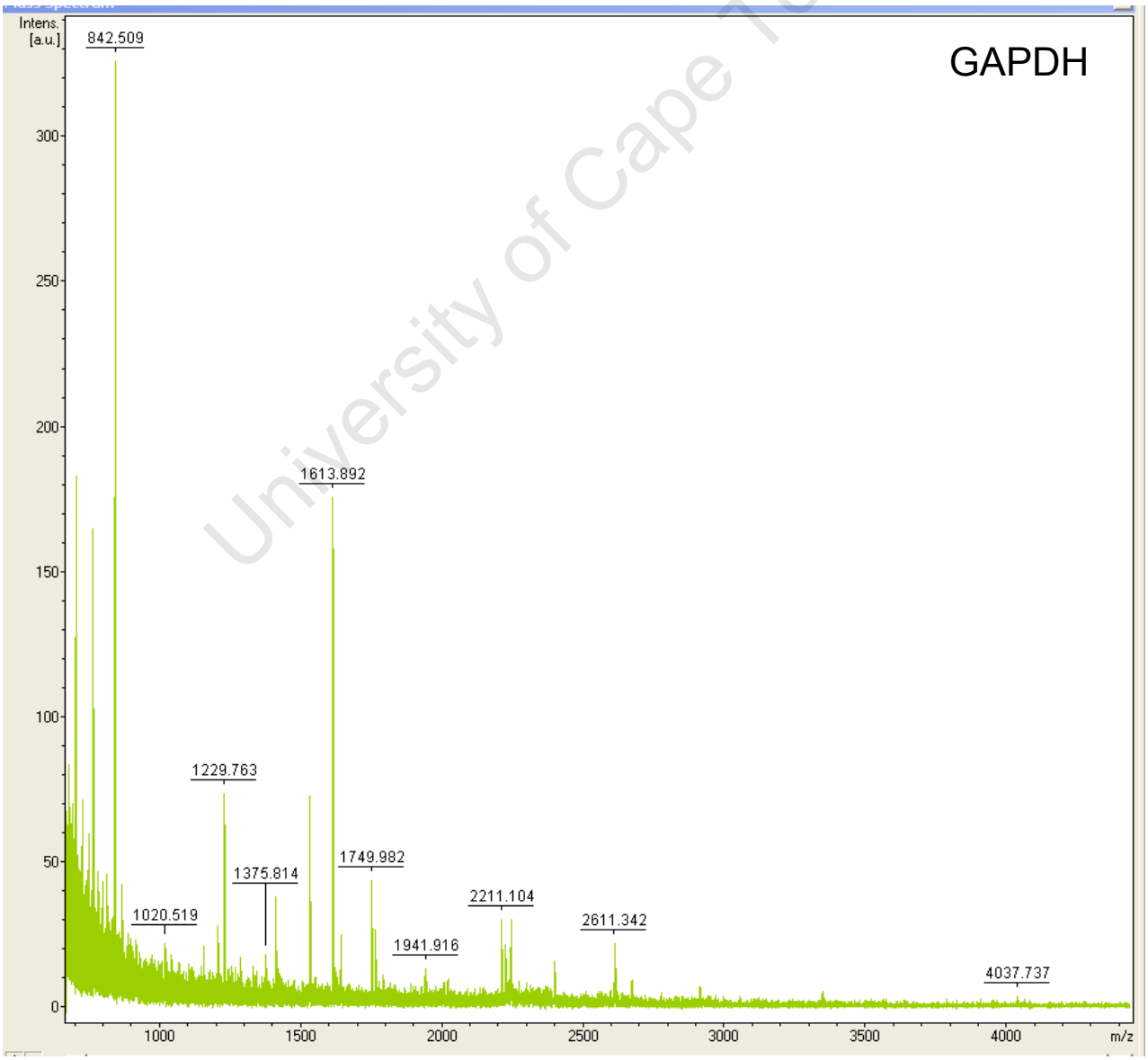

Figure B 4: Mass spectrum for GAPDH. The mass-to-charge ratio (*m/z)* is on the *x*-axis and signal intensity is represented on the *y*-axis. MS data was generated as described in materials and methods, and internally calibrated using trypsin autolysis peaks.

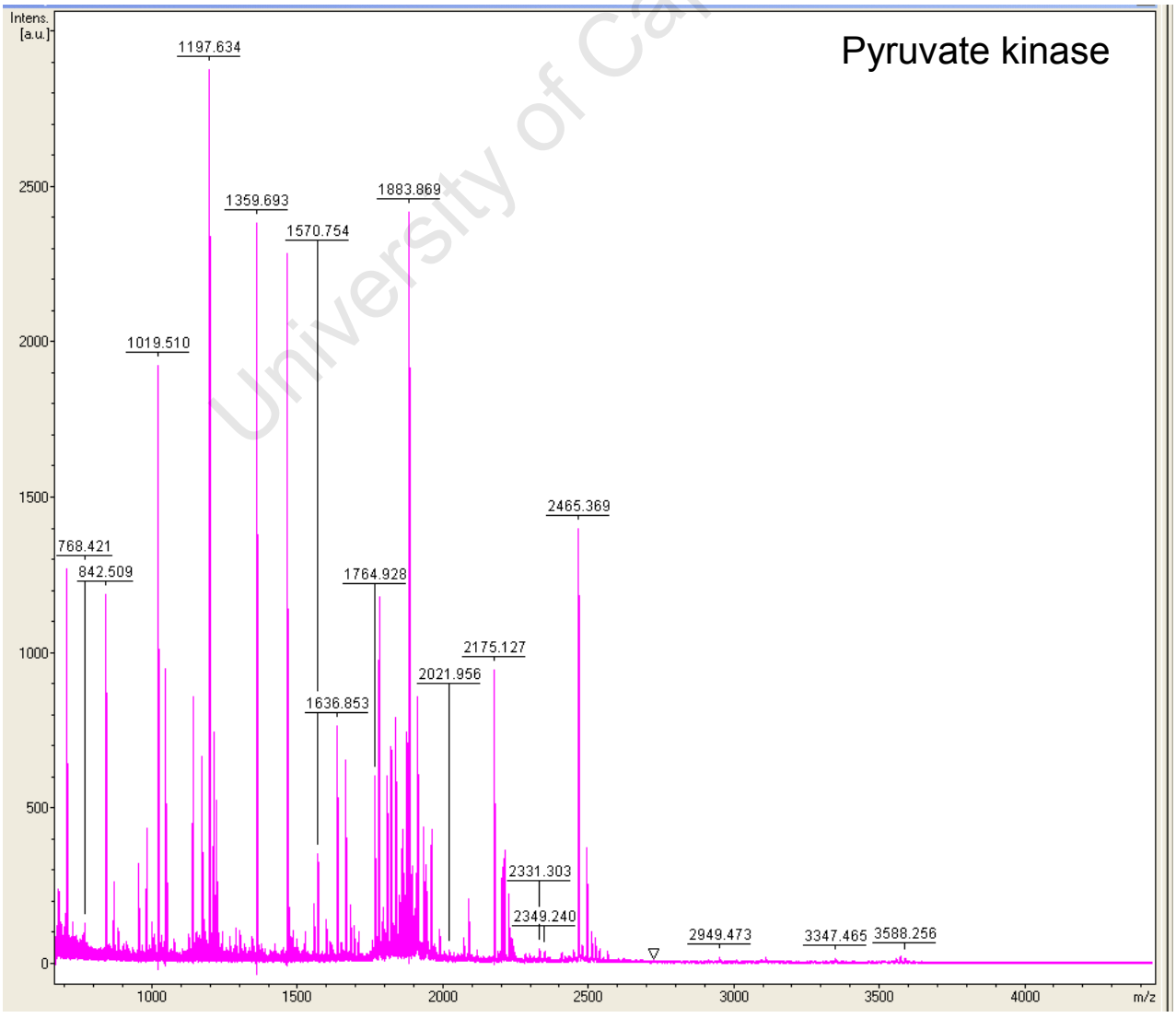

Figure B 5: Mass spectrum for pyruvate kinase. The mass-to-charge ratio (*m/z)* is on the *x*-axis and signal intensity is represented on the *y*-axis. MS data was generated as described in materials and methods, and internally calibrated using trypsin autolysis peaks.

References

(1) "epithelium" McGraw-Hill Encyclopedia of Science and Technology. New York: The McGraw-Hill Companies, Inc.; 2005.

(2) Normal oesophagus. www barretsinfo com 2008 January 11 [cited 2008 Oct 11];

(3) Stages of oesophageal cancer. www cancer gov 2008 October 11 [cited 2008 Oct 11];

(4) Gabbert HE, Shimoda T, Hainaut P, Nakamura Y, Field JK, Inoue H. Squamous cell carcinoma of the oesophagus. Pathology and Genetics. Tumours of the Digestive System (WHO Classification of Tumours, Volume 2 IARC WHO Classification of Tumours, No 2). 3 ed. Lyon: International Agency for Research on cancer (IARC) Press; 2000.

(5) Mqoqi N, Kellet P, Sitas F, Jula M. Incidence of histologically diagnosed cancer in South Africa, 1998 - 1999. Johannesburg: National Cancer Registry of South Africa, National Health Laboratory Service; 2004 Jan 12.

(6) Hendricks D, Parker MI. Oesophageal cancer in Africa. IUBMB Life 2002 Apr;53(4-5):263-8.

(7) Lam AK. Molecular biology of esophageal squamous cell carcinoma. Crit Rev Oncol Hematol 2000 Feb;33(2):71-90.

(8) Parkin DM, Pisani P, Ferlay J. Global cancer statistics. CA Cancer J Clin 1999 Jan;49(1):33-64, 1.

(9) Ferlay J, Bray F, Pisani P, Parkin DM. GLOBOCAN 2002: Cancer Incidence, Mortality and Prevalence Worldwide IARC CancerBase No. 5. version 2.0. Lyon: IARC Press; 2004.

(10) Norman R, Bradshaw D, Schneider M, Pieterse D, Groenerwald P. Revised Burden of Disease Estimates for the Comparative Risk Factor Assessment, South Africa 2000. Cape Town: South African Medical Research Council; 2006.

(11) Enzinger PC, Mayer RJ. Esophageal cancer. N Engl J Med 2003 Dec 4;349(23):2241-52.

(12) Pacella-Norman R, Urban MI, Sitas F, Carrara H, Sur R, Hale M, et al. Risk factors for oesophageal, lung, oral and laryngeal cancers in black South Africans. Br J Cancer 2002 Jun 5;86(11):1751-6.

(13) Matsha T, Erasmus R, Kafuko AB, Mugwanya D, Stepien A, Parker MI. Human papillomavirus associated with oesophageal cancer. J Clin Pathol 2002 Aug;55(8):587-90.

(14) Dlamini Z, Bhoola K. Esophageal cancer in African blacks of Kwazulu Natal, South Africa: an epidemiological brief. Ethn Dis 2005;15(4):786-9.

(15) Marasas WF, Jaskiewicz K, Venter FS, Van Schalkwyk DJ. Fusarium moniliforme contamination of maize in oesophageal cancer areas in Transkei. S Afr Med J 1988 Aug 6;74(3):110-4.

(16) Marasas WF. Discovery and occurrence of the fumonisins: a historical perspective. Environ Health Perspect 2001 May;109 Suppl 2:239-43.

(17) Walker AR, Walker BF, Metz J. Acceptability trials of maize meal fortified with niacin, riboflavin and folic acid. S Afr Med J 1983 Sep 3;64(10):343-6.

(18) Ghavamzadeh A, Moussavi A, Jahani M, Rastegarpanah M, Iravani M. Esophageal cancer in Iran. Semin Oncol 2001 Apr;28(2):153-7.

(19) Van Rensburg SJ, Bradshaw ES, Bradshaw D, Rose EF. Oesophageal cancer in Zulu men, South Africa: a case-control study. Br J Cancer 1985 Mar;51(3):399-405.

(20) Coussens LM, Werb Z. Inflammation and cancer. Nature 2002 Dec 19;420(6917):860-7.

(21) Balleine RL, Kefford RF. Targeting molecular mechanisms in cancer. ANZ J Surg 2002 Oct;72(10):760-3.

(22) Hanahan D, Weinberg RA. The hallmarks of cancer. Cell 2000 Jan 7;100(1):57-70.

(23) Ullah MF, Aatif M. The footprints of cancer development: Cancer biomarkers. Cancer Treat Rev 2009 May;35(3):193-200.

(24) Zhang HT, Wang Q, Greene MI, Murali R. New perspectives on anti-HER2/neu therapeutics. Drug News Perspect 2000 Aug;13(6):325-9.

(25) Albanell J, Codony J, Rovira A, Mellado B, Gascon P. Mechanism of action of anti-HER2 monoclonal antibodies: scientific update on trastuzumab and 2C4. Adv Exp Med Biol 2003;532:253-68.

(26) Romond EH, Perez EA, Bryant J, Suman VJ, Geyer CE, Jr., Davidson NE, et al. Trastuzumab plus adjuvant chemotherapy for operable HER2-positive breast cancer. N Engl J Med 2005 Oct 20;353(16):1673-84.

(27) Absi A, Adelstein DJ. Esophageal cancer. In: Carey WD, editor. Disease Management Project.Cleveland: The Cleveland Clinic Foundation; 2008.

(28) Bast RC, Jr., Klug TL, St JE, Jenison E, Niloff JM, Lazarus H, et al. A radioimmunoassay using a monoclonal antibody to monitor the course of epithelial ovarian cancer. N Engl J Med 1983 Oct 13;309(15):883-7.

(29) Buys SS, Partridge E, Greene MH, Prorok PC, Reding D, Riley TL, et al. Ovarian cancer screening in the Prostate, Lung, Colorectal and Ovarian (PLCO) cancer screening trial: findings from the initial screen of a randomized trial. Am J Obstet Gynecol 2005 Nov;193(5):1630-9.

(30) Guppy AE, Rustin GJ. CA125 response: can it replace the traditional response criteria in ovarian cancer? Oncologist 2002;7(5):437-43.

(31) Polascik TJ, Oesterling JE, Partin AW. Prostate specific antigen: a decade of discovery--what we have learned and where we are going. J Urol 1999 Aug;162(2):293-306.

(32) Makarov DV, Carter HB. The discovery of prostate specific antigen as a biomarker for the early detection of adenocarcinoma of the prostate. J Urol 2006 Dec;176(6 Pt 1):2383-5.

(33) Grossklaus DJ, Smith JA, Jr., Shappell SB, Coffey CS, Chang SS, Cookson MS. The free/total prostate-specific antigen ratio (%fPSA) is the best predictor of tumor

involvement in the radical prostatectomy specimen among men with an elevated PSA. Urol Oncol 2002 Sep;7(5):195-8.

(34) Baron AT, Maihle N. Nadir CA125 concentration as a prognostic indicator in ovarian cancer. Nat Clin Pract Oncol 2005 Jun;2(6):288-9.

(35) Stenman UH, Abrahamsson PA, Aus G, Lilja H, Bangma C, Hamdy FC, et al. Prognostic value of serum markers for prostate cancer. Scand J Urol Nephrol Suppl 2005 May;(216):64-81.

(36) Tenke P, Horti J, Balint P, Kovacs B. Prostate cancer screening. Recent Results Cancer Res 2007;175:65-81.

(37) Conrads TP, Zhou M, Petricoin EF, III, Liotta L, Veenstra TD. Cancer diagnosis using proteomic patterns. Expert Rev Mol Diagn 2003 Jul;3(4):411-20.

(38) Cancer Biomarkers: The Promises and Challenges of Improving Detection and Treatment. Washington DC: National Academic Press; 2007.

(39) Physician's Desk Reference. 50th ed. Montvale, NJ: Medical Economics Company; 1996.

(40) Sun CC, Ramirez PT, Bodurka DC. Quality of life for patients with epithelial ovarian cancer. Nat Clin Pract Oncol 2007 Jan;4(1):18-29.

(41) Planting AS, de Mulder PH, de GA, Verweij J. Phase II study of weekly high-dose cisplatin for six cycles in patients with locally advanced squamous cell carcinoma of the head and neck. Eur J Cancer 1997 Jan;33(1):61-5.

(42) Press OW. Emerging immunotherapies for non-Hodgkin lymphomas: the tortoise approaches the finish line. Ann Intern Med 2000 Jun 6;132(11):916-8.

(43) Kalyn R. Overview of targeted therapies in oncology. J Oncol Pharm Pract 2007 Dec;13(4):199-205.

(44) Hamann PR, Hinman LM, Hollander I, Beyer CF, Lindh D, Holcomb R, et al. Gemtuzumab ozogamicin, a potent and selective anti-CD33 antibody-calicheamicin conjugate for treatment of acute myeloid leukemia. Bioconjug Chem 2002 Jan;13(1):47-58.

(45) Bernstein ID. CD33 as a target for selective ablation of acute myeloid leukemia. Clin Lymphoma 2002 Mar;2 Suppl 1:S9-11.

(46) Hamann PR, Hinman LM, Beyer CF, Lindh D, Upeslacis J, Flowers DA, et al. An anti-CD33 antibody-calicheamicin conjugate for treatment of acute myeloid leukemia. Choice of linker. Bioconjug Chem 2002 Jan;13(1):40-6.

(47) al-Kasspooles M, Moore JH, Orringer MB, Beer DG. Amplification and over-expression of the EGFR and erbB-2 genes in human esophageal adenocarcinomas. Int J Cancer 1993 May 8;54(2):213-9.

(48) Grandis JR, Tweardy DJ. Elevated levels of transforming growth factor alpha and epidermal growth factor receptor messenger RNA are early markers of carcinogenesis in head and neck cancer. Cancer Res 1993 Aug 1;53(15):3579-84.

(49) Normanno N, De LA, Bianco C, Strizzi L, Mancino M, Maiello MR, et al. Epidermal growth factor receptor (EGFR) signaling in cancer. Gene 2006 Jan 17;366(1):2-16.

(50) Harari PM. Epidermal growth factor receptor inhibition strategies in oncology. Endocr Relat Cancer 2004 Dec;11(4):689-708.

(51) Martin P, Kelly CM, Carney D. Epidermal growth factor receptor-targeted agents for lung cancer. Cancer Control 2006 Apr;13(2):129-40.

(52) Cohen MH, Williams GA, Sridhara R, Chen G, Pazdur R. FDA drug approval summary: gefitinib (ZD1839) (Iressa) tablets. Oncologist 2003;8(4):303-6.

(53) Raffo AJ, Perlman H, Chen MW, Day ML, Streitman JS, Buttyan R. Overexpression of bcl-2 protects prostate cancer cells from apoptosis in vitro and confers resistance to androgen depletion in vivo. Cancer Res 1995 Oct 1;55(19):4438-45.

(54) Cox AG, Hampton MB. Bcl-2 over-expression promotes genomic instability by inhibiting apoptosis of cells exposed to hydrogen peroxide. Carcinogenesis 2007 Oct;28(10):2166-71.

(55) Del PG, Bruno A, Del Principe MI, Venditti A, Maurillo L, Buccisano F, et al. Deregulation of the mitochondrial apoptotic machinery and development of molecular targeted drugs in acute myeloid leukemia. Curr Cancer Drug Targets 2008 May;8(3):207-22.

(56) Moreira JN, Santos A, Simoes S. Bcl-2-targeted antisense therapy (Oblimersen sodium): towards clinical reality. Rev Recent Clin Trials 2006 Sep;1(3):217-35.

(57) Cheson BD. Oblimersen for the treatment of patients with chronic lymphocytic leukemia. Ther Clin Risk Manag 2007 Oct;3(5):855-70.

(58) Lee S, Chen J, Zhou G, Shi RZ, Bouffard GG, Kocherginsky M, et al. Gene expression profiles in acute myeloid leukemia with common translocations using SAGE. Proc Natl Acad Sci U S A 2006 Jan 24;103(4):1030-5.

(59) Muller-Hagen G, Beinert T, Sommer A. Aspects of lung cancer gene expression profiling. Curr Opin Drug Discov Devel 2004 May;7(3):290-303.

(60) Pospisilova S, Mayer J. [A modern method for differential gene expression analysis and its significance for cancer diagnostics and therapy]. Cas Lek Cesk 2005;144(1):11-7.

(61) Kim B, Lee HJ, Choi HY, Shin Y, Nam S, Seo G, et al. Clinical validity of the lung cancer biomarkers identified by bioinformatics analysis of public expression data. Cancer Res 2007 Aug 1;67(15):7431-8.

(62) Argani P, Iacobuzio-Donahue C, Ryu B, Rosty C, Goggins M, Wilentz RE, et al. Mesothelin is overexpressed in the vast majority of ductal adenocarcinomas of the pancreas: identification of a new pancreatic cancer marker by serial analysis of gene expression (SAGE). Clin Cancer Res 2001 Dec;7(12):3862-8.

(63) Hassan R, Bera T, Pastan I. Mesothelin: a new target for immunotherapy. Clin Cancer Res 2004 Jun 15;10(12 Pt 1):3937-42.

(64) Sparano JA, Paik S. Development of the 21-gene assay and its application in clinical practice and clinical trials. J Clin Oncol 2008 Feb 10;26(5):721-8.

(65) Paik S, Shak S, Tang G, Kim C, Baker J, Cronin M, et al. A multigene assay to predict recurrence of tamoxifen-treated, node-negative breast cancer. N Engl J Med 2004 Dec 30;351(27):2817-26.

(66) Kaklamani VG, Gradishar WJ. Gene expression in breast cancer. Curr Treat Options Oncol 2006 Mar;7(2):123-8.

(67) Cobleigh MA, Tabesh B, Bitterman P, Baker J, Cronin M, Liu ML, et al. Tumor gene expression and prognosis in breast cancer patients with 10 or more positive lymph nodes. Clin Cancer Res 2005 Dec 15;11(24 Pt 1):8623-31.

(68) Lyman GH, Cosler LE, Kuderer NM, Hornberger J. Impact of a 21-gene RT-PCR assay on treatment decisions in early-stage breast cancer: an economic analysis based on prognostic and predictive validation studies. Cancer 2007 Mar 15;109(6):1011-8.

(69) Azad NS, Rasool N, Annunziata CM, Minasian L, Whiteley G, Kohn EC. Proteomics in clinical trials and practice: present uses and future promise. Mol Cell Proteomics 2006 Oct;5(10):1819-29.

(70) Zhou G, Li H, DeCamp D, Chen S, Shu H, Gong Y, et al. 2D differential in-gel electrophoresis for the identification of esophageal scans cell cancer-specific protein markers. Mol Cell Proteomics 2002 Feb;1(2):117-24.

(71) Washburn MP, Wolters D, Yates JR, III. Large-scale analysis of the yeast proteome by multidimensional protein identification technology. Nat Biotechnol 2001 Mar;19(3):242-7.

(72) Gygi SP, Rist B, Gerber SA, Turecek F, Gelb MH, Aebersold R. Quantitative analysis of complex protein mixtures using isotope-coded affinity tags. Nat Biotechnol 1999 Oct;17(10):994-9.

(73) DeSouza L, Diehl G, Rodrigues MJ, Guo J, Romaschin AD, Colgan TJ, et al. Search for cancer markers from endometrial tissues using differentially labeled tags iTRAQ and cICAT with multidimensional liquid chromatography and tandem mass spectrometry. J Proteome Res 2005 Mar;4(2):377-86.

(74) Everley PA, Krijgsveld J, Zetter BR, Gygi SP. Quantitative cancer proteomics: stable isotope labeling with amino acids in cell culture (SILAC) as a tool for prostate cancer research. Mol Cell Proteomics 2004 Jul;3(7):729-35.

(75) Mann M. Functional and quantitative proteomics using SILAC. Nat Rev Mol Cell Biol 2006 Dec;7(12):952-8.

(76) Tabb DL, McDonald WH, Yates JR, III. DTASelect and Contrast: tools for assembling and comparing protein identifications from shotgun proteomics. J Proteome Res 2002 Jan;1(1):21-6.

(77) Bridges SM, Magee GB, Wang N, Williams WP, Burgess SC, Nanduri B. ProtQuant: a tool for the label-free quantification of MudPIT proteomics data. BMC Bioinformatics 2007;8 Suppl 7:S24.

(78) Wu WW, Wang G, Baek SJ, Shen RF. Comparative study of three proteomic quantitative methods, DIGE, cICAT, and iTRAQ, using 2D gel- or LC-MALDI TOF/TOF. J Proteome Res 2006 Mar;5(3):651-8.

(79) Hanash SM, Madoz-Gurpide J, Misek DE. Identification of novel targets for cancer therapy using expression proteomics. Leukemia 2002 Apr;16(4):478-85.

(80) Li J, Zhang Z, Rosenzweig J, Wang YY, Chan DW. Proteomics and bioinformatics approaches for identification of serum biomarkers to detect breast cancer. Clin Chem 2002 Aug;48(8):1296-304.

(81) Kiehntopf M, Siegmund R, Deufel T. Use of SELDI-TOF mass spectrometry for identification of new biomarkers: potential and limitations. Clin Chem Lab Med 2007;45(11):1435-49.

(82) Vanhoutte KJ, Laarakkers C, Marchiori E, Pickkers P, Wetzels JF, Willems JL, et al. Biomarker discovery with SELDI-TOF MS in human urine associated with early renal injury: evaluation with computational analytical tools. Nephrol Dial Transplant 2007 Oct;22(10):2932-43.

(83) Liotta LA, Espina V, Mehta AI, Calvert V, Rosenblatt K, Geho D, et al. Protein microarrays: meeting analytical challenges for clinical applications. Cancer Cell 2003 Apr;3(4):317-25.

(84) Espina V, Woodhouse EC, Wulfkuhle J, Asmussen HD, Petricoin EF, III, Liotta LA. Protein microarray detection strategies: focus on direct detection technologies. J Immunol Methods 2004 Jul;290(1-2):121-33.

(85) Gevaert K, Van DJ, Goethals M, Thomas GR, Hoorelbeke B, Demol H, et al. Chromatographic isolation of methionine-containing peptides for gel-free proteome analysis: identification of more than 800 Escherichia coli proteins. Mol Cell Proteomics 2002 Nov;1(11):896-903.

(86) Conrads TP, Anderson GA, Veenstra TD, Pasa-Tolic L, Smith RD. Utility of accurate mass tags for proteome-wide protein identification. Anal Chem 2000 Jul 15;72(14):3349-54.

(87) Ji J, Chakraborty A, Geng M, Zhang X, Amini A, Bina M, et al. Strategy for qualitative and quantitative analysis in proteomics based on signature peptides. J Chromatogr B Biomed Sci Appl 2000 Aug 4;745(1):197-210.

(88) Wang S, Regnier FE. Proteomics based on selecting and quantifying cysteine containing peptides by covalent chromatography. J Chromatogr A 2001 Jul 27;924(1-2):345-57.

(89) Oda Y, Nagasu T, Chait BT. Enrichment analysis of phosphorylated proteins as a tool for probing the phosphoproteome. Nat Biotechnol 2001 Apr;19(4):379-82.

(90) Zhou H, Watts JD, Aebersold R. A systematic approach to the analysis of protein phosphorylation. Nat Biotechnol 2001 Apr;19(4):375-8.

(91) Spahr CS, Susin SA, Bures EJ, Robinson JH, Davis MT, McGinley MD, et al. Simplification of complex peptide mixtures for proteomic analysis: reversible biotinylation of cysteinyl peptides. Electrophoresis 2000 May;21(9):1635-50.

(92) Gerber SA, Rush J, Stemman O, Kirschner MW, Gygi SP. Absolute quantification of proteins and phosphoproteins from cell lysates by tandem MS. Proc Natl Acad Sci U S A 2003 Jun 10;100(12):6940-5.

(93) Timms JF, Cramer R. Difference gel electrophoresis. Proteomics 2008 Nov 10.

(94) Gharbi S, Gaffney P, Yang A, Zvelebil MJ, Cramer R, Waterfield MD, et al. Evaluation of two-dimensional differential gel electrophoresis for proteomic expression analysis of a model breast cancer cell system. Mol Cell Proteomics 2002 Feb;1(2):91-8.

(95) Graham RL, Sharma MK, Ternan NG, Weatherly DB, Tarleton RL, McMullan G. A semi-quantitative GeLC-MS analysis of temporal proteome expression in the emerging nosocomial pathogen Ochrobactrum anthropi. Genome Biol 2007;8(6):R110.

(96) Thilo L. Labeling of plasma membrane glycoconjugates by terminal glycosylation (galactosyltransferase and glycosidase). Methods Enzymol 1983;98:415-21.

(97) de CC, Ryter A, Thilo L. Membrane shuttle between plasma membrane, phagosomes, and pinosomes in Dictyostelium discoideum amoeboid cells. Eur J Cell Biol 1983 May;30(2):233-43.

(98) Burgert HG, Thilo L. Internalization and recycling of plasma membrane glycoconjugates during pinocytosis in the macrophage cell line, P388D1. Kinetic evidence for compartmentation of internalized membranes. Exp Cell Res 1983 Mar;144(1):127-42.

(99) O'Farrell PH. High resolution two-dimensional electrophoresis of proteins. J Biol Chem 1975 May 25;250(10):4007-21.

(100) Unlu M, Morgan ME, Minden JS. Difference gel electrophoresis: a single gel method for detecting changes in protein extracts. Electrophoresis 1997 Oct;18(11):2071-7.

(101) Wang B, Hendricks DT, Wamunyokoli F, Parker MI. A growth-related oncogene/CXC chemokine receptor 2 autocrine loop contributes to cellular proliferation in esophageal cancer. Cancer Res 2006 Mar 15;66(6):3071-7.

(102) Brower V. Proteomics: biology in the post-genomic era. Companies all over the world rush to lead the way in the new post-genomics race. EMBO Rep 2001 Jul;2(7):558-60.

(103) Gharbi S, Gaffney P, Yang A, Zvelebil MJ, Cramer R, Waterfield MD, et al. Evaluation of two-dimensional differential gel electrophoresis for proteomic expression analysis of a model breast cancer cell system. Mol Cell Proteomics 2002 Feb;1(2):91-8.

(104) Somiari RI, Somiari S, Russell S, Shriver CD. Proteomics of breast carcinoma. J Chromatogr B Analyt Technol Biomed Life Sci 2005 Feb 5;815(1-2):215-25.

(105) Zhou G, Li H, Gong Y, Zhao Y, Cheng J, Lee P, et al. Proteomic analysis of global alteration of protein expression in squamous cell carcinoma of the esophagus. Proteomics 2005 Sep;5(14):3814-21.

(106) Shen J, Person MD, Zhu J, Abbruzzese JL, Li D. Protein expression profiles in pancreatic adenocarcinoma compared with normal pancreatic tissue and tissue affected by pancreatitis as detected by two-dimensional gel electrophoresis and mass spectrometry. Cancer Res 2004 Dec 15;64(24):9018-26.

(107) Friedman DB, Hill S, Keller JW, Merchant NB, Levy SE, Coffey RJ, et al. Proteome analysis of human colon cancer by two-dimensional difference gel electrophoresis and mass spectrometry. Proteomics 2004 Mar;4(3):793-811.

(108) Lee IN, Chen CH, Sheu JC, Lee HS, Huang GT, Yu CY, et al. Identification of human hepatocellular carcinoma-related biomarkers by two-dimensional difference gel electrophoresis and mass spectrometry. J Proteome Res 2005 Nov;4(6):2062-9.

(109) Flanagan CA, Tetaz T, Smith AI, Millar RP. Development of methods for purification of membrane associated gonadotropin-releasing hormone binding proteins. Biomed Chromatogr 1996 Mar;10(2):83-8.

(110) Weeks ME, Sinclair J, Butt A, Chung YL, Worthington JL, Wilkinson CR, et al. A parallel proteomic and metabolomic analysis of the hydrogen peroxide- and Sty1p-dependent stress response in Schizosaccharomyces pombe. Proteomics 2006 May;6(9):2772-96.

(111) Neuhoff V, Arold N, Taube D, Ehrhardt W. Improved staining of proteins in polyacrylamide gels including isoelectric focusing gels with clear background at nanogram sensitivity using Coomassie Brilliant Blue G-250 and R-250. Electrophoresis 1988 Jun;9(6):255-62.

(112) Neuhoff V, Stamm R, Pardowitz I, Arold N, Ehrhardt W, Taube D. Essential problems in quantification of proteins following colloidal staining with coomassie brilliant blue dyes in polyacrylamide gels, and their solution. Electrophoresis 1990 Feb;11(2):101-17.

(113) Dupont WD, Plummer WD, Jr. Power and sample size calculations. A review and computer program. Control Clin Trials 1990 Apr;11(2):116-28.

(114) Park SG, Ewalt KL, Kim S. Functional expansion of aminoacyl-tRNA synthetases and their interacting factors: new perspectives on housekeepers. Trends Biochem Sci 2005 Oct;30(10):569-74.

(115) Yagui-Beltran A, Craig AL, Lawrie L, Thompson D, Pospisilova S, Johnston D, et al. The human oesophageal squamous epithelium exhibits a novel type of heat shock protein response. Eur J Biochem 2001 Oct;268(20):5343-55.

(116) Imai FL, Uzawa K, Nimura Y, Moriya T, Imai MA, Shiiba M, et al. Chromosome 1 open reading frame 10 (C1orf10) gene is frequently down-regulated and inhibits cell proliferation in oral squamous cell carcinoma. Int J Biochem Cell Biol 2005 Aug;37(8):1641-55.

(117) Tzivion G, Gupta VS, Kaplun L, Balan V. 14-3-3 proteins as potential oncogenes. Semin Cancer Biol 2006 Jun;16(3):203-13.

(118) Bonner JC, Osornio-Vargas AR. Differential binding and regulation of platelet-derived growth factor A and B chain isoforms by alpha 2-macroglobulin. J Biol Chem 1995 Jul 7;270(27):16236-42.

(119) Lepretre C, Fleurier Y, Martin E, Torriglia A. Nuclear export of LEI/L-DNase II by Crm1 is essential for cell survival. Biochim Biophys Acta 2008 Jun;1783(6):1068-75.

(120) Silverman GA, Bird PI, Carrell RW, Church FC, Coughlin PB, Gettins PG, et al. The serpins are an expanding superfamily of structurally similar but functionally diverse proteins. Evolution, mechanism of inhibition, novel functions, and a revised nomenclature. J Biol Chem 2001 Sep 7;276(36):33293-6.

(121) Suriano R, Ghosh SK, Ashok BT, Mittelman A, Chen Y, Banerjee A, et al. Differences in glycosylation patterns of heat shock protein, gp96: implications for prostate cancer prevention. Cancer Res 2005 Jul 15;65(14):6466-75.

(122) Melendez K, Wallen ES, Edwards BS, Mobarak CD, Bear DG, Moseley PL. Heat shock protein 70 and glycoprotein 96 are differentially expressed on the surface of malignant and nonmalignant breast cells. Cell Stress Chaperones 2006;11(4):334-42.

(123) Shieh DB, Chen IW, Wei TY, Shao CY, Chang HJ, Chung CH, et al. Tissue expression of gelsolin in oral carcinogenesis progression and its clinicopathological implications. Oral Oncol 2006 Jul;42(6):599-606.

(124) Noske A, Denkert C, Schober H, Sers C, Zhumabayeva B, Weichert W, et al. Loss of Gelsolin expression in human ovarian carcinomas. Eur J Cancer 2005 Feb;41(3):461-9.

(125) Tatenhorst L, Rescher U, Gerke V, Paulus W. Knockdown of annexin 2 decreases migration of human glioma cells in vitro. Neuropathol Appl Neurobiol 2006 Jun;32(3):271-7.

(126) Vishwanatha JK, Chiang Y, Kumble KD, Hollingsworth MA, Pour PM. Enhanced expression of annexin II in human pancreatic carcinoma cells and primary pancreatic cancers. Carcinogenesis 1993 Dec;14(12):2575-9.

(127) Gerke V, Moss SE. Annexins: from structure to function. Physiol Rev 2002 Apr;82(2):331-71.

(128) Kwiatkowski DJ, Mehl R, Yin HL. Genomic organization and biosynthesis of secreted and cytoplasmic forms of gelsolin. J Cell Biol 1988 Feb;106(2):375-84.

(129) Kwiatkowski DJ, Janmey PA, Yin HL. Identification of critical functional and regulatory domains in gelsolin. J Cell Biol 1989 May;108(5):1717-26.

(130) Kwiatkowski DJ. Functions of gelsolin: motility, signaling, apoptosis, cancer. Curr Opin Cell Biol 1999 Feb;11(1):103-8.

(131) WARBURG O. On the origin of cancer cells. Science 1956 Feb 24;123(3191):309-14.

(132) Karp NA, Lilley KS. Investigating sample pooling strategies for DIGE experiments to address biological variability. Proteomics 2008 Dec 22;9(2):388-97.

(133) Arany I, Rady P, Kertai P. Regulation of glycolysis and oxygen consumption in lymph-node cells of normal and leukaemic mice. Br J Cancer 1981 Jun;43(6):804-8.

(134) Farrow SM, Jones CT. Membrane-associated pyruvate kinase in developing guinea-pig liver. Biochem J 1986 Apr 1;235(1):103-10.

(135) Tarze A, Deniaud A, Le BM, Maillier E, Molle D, Larochette N, et al. GAPDH, a novel regulator of the pro-apoptotic mitochondrial membrane permeabilization. Oncogene 2007 Apr 19;26(18):2606-20.

(136) Mazzola JL, Sirover MA. Subcellular localization of human glyceraldehyde-3-phosphate dehydrogenase is independent of its glycolytic function. Biochim Biophys Acta 2003 Jun 20;1622(1):50-6.

(137) Mikuriya K, Kuramitsu Y, Ryozawa S, Fujimoto M, Mori S, Oka M, et al. Expression of glycolytic enzymes is increased in pancreatic cancerous tissues as evidenced by proteomic profiling by two-dimensional electrophoresis and liquid chromatography-mass spectrometry/mass spectrometry. Int J Oncol 2007 Apr;30(4):849-55.

(138) Shaw RJ. Glucose metabolism and cancer. Curr Opin Cell Biol 2006 Dec;18(6):598-608.

(139) Bonnet S, Archer SL, Ialunis-Turner J, Haromy A, Beaulieu C, Thompson R, et al. A mitochondria-K+ channel axis is suppressed in cancer and its normalization promotes apoptosis and inhibits cancer growth. Cancer Cell 2007 Jan;11(1):37-51.

(140) Qi W, Liu X, Qiao D, Martinez JD. Isoform-specific expression of 14-3-3 proteins in human lung cancer tissues. Int J Cancer 2005 Jan 20;113(3):359-63.

(141) Jang JS, Cho HY, Lee YJ, Ha WS, Kim HW. The differential proteome profile of stomach cancer: identification of the biomarker candidates. Oncol Res 2004;14(10):491-9.

(142) Zang L, Palmer TD, Hancock WS, Sgroi DC, Karger BL. Proteomic analysis of ductal carcinoma of the breast using laser capture microdissection, LC-MS, and 16O/18O isotopic labeling. J Proteome Res 2004 May;3(3):604-12.

(143) Somiari RI, Somiari S, Russell S, Shriver CD. Proteomics of breast carcinoma. J Chromatogr B Analyt Technol Biomed Life Sci 2005 Feb 5;815(1-2):215-25.

(144) Poschl E, Schlotzer-Schrehardt U, Brachvogel B, Saito K, Ninomiya Y, Mayer U. Collagen IV is essential for basement membrane stability but dispensable for initiation of its assembly during early development. Development 2004 Apr;131(7):1619-28.

(145) Khoshnoodi J, Pedchenko V, Hudson BG. Mammalian collagen IV. Microsc Res Tech 2008 May;71(5):357-70.

(146) Tanjore H, Kalluri R. The role of type IV collagen and basement membranes in cancer progression and metastasis. Am J Pathol 2006 Mar;168(3):715-7.

(147) Ikeda K, Iyama K, Ishikawa N, Egami H, Nakao M, Sado Y, et al. Loss of expression of type IV collagen alpha5 and alpha6 chains in colorectal cancer associated with the hypermethylation of their promoter region. Am J Pathol 2006 Mar;168(3):856-65.

(148) Rommelaere H, Van TM, Gao Y, Melki R, Cowan NJ, Vandekerckhove J, et al. Eukaryotic cytosolic chaperonin contains t-complex polypeptide 1 and seven related subunits. Proc Natl Acad Sci U S A 1993 Dec 15;90(24):11975-9.

(149) Winston JS, Asch HL, Zhang PJ, Edge SB, Hyland A, Asch BB. Downregulation of gelsolin correlates with the progression to breast carcinoma. Breast Cancer Res Treat 2001 Jan;65(1):11-21.

(150) Yang J, Tan D, Asch HL, Swede H, Bepler G, Geradts J, et al. Prognostic significance of gelsolin expression level and variability in non-small cell lung cancer. Lung Cancer 2004 Oct;46(1):29-42.

(151) Dissmann E, Hinssen H. Immunocytochemical localization of gelsolin in fibroblasts, myogenic cells, and isolated myofibrils. Eur J Cell Biol 1994 Apr;63(2):336-44.

(152) Bernal SD, Stahel RA. Cytoskeleton-associated proteins: their role as cellular integrators in the neoplastic process. Crit Rev Oncol Hematol 1985;3(3):191-204.

(153) Hayes MJ, Rescher U, Gerke V, Moss SE. Annexin-actin interactions. Traffic 2004 Aug;5(8):571-6.

(154) Rescher U, Gerke V. Annexins--unique membrane binding proteins with diverse functions. J Cell Sci 2004 Jun 1;117(Pt 13):2631-9.

(155) Takahashi H, Shikata N, Senzaki H, Shintaku M, Tsubura A. Immunohistochemical staining patterns of keratins in normal oesophageal epithelium and carcinoma of the oesophagus. Histopathology 1995 Jan;26(1):45-50.

(156) Viaene AI, Baert JH. Expression of cytokeratin-mRNAs in squamous-cell carcinoma and balloon-cell formation of human oesophageal epithelium. Histochem J 1995 Jan;27(1):69-78.

(157) Viaene AI, Baert JH. Expression of cytokeratin mRNAs in normal human esophageal epithelium. Anat Rec 1995 Jan;241(1):88-98.

(158) Vaidya MM, Kanojia D. Keratins: markers of cell differentiation or regulators of cell differentiation? J Biosci 2007 Jun;32(4):629-34.

(159) Lloyd C, Yu QC, Cheng J, Turksen K, Degenstein L, Hutton E, et al. The basal keratin network of stratified squamous epithelia: defining K15 function in the absence of K14. J Cell Biol 1995 Jun;129(5):1329-44.

(160) Ko YG, Kim EY, Kim T, Park H, Park HS, Choi EJ, et al. Glutamine-dependent antiapoptotic interaction of human glutaminyl-tRNA synthetase with apoptosis signal-regulating kinase 1. J Biol Chem 2001 Feb 23;276(8):6030-6.

(161) Yang X, Khosravi-Far R, Chang HY, Baltimore D. Daxx, a novel Fas-binding protein that activates JNK and apoptosis. Cell 1997 Jun 27;89(7):1067-76.

(162) Uemura N, Nakanishi Y, Kato H, Saito S, Nagino M, Hirohashi S, et al. Transglutaminase 3 as a prognostic biomarker in esophageal cancer revealed by proteomics. Int J Cancer 2008 Dec 3.

(163) Liu W, Yu ZC, Cao WF, Ding F, Liu ZH. Functional studies of a novel oncogene TGM3 in human esophageal squamous cell carcinoma. World J Gastroenterol 2006 Jun 28;12(24):3929-32.

(164) Dawson DM, Eppenberger HM, Eppenberger ME. Multiple molecular forms of creatine kinases. Ann N Y Acad Sci 1968 Jun 14;151(1):616-26.

(165) Klein SC, Haas RC, Perryman MB, Billadello JJ, Strauss AW. Regulatory element analysis and structural characterization of the human sarcomeric mitochondrial creatine kinase gene. J Biol Chem 1991 Sep 25;266(27):18058-65.

(166) Pretlow TG, Whitehurst GB, Pretlow TP, Hunt RS, Jacobs JM, McKenzie DR, et al. Decrease in creatine kinase in human prostatic carcinoma compared to benign prostatic hyperplasia. Cancer Res 1982 Nov;42(11):4842-8.

(167) Fukao T, Song XQ, Mitchell GA, Yamaguchi S, Sukegawa K, Orii T, et al. Enzymes of ketone body utilization in human tissues: protein and messenger RNA levels of succinyl-coenzyme A (CoA):3-ketoacid CoA transferase and mitochondrial and cytosolic acetoacetyl-CoA thiolases. Pediatr Res 1997 Oct;42(4):498-502.

(168) Williamson DH, Bates MW, Page MA, Krebs HA. Activities of enzymes involved in acetoacetate utilization in adult mammalian tissues. Biochem J 1971 Jan;121(1):41-7.

(169) Singh MS, Michael M. Role of xenobiotic metabolic enzymes in cancer epidemiology. Methods Mol Biol 2009;472:243-64.

(170) Board PG, Coggan M, Chelvanayagam G, Easteal S, Jermiin LS, Schulte GK, et al. Identification, characterization, and crystal structure of the Omega class glutathione transferases. J Biol Chem 2000 Aug 11;275(32):24798-806.

(171) Yin ZL, Dahlstrom JE, Le Couteur DG, Board PG. Immunohistochemistry of omega class glutathione S-transferase in human tissues. J Histochem Cytochem 2001 Aug;49(8):983-7.

(172) Aksoy S, Szumlanski CL, Weinshilboum RM. Human liver nicotinamide N-methyltransferase. cDNA cloning, expression, and biochemical characterization. J Biol Chem 1994 May 20;269(20):14835-40.

(173) Jang JS, Cho HY, Lee YJ, Ha WS, Kim HW. The differential proteome profile of stomach cancer: identification of the biomarker candidates. Oncol Res 2004;14(10):491-9.

(174) Roessler M, Rollinger W, Palme S, Hagmann ML, Berndt P, Engel AM, et al. Identification of nicotinamide N-methyltransferase as a novel serum tumor marker for colorectal cancer. Clin Cancer Res 2005 Sep 15;11(18):6550-7.

(175) Fukumoto S, Yamauchi N, Moriguchi H, Hippo Y, Watanabe A, Shibahara J, et al. Overexpression of the aldo-keto reductase family protein AKR1B10 is highly correlated

with smokers' non-small cell lung carcinomas. Clin Cancer Res 2005 Mar 1;11(5):1776-85.

(176) Yan R, Zu X, Ma J, Liu Z, Adeyanju M, Cao D. Aldo-keto reductase family 1 B10 gene silencing results in growth inhibition of colorectal cancer cells: Implication for cancer intervention. Int J Cancer 2007 Nov 15;121(10):2301-6.

(177) Aisen P, Brown EB. Structure and function of transferrin. Prog Hematol 1975;9:25-56.

(178) Cheng Y, Zak O, Aisen P, Harrison SC, Walz T. Structure of the human transferrin receptor-transferrin complex. Cell 2004 Feb 20;116(4):565-76.

(179) Vostrejs M, Moran PL, Seligman PA. Transferrin synthesis by small cell lung cancer cells acts as an autocrine regulator of cellular proliferation. J Clin Invest 1988 Jul;82(1):331-9.

(180) Erickson JD, Varoqui H. Molecular analysis of vesicular amine transporter function and targeting to secretory organelles. FASEB J 2000 Dec;14(15):2450-8.

(181) Koch J, Foekens J, Timmermans M, Fink W, Wirzbach A, Kramer MD, et al. Human VAT-1: a calcium-regulated activation marker of human epithelial cells. Arch Dermatol Res 2003 Sep;295(5):203-10.

(182) Welss T, Sun J, Irving JA, Blum R, Smith AI, Whisstock JC, et al. Hurpin is a selective inhibitor of lysosomal cathepsin L and protects keratinocytes from ultraviolet-induced apoptosis. Biochemistry 2003 Jun 24;42(24):7381-9.

(183) Abts HF, Welss T, Mirmohammadsadegh A, Kohrer K, Michel G, Ruzicka T. Cloning and characterization of hurpin (protease inhibitor 13): A new skin-specific, UV-repressible serine proteinase inhibitor of the ovalbumin serpin family. J Mol Biol 1999 Oct 15;293(1):29-39.

(184) Spring P, Nakashima T, Frederick M, Henderson Y, Clayman G. Identification and cDNA cloning of headpin, a novel differentially expressed serpin that maps to chromosome 18q. Biochem Biophys Res Commun 1999 Oct 14;264(1):299-304.

(185) Lepretre C, Scovassi AI, Shah GM, Torriglia A. Regulation of poly(ADP-ribose) polymerase-1 functions by leukocyte elastase inhibitor/LEI-derived DNase II during caspase-independent apoptosis. Int J Biochem Cell Biol 2008 Oct 4.

(186) Young RA. Stress proteins and immunology. Annu Rev Immunol 1990;8:401-20.

(187) Zhu XD, Li CL, Lang ZW, Gao GF, Tien P. Significant correlation between expression level of HSP gp96 and progression of hepatitis B virus induced diseases. World J Gastroenterol 2004 Apr 15;10(8):1141-5.

(188) Qi Y, Chiu JF, Wang L, Kwong DL, He QY. Comparative proteomic analysis of esophageal squamous cell carcinoma. Proteomics 2005 Jul;5(11):2960-71.

(189) Essentials of Glycobiology. 2nd ed. Cold Spring Harbor, New York: Cold Spring Harbor Laboratory Press; 1999.

(190) Ohtsubo K, Marth JD. Glycosylation in cellular mechanisms of health and disease. Cell 2006 Sep 8;126(5):855-67.

(191) Types of glycosylation. http://www premierbiosoft com/glycan/glossary/glycosylation html 2009 January 1 [cited 2009 Oct 11];

(192) Haynes BF, Hemler ME, Mann DL, Eisenbarth GS, Shelhamer J, Mostowski HS, et al. Characterization of a monoclonal antibody (4F2) that binds to human monocytes and to a subset of activated lymphocytes. J Immunol 1981 Apr;126(4):1409-14.

(193) Pietersen R, Thilo L, de CC. Mycobacterium tuberculosis and Mycobacterium avium modify the composition of the phagosomal membrane in infected macrophages by selective depletion of cell surface-derived glycoconjugates. Eur J Cell Biol 2004 May;83(4):153-8.

(194) de CC, Lang T, Thilo L. Phagocytic processing of the macrophage endoparasite, Mycobacterium avium, in comparison to phagosomes which contain Bacillus subtilis or latex beads. Eur J Cell Biol 1995 Oct;68(2):167-82.

(195) Hoffmann R, Valencia A. A gene network for navigating the literature. Nat Genet 2004 Jul;36(7):664.

(196) Wagner CA, Lang F, Broer S. Function and structure of heterodimeric amino acid transporters. Am J Physiol Cell Physiol 2001 Oct;281(4):C1077-C1093.

(197) Estevez R, Camps M, Rojas AM, Testar X, Deves R, Hediger MA, et al. The amino acid transport system y+L/4F2hc is a heteromultimeric complex. FASEB J 1998 Oct;12(13):1319-29.

(198) Haynes BF, Hemler M, Cotner T, Mann DL, Eisenbarth GS, Strominger JL, et al. Characterization of a monoclonal antibody (5E9) that defines a human cell surface antigen of cell activation. J Immunol 1981 Jul;127(1):347-51.

(199) Kanai Y, Segawa H, Miyamoto K, Uchino H, Takeda E, Endou H. Expression cloning and characterization of a transporter for large neutral amino acids activated by the heavy chain of 4F2 antigen (CD98). J Biol Chem 1998 Sep 11;273(37):23629-32.

(200) Feral CC, Nishiya N, Fenczik CA, Stuhlmann H, Slepak M, Ginsberg MH. CD98hc (SLC3A2) mediates integrin signaling. Proc Natl Acad Sci U S A 2005 Jan 11;102(2):355-60.

(201) Henderson NC, Collis EA, Mackinnon AC, Simpson KJ, Haslett C, Zent R, et al. CD98hc (SLC3A2) interaction with beta 1 integrins is required for transformation. J Biol Chem 2004 Dec 24;279(52):54731-41.

(202) Yagita H, Masuko T, Hashimoto Y. Inhibition of tumor cell growth in vitro by murine monoclonal antibodies that recognize a proliferation-associated cell surface antigen system in rats and humans. Cancer Res 1986 Mar;46(3):1478-84.

(203) Broer S, Broer A, Hamprecht B. Expression of the surface antigen 4F2hc affects system-L-like neutral-amino-acid-transport activity in mammalian cells. Biochem J 1997 Jun 1;324 (Pt 2):535-41.

(204) Campbell WA, Thompson NL. Overexpression of LAT1/CD98 light chain is sufficient to increase system L-amino acid transport activity in mouse hepatocytes but not fibroblasts. J Biol Chem 2001 May 18;276(20):16877-84.

(205) Warren AP, Patel K, McConkey DJ, Palacios R. CD98: a type II transmembrane glycoprotein expressed from the beginning of primitive and definitive hematopoiesis may play a critical role in the development of hematopoietic cells. Blood 1996 May 1;87(9):3676-87.

(206) Fenczik CA, Sethi T, Ramos JW, Hughes PE, Ginsberg MH. Complementation of dominant suppression implicates CD98 in integrin activation. Nature 1997 Nov 6;390(6655):81-5.

(207) Ohgimoto S, Tabata N, Suga S, Nishio M, Ohta H, Tsurudome M, et al. Molecular characterization of fusion regulatory protein-1 (FRP-1) that induces multinucleated giant cell formation of monocytes and HIV gp160-mediated cell fusion. FRP-1 and 4F2/CD98 are identical molecules. J Immunol 1995 Oct 1;155(7):3585-92.

(208) Hashimoto Y, Masuko T, Yagita H, Endo N, Kanazawa J, Tazawa J. A proliferation-associated rat cell surface antigen recognized by a murine monoclonal antibody. Gann 1983 Dec;74(6):819-21.

(209) Masuko T, Abe J, Yagita H, Hashimoto Y. Human bladder cancer cell-surface antigens recognized by murine monoclonal antibodies raised against T24 bladder cancer cells. Jpn J Cancer Res 1985 May;76(5):386-94.

(210) Quackenbush EJ, Gougos A, Baumal R, Letarte M. Differential localization within human kidney of five membrane proteins expressed on acute lymphoblastic leukemia cells. J Immunol 1986 Jan;136(1):118-24.

(211) Christensen HN. Role of amino acid transport and countertransport in nutrition and metabolism. Physiol Rev 1990 Jan;70(1):43-77.

(212) Kobayashi K, Ohnishi A, Promsuk J, Shimizu S, Kanai Y, Shiokawa Y, et al. Enhanced tumor growth elicited by L-type amino acid transporter 1 in human malignant glioma cells. Neurosurgery 2008 Feb;62(2):493-503.

(213) Kaira K, Oriuchi N, Imai H, Shimizu K, Yanagitani N, Sunaga N, et al. l-type amino acid transporter 1 and CD98 expression in primary and metastatic sites of human neoplasms. Cancer Sci 2008 Nov 17.

(214) Itoh K, Inoue K, Hayashi H, Suzuki T, Masuko T. Identification of cell proliferation-associated epitope on CD98 oncoprotein using phage display random peptide library. Cancer Sci 2007 Nov;98(11):1696-700.

(215) Endou H, Kanai Y, inventors; Method using neutral amino acid transporter expressing cell. United States patent 7335482. 2008 Feb 26.

(216) Stassar MJJG, Chahal FC, Cizeau JP, inventors; Antibodies specific for human CD98 heavy antigen. United States patent WO/2008/017828 . 2008 Feb 14.

(217) Xiao T, Ying W, Li L, Hu Z, Ma Y, Jiao L, et al. An approach to studying lung cancer-related proteins in human blood. Mol Cell Proteomics 2005 Oct;4(10):1480-6.

(218) Wong JY, Huggins GS, Debidda M, Munshi NC, De V, I. Dichloroacetate induces apoptosis in endometrial cancer cells. Gynecol Oncol 2008 Jun;109(3):394-402.

(219) Michelakis ED, Webster L, Mackey JR. Dichloroacetate (DCA) as a potential metabolic-targeting therapy for cancer. Br J Cancer 2008 Oct 7;99(7):989-94.

(220) Michelakis ED, Webster L, Mackey JR. Dichloroacetate (DCA) as a potential metabolic-targeting therapy for cancer. Br J Cancer 2008 Oct 7;99(7):989-94.

(221) Michelakis ED, Webster L, Mackey JR. Dichloroacetate (DCA) as a potential metabolic-targeting therapy for cancer. Br J Cancer 2008 Oct 7;99(7):989-94.

(222) Michelakis ED, Webster L, Mackey JR. Dichloroacetate (DCA) as a potential metabolic-targeting therapy for cancer. Br J Cancer 2008 Oct 7;99(7):989-94.

(223) Shimada Y, Imamura M, Wagata T, Yamaguchi N, Tobe T. Characterization of 21 newly established esophageal cancer cell lines. Cancer 1992 Jan 15;69(2):277-84.

(224) Harada H, Nakagawa H, Oyama K, Takaoka M, Andl CD, Jacobmeier B, et al. Telomerase induces immortalization of human esophageal keratinocytes without p16INK4a inactivation. Mol Cancer Res 2003 Aug;1(10):729-38.

(225) Fouque F, Brivet M, Boutron A, Vequaud C, Marsac C, Zabot MT, et al. Differential effect of DCA treatment on the pyruvate dehydrogenase complex in patients with severe PDHC deficiency. Pediatr Res 2003 May;53(5):793-9.

(226) Geoffroy V, Fouque F, Benelli C, Poggi F, Saudubray JM, Lissens W, et al. Defect in the X-lipoyl-containing component of the pyruvate dehydrogenase complex in a patient with neonatal lactic acidemia. Pediatrics 1996 Feb;97(2):267-72.

(227) Denyer GS, Lam D, Cooney GJ, Caterson ID. Effect of starvation and insulin in vivo on the activity of the pyruvate dehydrogenase complex in rat skeletal muscles. FEBS Lett 1989 Jul 3;250(2):464-8.

(228) Bradford MM. A rapid and sensitive method for the quantitation of microgram quantities of protein utilizing the principle of protein-dye binding. Anal Biochem 1976 May 7;72:248-54.

(229) Cao W, Yacoub S, Shiverick KT, Namiki K, Sakai Y, Porvasnik S, et al. Dichloroacetate (DCA) sensitizes both wild-type and over expressing Bcl-2 prostate cancer cells in vitro to radiation. Prostate 2008 Aug 1;68(11):1223-31.

(230) Naito E, Kuroda Y, Toshima K, Takeda E, Saijo T, Kobashi H, et al. Effect of sodium dichloroacetate on human pyruvate metabolism. Brain Dev 1989;11(3):195-7.

(231) Gambhir SS. Molecular imaging of cancer with positron emission tomography. Nat Rev Cancer 2002 Sep;2(9):683-93.

(232) Stacpoole PW, Henderson GN, Yan Z, James MO. Clinical pharmacology and toxicology of dichloroacetate. Environ Health Perspect 1998 Aug;106 Suppl 4:989-94.

(233) Anselm IA, Darras BT. Dichloroacetate causes toxic neuropathy in MELAS: a randomized, controlled clinical trial. Neurology 2006 Oct 10;67(7):1313.

(234) Pan JG, Mak TW. Metabolic targeting as an anticancer strategy: dawn of a new era? Sci STKE 2007 Apr 10;2007(381):e14.

(235) Wamunyokoli F. Differentially expressed genes in oesophageal cancer. Cape Town: University of Cape Town; 2002.